Bound States and Structural Properties of Trap-Imbalanced Fermions

Robert Alexander Henry

Supervisors:
Dr. Andrew M. Martin
A/Prof. Harry M. Quiney

Submitted in total fulfilment of the requirements
of the degree of Master of Philosophy

October 2016

School of Physics
University of Melbourne

Abstract

Ultracold quantum gases, which were only recently realised experimentally, have become one of the most active fields of modern research. This is due to the precision and power of the experiments, as well as the great variety of physical phenomena that they exhibit. In this thesis, the physics of few-body scattering in the strongly-interacting regime is studied. The study of few-body physics allows a better understanding of many-body systems, particularly with strong interactions, which make the usual many-body theoretical techniques untenable.

The particular topic of this thesis is few-body scattering in heteronuclear systems, which contain two species of atom with different masses and/or harmonic trapping frequencies. These mass and trap imbalances lead to a variety of interesting physics that is not present in homonuclear systems. Deeply-bound Efimov states with unusual properties appear in systems containing two species of fermions when the ratio of the two species' masses becomes sufficiently large. Other types of deeply bound states also appear above a lower critical mass ratio. We use an implementation of a stochastic variational method to study states of this type under a trap imbalance i.e. with two species of fermion with different harmonic trapping frequencies. The stochastic variational method works by randomly generating trial functions, then using a competitive selection scheme to select the best contributions to the approximate variational solution. Using this method, it is shown that the introduction of a trap imbalance has no effect ont the physics of these bound states.

Also using this variational method, the effect of trap imbalances on two- and three-body systems, with and without mass imbalances, is studied in detail. It is found that the trap imbalance has the immediate effect of lifting structural and energetic degeneracies between different total angular momentum states of the few-

body system. Furthermore, trap imbalances significantly alter the usual physics of the three-fermion system, in which two atoms form a deeply-bound dimer while the third remains unbound. The trap imbalance changes this picture and causes all three atoms to overlap considerably in the ground state, forming a loosely-bound trimer state. Such alterations to the few-body collision properties can have significant effects on the many-body physics of an atomic gas. Thus these results indicate the possibility of additional methods of tuning and control for heteronuclear many-body systems. These results may also be of interest in explicitly few-body experiments, which remain largely unexplored at this time.

Declaration

This to certify that:

1. This thesis is my original work towards the MPhil
2. All material from other sources is duly acknowledged in the text
3. This thesis is less than 40,000 words in length, exclusive of tables, bibliographies and appendices.

Robert Alexander Henry

Preface

Here the content of each Chapter, and what part of this content is the original work of the author, are outlined.

- **Chapter 2** reviews the scattering theory that underlies most ultracold few-body systems. All calculations and figures are the author's own work.
- **Chapter 3** describes the stochastic variational method used throughout the thesis. The particulars of the variational ansatz are the author's original work. All calculations and figures are the author's own work.
- **Chapter 4** reviews the analytic theory of two atoms in a harmonic trap, and compares to the author's own numerics. All calculations and figures are the author's own work.
- **Chapter 5** reviews the analytic theory of three atoms in a harmonic trap, and compares to the author's own numerics. All calculations and figures are the author's own work.
- **Chapter 6** reviews the theory and history of Efimov states and other effects found in mass-imbalanced fermionic systems, particularly non-universal bound states. All calculations and figures are the author's own work unless otherwise specified.
- **Chapter 7** presents new results on trap-imbalanced systems. All content in this Chapter is the author's original work, as yet unpublished.

Acknowledgements

I would first like to thank my supervisor Assoc. Prof. Andy Martin for his perpetual patience and enthusiasm throughout the course of my MPhil. I would also like to thank Assoc. Prof. Harry Quiney for his occasional but very helpful discussions, and his inspiring aura of erudition.

My sincere thanks go to Doctors Brendan Mulkerin and Chris Bradly, who guided me through much of my research, and generally to all members of the Theoretical Condensed Matter Physics group, who have made this an inspiring and enjoyable place to work these past years.

Finally, special thanks to Fiona Henry, Les Bursill and Vickie Zhang for their invaluable contributions to the structure and typography of this thesis. Extra special thanks go to Vickie Zhang, for her contributions to my life both noticed and unnoticed.

Contents

List of Figures

Definitions and Conventions

Various quantities and conventions which are used throughout the thesis are listed here.

- Throughout the thesis, dimensionless units are used i.e. $\hbar = 1$.
- The natural length and energy scales of a general 3D quantum harmonic oscillator with mass m and frequency ω are $a_{\text{ho}} = (m\omega)^{-1/2}$ and $E_{\text{ho}} = \omega$, respectively. These quantities are often used to rescale lengths and energies in calculations and results. Unless otherwise specified, a_{ho} refers to the harmonic oscillator length of the system's first Jacobi coordinate i.e. $a_{\text{ho}} = (m_r\omega_r)^{-1/2}$. This is used to rescale the pair correlations that make up a large part of the new results in Chapter 7. Expressions for m_r and ω_r are given in Eq. (7.10).
- The scattering length a_s is the effective physical extent of a scattering potential. Unless otherwise stated, all calculations are performed at $a_s \approx 10^8 a_{\text{ho}}$ i.e. approximately at unitarity. See Eq. (2.15) for details.

Chapter 1

Introduction

The field of ultracold atoms is a young one, yet it draws on the physics of the past century in a way that is conceptual and historical, and also practical and stylistic. This is because the physics of so many other quantum systems can be found in the ultracold gas. Ultracold atom physics is often viewed as a continuation of condensed matter physics. The familiar theories of crystalline structures are found at work in the optical lattice, and the mechanisms of superconductivity are reproduced in the phases of quantum gases. Closer to the heart of this thesis, nuclear physics and quantum chemistry have long explored the surprising and rich physics of few-body quantum systems. Many of the techniques used in this work descend directly from those fields.

Virtually all previous and current research in the ultracold atom field depends on a small set of remarkable experiments that have taken place in the past few decades. The most fundamental of these is the development by Chu, Cohen-Tannoudji and Phillips [27, 28] of techniques to trap and cool atoms at temperatures near absolute zero, for which they won the Nobel Prize in 1997. Since their invention, these techniques have been expanded and refined to facilitate a wide range of experiments [89]. Perhaps the best-known is the realisation of Bose-Einstein condensates (BECs) [5, 22, 33], in which a cloud of identical bosons is cooled to such low temperates that each boson occupies the same quantum state. This observation had long been anticipated, since Einstein theorised the state in 1925 [42] based on work by Satyendra Bose [19]. Cornell, Wieman and Ketterle shared the Nobel Prize in 2001 for its realisation [30]. Since the original experiments, many new

BEC systems have been created, notably including observations of superfluidity and quantum vortices [1, 87], and solitons [23, 74].

This work, however, is concerned with systems of ultracold fermions. A gas of identical fermions is in fact not directly susceptible to the cooling techniques developed by Chu, Tannoudji and Phillips. This is because evaporative cooling relies fundamentally on s-wave scattering to give large quantities of kinetic energy to some fraction of the atoms, causing them to escape from the shallow optical and/or magnetic potential [53]. However, scattering between identical fermions is heavily suppressed due to the Pauli exclusion principle, preventing these collisions and thus inhibiting evaporative cooling. Therefore, the first sample of ultracold fermions was a two-component system [34], with fermions in two different spin states, which are able to scatter. This was quickly followed by various experiments in which fermions of a single spin state were cooled sympathetically through contact with a cold gas of bosons [110, 124].

Fermi gases (from here on assumed to be two-component) exhibit a range of physics not found in Bose gases [53, 64]. In three dimensions, the Bose gas has a phase transition to a BEC superfluid phase as it approaches some critical temperature T_c. Fermions have a similar BEC phase, in which pairs of fermions form tight dimers. Being bosonic, these dimers then readily form a BEC with superfluid properties. Fermi gases also have a Bardeen Cooper Schrieffer (BCS) superfluid phase, which is analogous to that found in superconductors[7].

For bosons, the transition to a BEC state is well-defined and relatively well-understood. It is here that fermions show remarkably different physics. Fermi gases can exist in regions of the parameter space where Bose gases cannot. Specifically, those regions where the strength of the interaction between atoms is very high. This is due to the same suppression of three-body scattering that originally made fermions so difficult to cool. This is referred to as the strongly-interacting regime and is a major focus of ultracold fermion research. This regime can be approached from either the BEC or BCS side of phase space, with the notable result that the transition is *smooth* i.e. the fermions gradually transition from a BEC state to a BCS state [36, 81, 96]. The strongly-interacting regime can be characterised as where r_0, the range of the interaction, is much smaller than any other length scale, with the relevant length scales being the thermal de Broglie wavelength ($\lambda = hp$), the mean interparticle distance, and the Fermi length (the wavelength of a particle

at the Fermi energy). The situation is similar to many nuclear systems, but without the difficulties introduced by electric charges and other nuclear effects. Analogous transitions are found in neutron stars [102], and high-temperature superconductors [25, 80].

The first Fermi BECs, also known as molecular condensates, were observed in 2003 [71, 76, 136]. This was soon followed by many observations in the strongly-interacting regime [20, 56, 97, 108, 135] on both the BCS and BEC sides. These observations were enabled by a technique that has become fundamental to the cold atom field: the Feshbach (or Fano-Feshbach) resonance. By exploiting resonances between atomic bound states and two-particle scattering states, this technique allows the effective strength of the atomic interaction to be changed [26, 123]. An external magnetic field is sufficient to Zeeman shift the bound state and move the system across the resonance. In fact, this can be done with incredible range and precision for many species of atom, allowing the scattering length a_s, which characterises the interaction, to be tuned across many orders of magnitude. Like many cold atom phenomena, the Feshbach resonance was originally theorised and observed in nuclear systems [44, 49].

Feshbach resonances allow experimentalists to reach scattering lengths so large that all other length scales in the system are eclipsed by many orders of magnitude. This is known as the unitary regime, which lies at the centre of the BCS-BEC crossover, and has its own unique properties. The most impressive of these is universality. Under universality, all observable properties of the system can be expressed in terms of a single parameter, the scattering length a_s. This includes macroscopic quantities like entropy and pressure. The microscopic behaviour of the system also becomes universal: the few-body scattering processes come to depend only on a_s, and not on the detailed shape of the interatomic potential, a fact that will be used throughout this thesis. Universality is fundamentally a property of the scattering theory of two-body collisions, which is discussed extensively in Chapter 2. The problem of two trapped neutral atoms interacting at any scattering length was solved in 1998 by Busch et al. [24], assuming a zero-range pseudopotential as the interaction. As discussed in Chapter 3, this effectively gives the solution to a two-body system with *any* isotropic interaction at unitarity, due to universality. This tuning of the scattering length via Feshbach resonances was first demonstrated with bosons in 2000 [31]. However, bosons are unsuitable for

examining the strongly-interacting regime, as three-body losses scale with the increasing strength of the interaction [9, 43, 94, 129]. As mentioned, fermions do not have this problem because three-body collisions are heavily suppressed by the Fermi statistics [104].

An important variation on the atomic gas is the optical lattice, in which the atoms are trapped in a periodic laser potential on top of the harmonic trap common to most ultracold atom experiments [55, 98]. This gives an excellent realisation of the Bose-Hubbard (or Hubbard, for fermions) model, in which bosons are confined to discrete sites, can hop to adjacent sites, and experience a quadratic on-site interaction. These systems exhibit a rich variety of physics: most fundamentally, a phase transition between a superfluid phase and the Mott insulator phase [51, 68], in which each atom is localised to a particular site. Feshbach resonances and other techniques can be applied to create a variety of effects: there have been many proposals for Bose-Hubbard devices to control the movement of atoms and to emulate other quantum systems [13, 68].

Most of the results mentioned thus far are distinctly many-body in nature: BECs and phase transitions are properties of a system of hundreds or thousands of atoms. This research, however, is concerned with few-body systems containing only two or three atoms, which are naturally fundamental to many-body physics. Knowledge of few-body collisions can be used to calculate and understand many-body properties of a system. Cluster or virial expansions [65, 84, 125] allow the system's thermodynamic properties to be expressed as sums of terms depending on few-body collisions of different orders. These expansions have been applied successfully to fermionic systems up to third order [93]. Shina Tan recently derived an entirely different connection between few- and many-body physics. His relations describe the many-body properties in terms of a universal parameter that depends only on two-body physics [116–118].

In addition to their utility in describing many-body behaviour, few-body systems exhibit their own rich physics. One of the most striking examples is the Efimov state, in which three particles that do not form two-body bound states can form a bound trimer state [40]. In fact, an infinite series of such states can (in principle) form, related by geometric scaling laws. The signatures of these states have been recently observed in ultracold gas experiments [8, 10, 58, 59, 66, 78, 86, 92, 100, 107, 130, 134], despite remaining elusive in nuclear systems in the many

years since Efimov's original work. In the case of fermions, the Efimov effect is suppressed by the centrifugal barrier, but reappears in heteronuclear systems above a critical mass ratio of approximately 13.6 [103]. Other effects of mass imbalances have been explored extensively: Blume and Daily use a stochastic variational approach to observe in detail the onset of non-universal trimer states in trapped mass-imbalanced systems [17, 18]. While the ultracold atom field largely revolves around many-body experiments, some experiments have begun to probe few-body physics directly. Optical lattices with sufficiently weak tunnelling between sites are essentially arrays of ideal few-body systems, and recent experiments have isolated few-fermion systems directly by gradually evaporating a Fermi gas [112].

Since the field's inception, there has been growing interest in ultracold systems with exotic potentials. Many examples have appeared in both theory and experiment, including dipolar interactions [6, 79, 90] and Rydberg molecules [82]. Variations in the confining potential are also of great interest, the optical lattice being the most important example. By heavily tightening the trapping potential in one or two directions, quasi two- and one-dimensional systems can be realised, which have been the subject of much recent research [38, 60, 114]. This can also be achieved within an optical lattice, by weakening the lattice potential in one or two directions, to create an array of one- or two-dimensional systems [54].

Also of interest are direct variations in the confining harmonic potential such as rotating and anisotropic traps [29, 50, 111]. This research is concerned with a similar variation, the *trap-imbalance*, where a heteronuclear system has atoms of different species experiencing confining potentials of different strengths, in addition to having different masses. The trap imbalance has been investigated very little, being a major subject of only one paper [14] to the author's knowledge. As will be seen in Chapter 7, trap imbalances introduce couplings between different angular momentum channels, as well as between the centre of mass and relative coordinates. These new couplings significantly change the physics of the few-body system in a variety of novel ways.

This thesis follows a natural progression through the theory of few-body ultracold scattering problems, culminating in a discussion of the heteronuclear systems that are the focus of this research. In Chapter 2, the scattering theory that underlies the physics of ultracold atoms is described. This leads to the definition of the scattering length, and its relation to the important concepts of unitarity and universality.

In Chapter 3, a formulation of the stochastic variational method is given, which is a powerful numerical method for solving few-body problems in atomic as well as nuclear and molecular systems. This method is used to obtain numerical results throughout the thesis. Our implementation explicitly includes the centre of mass motion, and uses solid spherical harmonics as a basis for the angular part of the problem, both of which distinguish it from most implementations. Chapters 4 and 5 review the established analytic results on balanced two- and three-body systems, which are compared directly with results from the numerical methods described in Chapter 3. Chapter 6 comprises an extensive review of the Efimov effect, as well as similar effects leading to non-universal bound states in three-fermion systems.

In Chapter 7, trap-imbalanced two- and three-fermion systems, both with and without mass imbalances, are explored in detail. A series of novel effects resulting from trap imbalances are described. The ability of trap imbalances to lift structural and energetic degeneracies is shown, arising from anisotropic terms introduced into the Jacobi coordinate form of the Hamiltonian. The effect of trap imbalances on the formation of deeply-bound non-universal trimers above the critical mass ratio is investigated. Structural variations induced by the imbalance are described; particularly, it is shown that trap imbalances can modify the simple atom-dimer physics of three-fermion systems to produce loosely-bound trimer states in which all three fermions overlap significantly. Finally, combinations of mass and trap imbalances are explored. These lead to interesting ground state degeneracies and structural variations not seen in any balanced system.

Chapter 2

Scattering Theory

2.1 Introduction

The great attraction of ultracold quantum gases is the simplicity and controllability of the atomic interactions which determine the system's state. In this Chapter, elementary scattering theory is used to show that these interactions can be described by a single parameter, the scattering length a_s. In particular, when a_s is much greater than any other length scale, the unitary regime is reached, where a_s is the only parameter that influences the atomic interactions. Importantly, the physics becomes independent of the short-range form of the interaction potential, a phenomenon known as universality. Finally, it is detailed how, experimentally, the scattering length can be tuned to any desired value using Feshbach resonances.

Physically, the interaction is well-modelled by a Van der Waals potential of the form V_0/r^6. At unitarity, this can be substituted for more convenient potentials, provided they share the same scattering length. In this work, Gaussian potentials of the form $V_0 e^{-r^2/2r_0^2}$, and zero-range delta-function pseudopotentials of the form $V_0\delta(\mathbf{r})\partial_r r$ are used in all cases. The Gaussian potential will be of great use in numerical simulations, while the pseudopotential will be useful for theoretical calculations. The primary purpose of this Chapter is therefore to define and understand the scattering length a_s, and to find relations between V_0 and a_s for these potentials, which will allow their direct substitution in the unitary regime. This requires two assumptions about the quantum gas. Firstly, it must be dilute, meaning that the interatomic spacing is much larger than the range of the interaction potential.

This means that three-body and higher collisions can be neglected. Secondly, the collision energies must be small, which follows from the very low temperature of the gas. As discussed in Chapter 1, these assumptions have been shown to be satisfiable in a variety of experimental scenarios.

2.2 Fundamentals of Scattering Theory

A general single-particle scattering system can be formulated as follows: a single particle with state $|\psi\rangle$ is scattered by some arbitrary potential (of finite extent) $V(\mathbf{r})$, and is hence subject to the Hamiltonian $H = H_0 + V$, where $H_0 = \frac{\mathbf{p}^2}{2m}$ is the kinetic energy. The general time-independent problem is to find solutions to the Schrödinger equation:

$$(H_0 + V)|\psi\rangle = E|\psi\rangle. \tag{2.1}$$

Since the space is continuous, it is required that as $V \to 0$, any solution $|\psi\rangle$ should reduce to a solution of the free-particle Schrödinger equation. This limiting free-particle solution is taken to be a plane-wave of the form $e^{i\mathbf{k}\cdot\mathbf{x}}$, for some momentum $\mathbf{k}$, where $\mathbf{x}$ are the particle's Cartesian coordinates, with $\mathbf{r}$ being the corresponding spherical coordinates. This can be identified as the *incoming wave*, i.e. the state of the particle as it approaches the scattering potential. It is assumed that the interaction has some effective range r_0 such that $V \approx 0$ for $r \gg r_0$, while the solutions of Eq. (2.1) vary over length scales much larger than r_0 i.e. the interaction is *short-range*, compared to the size of the system. In this case, the solution is well-described as the incoming plane wave, plus a scattered spherical wave with the same total momentum k, the amplitude of which of which depends on $\mathbf{k}$ and the scattering angle θ [109]:

$$\langle \mathbf{x}|\psi\rangle \approx \frac{1}{(2\pi)^{3/2}}\left[e^{i\mathbf{k}\cdot\mathbf{x}} + f(\mathbf{k},\theta)e^{ikr}/r\right], \tag{2.2}$$

where $f(\mathbf{k},\theta)$ is the scattering amplitude, which contains all the information about the scattering process. One can also define the problem in terms of an incoming spherical wave and an outgoing plane wave. However, the boundary conditions of this definition are not applicable to this situation, so for simplicity only the case of an outgoing spherical wave is considered. The differential cross-section is related to the scattering amplitude as:

$$\frac{d\sigma}{d\Omega} = |f(\mathbf{k},\theta)|^2, \tag{2.3}$$

where $\mathrm{d}\Omega$ is a differential of the solid scattering angle, and $\mathrm{d}\sigma$ is the corresponding area of the scatterer that produces scattering through $\mathrm{d}\Omega$. The total cross-section $\sigma_{\text{total}} = \int \frac{\mathrm{d}\sigma}{\mathrm{d}\Omega}\mathrm{d}\Omega$ represents the effective geometric area of the scattering potential; the larger σ_{total}, the greater the total amount of scattering, with 100% of incident particles being scattered as $\sigma_{\text{total}} \to \infty$. The method of partial-waves gives an expansion of the scattering amplitude in terms of polynomials of the angle θ:

$$f(\mathbf{k}, \theta) = \sum_l (2l + 1) P_l(\cos\theta) f_l(k), \tag{2.4}$$

where P_l is a Legendre polynomial [2], and $f_l(k)$ is called the partial-wave amplitude. Using Eqs. (2.4) and (2.2), a new expression is obtained for the large-r behaviour of the wavefunction:

$$\langle \mathbf{x}|\psi\rangle \approx \frac{1}{(2\pi)^{3/2}} \sum_l (2l + 1) \frac{P_l(\cos\theta)}{2ik} \left[(1 + 2ikf_l(k)) \frac{e^{ikr}}{r} - \frac{e^{-i(kr - l\pi)}}{r} \right]. \tag{2.5}$$

This form partially illuminates the physics of the scattering process. In the absence of the scatterer ($f_l(k) = 0$), there is only the initial plane wave, which has been re-expressed as a sum over l of outgoing spherical waves e^{ikr}/r and incoming spherical waves $-e^{-i(kr-l\pi)}/r$. The effect of the scatterer is to multiply the coefficients of the outgoing waves by $S_l(k) \equiv 1 + 2ikf_l(k)$, while leaving the incoming wave entirely unaffected.

2.2.1 Phase Shifts

Probability conservation requires that the outgoing flux equals the incoming flux. Combined with conservation of angular momentum, this implies that the coefficient of each outgoing partial wave in Eq. (2.5) must equal the coefficient of the corresponding incoming wave, i.e. $|S_l(k)| = 1$. Thus the important result is reached that the only influence of a scattering potential on the wavefunction at large r is a phase shift of δ_l, where $S_l(k) = e^{2i\delta_l}$. More can be deduced about the scattering process by examining this phase shift. First, the scattering amplitude is rewritten in terms of δ_l:

$$f_l(k) = \frac{e^{2i\delta_l} - 1}{2ik} = \frac{1}{k\cot\delta_l - ik}. \tag{2.6}$$

The next step is determining the phase shift for some potential $V(\mathbf{x})$ which vanishes for $r > R$. In the region outside the potential ($r > R$), the wavefunction must satisfy

the free Schrödinger equation. As such, the wavefunction is expanded in a basis of spherical waves [109]:

$$\langle \mathbf{x}|\psi\rangle \approx \frac{1}{(2\pi)^{3/2}} \sum_l i^l (2l+1) A_l(r) P_l(\cos\theta), \tag{2.7}$$

where the radial wavefunction $A_l(r) = c_l^{(1)} h_l^{(1)}(kr) + c_l^{(2)} h_l^{(2)}$, and $h_l^{(1)}$ and $h_l^{(2)}$ are spherical Hankel functions, related to the spherical Bessel functions j_l and n_l by [2]

$$h_l^{(1)} = j_l + i n_l \quad \text{and} \quad h_l^{(2)} = j_l - i n_l. \tag{2.8}$$

Equation (2.7) must match Eq. (2.5) in the large-r limit. Examining the large-r behaviour of the Hankel functions [2], this allows the coefficients in $A_l(r)$ to be determined as:

$$c_l^{(1)} = \frac{1}{2} e^{2i\delta_l} \quad \text{and} \quad c_l^{(2)} = \frac{1}{2}. \tag{2.9}$$

The radial wavefunction for $r > R$ can now be rewritten as

$$A_l(r) = e^{i\delta_l} \left[\cos\delta_l j_l(kr) - \sin\delta_l n_l(kr)\right]. \tag{2.10}$$

As the only free parameter remaining is the phase shift δ_l, only one additional physical constraint must be applied to the radial wavefunction to determine δ_l. Naturally, this must come from the form of the potential $V(\mathbf{x})$, which has not thus far been used in this derivation. Specifically, the logarithmic derivative of $A_l(r)$ at $r = R$ is matched with that of the wavefunction for $r < R$. The logarithmic derivative of A_l can be written as

$$\begin{aligned} \beta_l &\equiv \left(\frac{r}{A_l}\frac{dA_l}{dr}\right)_{r=R} \\ &= kR\left[\frac{j_l'(kR)\cos\delta_l - n_l'(kR)\sin\delta_l}{j_l(kR)\cos\delta_l - n_l(kR)\sin\delta_l}\right]. \end{aligned} \tag{2.11}$$

This can be inverted to express the phase shift in terms of β_l:

$$\tan\delta_l = \frac{kRj_l'(kR) - \beta_l j_l(kR)}{kRn_l'(kR) - \beta_l n_l(kR)}. \tag{2.12}$$

All that remains is to determine β_l from the inner ($r < R$) wavefunction. A spherically symmetric potential is assumed, so the following radial Schrödinger equation applies to the radial component $u_l(r) = rA_l(r)$ of the inner wavefunction:

$$\frac{d^2u_l}{dr^2} + \left(k^2 - \frac{2m}{\hbar}V - \frac{l(l+1)}{r^2}\right)u_l = 0, \tag{2.13}$$

where u_l is subject to the boundary condition $u_l|_{r=0} = 0$. Generally, this differential equation is integrated numerically from $r = 0$ to $r = R$ to determine β_l and hence δ_l. In the case of a potential that is technically infinite in extent, such as the Gaussian interaction $V = V_0 e^{-r^2/2r_0^2}$, one needs to choose a value of R that is considerably greater than the effective range of the potential, to satisfy the assumption that $V = 0$ for $r > R$ to a good approximation.

2.2.2 The Scattering Length

From the preceding theory, the phase shift δ_l can be determined for a large class of spherically symmetric potentials. The final step is to determine the scattering length, which is defined in terms of the momentum and the phase shift of the $l = 0$ channel by the following expansion:

$$k \cot \delta(k) = -\left(\frac{1}{a_s}\right) + O(k^2), \tag{2.14}$$

where a_s is the scattering length. Higher order terms in the expansion are referred to as range-dependent or energy-dependent, and by definition disappear in the low-momentum limit. The scattering length can hence be written as

$$a_s = -\lim_{k \to 0} \frac{\tan \delta(k)}{k}. \tag{2.15}$$

The scattering length is sufficient to describe the $l = 0$ scattering process in the low-momentum limit, but the possibility of higher-l scattering contributions has not been addressed. Examining Eq. (2.12) at low energy, gives $\delta_l(k) \approx k^{2l+1}$. This implies that only $l = 0$ (s-wave) states contribute to the scattering at low energies, meaning that higher-l contributions can indeed be neglected. This is reflected in the $-l(l+1)/r^2$ term in the radial Schrödinger equation (2.13), which creates an effective repulsive interaction when $l \neq 0$, often referred to as the *centrifugal barrier* term.

Thus it has been determined that under the assumptions of low energy and short interaction range, the entire scattering process is governed by the scattering length a_s. For a given potential, a_s can be readily determined from Eqs. (2.12) and (2.15), by appropriately integrating the radial Schrödinger equation (2.13) to determine the logarithmic derivative β_l. Thus the value of V_0 that gives the unitary regime

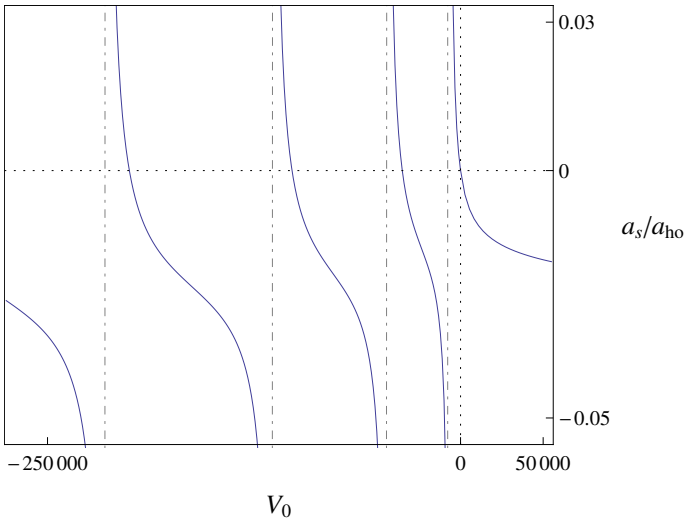

Figure 2.1: Scattering length a_s as a function of the interaction strength V_0 for a Gaussian potential $V_0 e^{-r^2/2r_0^2}$ with $r_0 = 0.01 a_{\mathrm{ho}}$, demonstrating the cyclic repetition of all possible values of a_s.

can be found for an arbitrary spherical interaction potential by, for example, numerically finding roots of the equation $[a_s(V_0)]^{-1} = 0$. This process typically takes less than a second and easily reaches scattering lengths upwards of 10^8 oscillator lengths, sufficient to provide a numerically adequate approximation of unitarity. In fact, any desired scattering length b can be achieved by solving $[a_s(V_0)]^{-1} = 1/b$. Throughout the numerical sections of this work, this method is used to achieve unitarity and other desired scattering lengths.

2.2.3 The Physics of the Scattering Length

In the above theory, the scattering length is introduced as an abstract quantity with no clear link to the physics of the system. One naturally asks why it is called the scattering length, and particularly to what physical length it refers. Most importantly, the scattering length can be related to the total cross-section as [109]

$$\sigma_{\mathrm{total}} = 4\pi a_s^2. \tag{2.16}$$

In other words, a_s is the effective geometric width of the scattering potential at low energies, as seen by the incident particle. The larger a_s is, the more likely the particle is to be scattered. Note that a_s is not in most cases geometrically related

to the physical width of the scattering potential. For instance, a Gaussian potential of a given width r_0 can result in any value of a_s given the right coefficient V_0. In fact, when sweeping through a large range of V_0 values, a_s will cyclically take all possible values, as shown in Fig. 2.1. This is because scattering is determined by the accumulation of the phase shift δ_l; phase is accumulated cyclically, resulting in this cyclic behaviour of a_s as $|V_0|$ is increased. Further insight into the physics of the scattering length can be gained by examining Eq. (2.10) to determine the behaviour of the outer ($r > R$) radial wavefunction in the low-k limit:

$$\begin{aligned} \lim_{k\to 0} u_0(r) &= \lim_{k\to 0} rA_l(r) = \lim_{k\to 0} e^{i\delta}[\cos(\delta_l) j_l(kr) - \sin(\delta_l) n_l(kr)] \\ &= c_1(r - a_s), \end{aligned} \tag{2.17}$$

for some constant c_1. In this limit, the outer radial wavefunction is a line that crosses zero at $r = a_s$, giving a simple geometric meaning to the scattering length, as demonstrated in Fig. 2.2. Alternatively, this can be inferred by noting that if $k = 0$, u obeys $\mathrm{d}^2u/\mathrm{d}r^2 = 0$, defining a straight line. Physically, this is interpreted as the limit where the wavelength becomes infinitely long, removing the usual oscillatory behaviour from the outside wavefunction. This r-intercept may occur in the region $r < R$, in which case it is not a zero of the actual wavefunction, but only of the outer wavefunction when extrapolated into the region described by the inner wavefunction. For large positive scattering lengths $a_s \gg R$, however, it will correspond to an actual zero of the wavefunction, as in Fig. 2.2(c).

In the second case, a relation can be deduced between the scattering length and the energy of a shallow $E \approx 0$ bound state. For a_s large and positive, Eq. (2.17) is equal to $c_2 e^{-\kappa r}$ for some constants c_2 and $\kappa \approx 0$, which is a bound state wavefunction with E very small and negative ($E = 0^-$). A relation can be found between κ and a_s by equating the logarithmic derivatives of the two cases at $r = R$ (the two cases being $\psi \approx c_2 e^{-\kappa r}$ for $E = 0^-$ and $\psi \approx c_1(r - a_s)$ for $E = 0$), giving

$$-\left.\frac{\kappa e^{-\kappa r}}{e^{-\kappa r}}\right|_{r=R} = \left.\left(\frac{1}{r - a_s}\right)\right|_{r=R}, \tag{2.18}$$

which, if $R \ll a_s$, determines $\kappa = \frac{1}{a_s}$ and

$$E_{\text{bound state}} = -\frac{\hbar^2\kappa^2}{2m} = -\frac{\hbar^2}{2ma_s^2}. \tag{2.19}$$

Experimentally, this means that the energy of a loosely bound state can be determined by performing simple scattering experiments, which determine a_s from the total cross section in Eq. (2.16).

2.2.4 Zero-Range Interactions

A zero-range interaction of the form $V_0\delta(\mathbf{r})\partial_r r$ is of great utility in theoretical treatments of scattering systems. Therefore, it is useful to apply the above theory of low-energy scattering to relate V_0 in the zero-range case to the scattering length a_s. When two interacting particles get very close together, and the interaction range $r_0 \to 0$, the scattered wavefunction must have the "long range" behaviour everywhere, i.e. Eq. (2.10) describes the wavefunction at all points. Examining the low-r limit, this gives

$$\lim_{r\to 0}\psi = A\left(\frac{1}{r} - \frac{1}{a_s}\right), \tag{2.20}$$

where A depends on the other coordinates of the system. This can be rewritten as

$$\lim_{r\to 0}\frac{\partial(r\psi)}{\partial r} = -\frac{r\psi}{a_s}, \tag{2.21}$$

which is known as the Bethe-Peierls boundary condition [11]. This is equivalent to a delta-function pseudopotential [24],

$$V_{\text{zero range}}(r) = \frac{4\pi\hbar^2 a_s}{m}\delta(\mathbf{r})\frac{\partial}{\partial r}r. \tag{2.22}$$

Hence the coefficient V_0 of the zero-range interaction that corresponds to a given scattering length has been determined, as was done for the Gaussian interaction in the previous subsections. The goal of being able to use these two potentials interchangeably in the low-energy unitary ($a_s \to \infty$) limit has now been achieved, since in this limit the short-range form of the potential is inconsequential, and the coefficient of either potential which corresponds to a desired scattering length can be found. Note that this does not involve taking the $a_s \to \infty$ limit of the above potential. Rather, a_s is left as a finite quantity during the calculation, and the unitary limit is taken as appropriate to interpret the results.

2.2.5 Feshbach Resonances and the Two-Channel Model

The above low-energy scattering theory is an accurate description of two-body scattering in a dilute ultracold quantum gas, provided the scattering length a_s is

known. However, it is useful to understand how a_s can be related to the experimental parameters of an ultracold gas system. In fact, understanding this relationship will reveal an important and appealing property of these systems: the experimental tunability of a_s. To do this, a more complicated two-channel model involving Fano-Feshbach resonances must be considered [26, 67]. This model includes the hyperfine splitting of the atoms, allowing scattering to occur in two channels: the open (triplet) and closed (singlet) channels, differentiated physically by the configurations of the outer electrons of the atom. These two channels each behave individually as a scattering process of the type discussed throughout this Chapter. However, the scattered atom now has access to the states of both channels, and may be in an arbitrary superposition of those states.

It is now assumed that the incident atom has energy E, which lies between the energies of the lowest state in each scattering channel: E_{open} and E_{closed}, and that the open channel supports a continuum state, while the closed channel supports a bound state, which is inaccessible since $E < E_{\text{closed}}$. However, if the energy of the channels is gradually modified so that $E_{\text{closed}} \to E_{\text{open}}$, the closed channel state becomes accessible and begins to affect the scattering process. Physically, this can be thought of as the incident atom hitting the two-channel potential, then entering a long-lived state with a large component of the closed channel bound state, which eventually decays back to the open channel state, resulting in the incident atom being ejected. This process causes the incident atom to accumulate additional phase, modifying δ and thus affecting the scattering process. This phenomenon is known as a Fano-Feshbach resonance, which originated in atomic and nuclear physics [45, 49].

This tuning of E_{open} and E_{closed} is commonly achieved by exploiting the different magnetic moments of the two states, which are assumed to differ by $\Delta\mu$. The states are then tunable via an external magnetic field B, which causes a Zeeman shift in the energy difference between the states of $\Delta\mu B$. By smoothly varying B, an experimentalist can sweep across the resonance. A maximal phase shift of π can be achieved in such a sweep, allowing for large modifications to a_s even over a small change in B. The change in the scattering length can be quantified in terms of the non-resonant scattering length a_{nr}, a parameter B_0 describing the location of the resonance (typically determined experimentally), and a parameter ΔB describ-

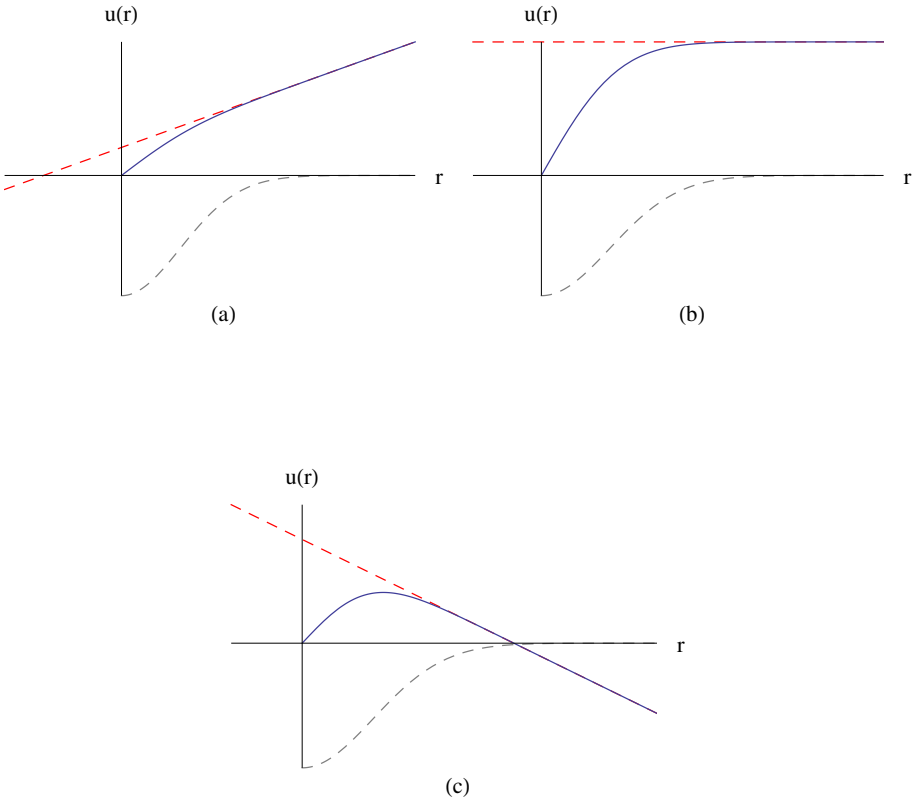

Figure 2.2: Three examples of low-energy scattering processes for Gaussian potentials with different scattering lengths. Blue lines show the radial wavefunction $u(r)$; dotted red lines show the (extrapolated) long-range behaviour of the wavefunction, with the r-intercept being a_s; dotted grey lines show the Gaussian potential, rescaled arbitrarily to fit the graph. Plot (a) shows a negative scattering length, plot (b) an infinite scattering length, and plot (c) a positive scattering length, which must support a bound state as $u(r)$ has a root.

ing the width of the external magnetic field:

$$a_s = a_{\rm nr}\left(1 + \frac{\Delta B}{B - B_0}\right). \tag{2.23}$$

In the above equation, a_s refers to the effective scattering length of the two-channel system, which can now be understood as a single two-body scattering system, of the type presented earlier in the Chapter. Experimentally, any desired value of a_s

can be readily achieved, including the unitary regime $a_s \to \infty$ [67]. This tunability is one of the great advantages of the ultracold gas system, for the obvious reason that it allows the exploration of many different physical regimes (as parametrised by a_s) within a single system, the unitary regime being of particular interest.

2.2.6 Conclusion

Using the assumptions of diluteness and low collision energy, it has been deduced that the interactions within an ultracold quantum gas can be described in terms of a single parameter a_s, known as the scattering length. Particularly, as $a_s \to \infty$, the short-range form of the interaction potential becomes irrelevant, allowing different potentials to be used interchangeably at unitarity. To facilitate this, it has been how to compute the scattering length for a large class of spherically symmetric potentials. Finally, it has been discussed how a_s can be tuned experimentally via Feshbach resonances, allowing (amongst other things) the unitary regime to be achieved.

Chapter 3

Numerical Methods

3.1 Introduction

Beyond a handful of simple cases, few-body systems are unsolvable analytically, and numerical methods must be used. The stochastic variational approach has broad applicability and proven effectiveness in dealing with systems of this class. The essential idea of this approach is to approximate the unknown wavefunction by some other function containing free parameters (the "trial" wavefunction), usually chosen for its analytical and/or numerical tractability. The system's Hamiltonian is then applied to this function, allowing an approximation of the system's energy to be found. In a numerical variational approach, the power of a computer allows the use of a trial function containing a very large number of free parameters, and potentially allows stochastic variation of these parameters. In this Chapter, the theory and principles of the variational approach are introduced. A choice of basis functions, which is the fundamental choice in formulating a variational method, is then described and justified.

There are many variations of the stochastic variational method. Ours is largely derived from the excellent textbook by Suzuki and Varga [115], which describes most aspects of the implementation, including the use of solid spherical harmonics as basis functions (which remains relatively uncommon, as a global angular momentum vector approach, also described in the textbook, is often more straightforward). The key extensions in our implementation are the inclusion of the centre of mass motion, and the computation of various integrals of the trap-imbalanced

Hamiltonian, which are somewhat more difficult than the standard case. These integrals are included in the Appendix.

3.2 Fundamentals of the Method

The general system of interest is some quantum system described by a Hamiltonian H, containing N particles, with particle i having coordinates $\mathbf{r}_i$, and the vector $\vec{x} = (\mathbf{r}_1, \cdots, \mathbf{r}_2)$ containing all the system's coordinates. The system has unknown energy eigenstates $|\psi_i(\vec{x})\rangle$ with eigenvalues E_i. The trial wavefunction $|\Phi(\vec{x})\rangle$ is then defined as some linear combination of a set of n basis functions $\{|\phi_i(\vec{x})\rangle\}$:

$$|\Phi\rangle = \sum_{1}^{n} c_i |\phi_i\rangle. \tag{3.1}$$

The basis functions may have any arbitrary dependence on the system's coordinates, provided they satisfy the axioms of the Hilbert space. The energy of this state can immediately be computed from the system's Hamiltonian as $\epsilon = \langle\Phi|H|\Phi\rangle/\langle\Phi|\Phi\rangle$. This finite set of basis functions is not a basis of the full Hilbert space, but rather a basis of some subspace, which is referred to as the reduced space. The idea is that for appropriate choices of the basis functions, the trial wavefunction can be made to serve as a good approximation of one of the system's true energy eigenstates. In other words, one seeks to define some finitely-generated and numerically tractable subspace of the full incomputable Hilbert space, such that this subspace contains a very good approximation of some eigenstates in the full Hilbert space. However, there is *a priori* no reason to believe that this will work. The essential problem is that the system's true eigenvalues are not known in advance, so there is no way to test the quality of the approximation. The solution comes from the fact that the ground state $|\psi_1\rangle$ is in fact the only function in the Hilbert space which minimises the system's energy, as per the variational principle (ignoring the possibility of degeneracy). This means that, since the trial wavefunction is still in the Hilbert space, its energy will necessarily be higher than that of the true ground state, a result known as the Ritz theorem:

$$\epsilon \equiv \frac{\langle\Phi|H|\Phi\rangle}{\langle\Phi|\Phi\rangle} \geq E_1, \tag{3.2}$$

where ϵ is the trial wavefunction's energy expectation value. In fact, the above statement is true of any function in the Hilbert space, regardless of its status as

a trial wavefunction, which makes sense since the only essential requirement on the trial wavefunction thus far is that it be in the Hilbert space. The Ritz theorem indicates that one can keep trying different trial wavefunctions, and will always compute an energy that is greater than or equal to the true ground state energy. Therefore, if one tries a sufficiently varied set of functions, a good approximation of the true energy will be found, as the trial function that gives the lowest energy can safely be identified as the best choice.

This idea can be made less haphazard by restricting ourselves to a particular set of trial wavefunctions, related in their dependence on some free parameter(s). A simple (and useful) example is Gaussians of varying width. If the system has only a single coordinate r, Gaussians of the form $e^{-\frac{r^2}{w^2}}$ can be tried with many different widths w. Then, the one giving the lowest value of ϵ can be selected, since of all the trial Gaussians, this will be the closest to the system's ground state. However, this will be near the right answer if the true ground state happens to be a Gaussian or similar function. One could try functions of other forms, but there is no guarantee that one will stumble on a functional form that adequately resembles the ground state (in fact, one almost certainly will not). This issue can be avoided by using a trial wavefunction of the form of Eq. (3.1), in this case taking the basis functions $|\phi_i\rangle$ as Gaussians of various widths i.e.

$$|\Phi(r)\rangle = \sum_{1}^{n} c_i e^{-\frac{r^2}{w_i^2}}, \tag{3.3}$$

for some expansion coefficients c_i. By changing the expansion coefficients, this trial function has considerable flexibility to mimic any functional form in the ground state $|\psi_1(r)\rangle$, provided the set of basis Gaussians is sufficiently large, and provided the variation occurs on a length scale encapsulated by the set of Gaussians. In fact, the infinite set of all Gaussians of this form is a formal basis for the entire Hilbert space of functions in r. Therefore, if the set of basis functions is continually made larger, a basis of the full Hilbert space is approached, which must give an exact representation of the true ground state with the appropriate expansion coefficients. This process is directly analogous to approximating a periodic function with a finite truncation of its Fourier series.

Thus it can reasonably be expected that if a trial wavefunction which is a sum of a large number of Gaussians is used, one will arrive at a good approximation

of the true wavefunction. The only remaining concern is the determination of the optimal expansion coefficients c_i. To do this, an eigenvalue problem must be solved on the subspace defined by the set of basis states. To construct this, the generalised Ritz theorem is required, which states that the energy is stationary in perturbations of the wavefunction only at the energy eigenstates. A proof of this theorem begins with the expression for the energy of an arbitrary state in the subspace, $E\langle\Psi|\Psi\rangle = \langle\Psi|H|\Psi\rangle$, which is then perturbed by changing $\Psi \to \Psi + \delta\Psi$, giving an expression for δE:

$$\begin{aligned} \langle\Psi|\Psi\rangle\delta E &= \delta(\langle\Psi|H|\Psi\rangle) - E\delta\langle\Psi|\Psi\rangle) \\ &= \langle\delta\Psi|H - E|\Psi\rangle + \langle\Psi|H - E|\delta\Psi\rangle. \end{aligned} \tag{3.4}$$

Letting $\delta\Psi = \eta(H - E)\Psi$, with η some small real number, the above reduces to $2\eta\langle(H - E)\Psi|(H - E)\Psi\rangle = \langle\Psi|\Psi\rangle$. Thus if $\delta E = 0$, the function $(H - E)\Psi$ is zero, giving an eigenstate. Reversing the implication, if $(H - E)\Psi = 0$, then the right hand side is zero and $\delta E = 0$. Therefore Ψ is an eigenstate if and only if $\delta E = 0$ i.e. eigenstates are precisely the functions with stationary expectation values of the Hamiltonian.

The expansion coefficients c_i must be optimised by defining an energy eigenvalue problem on the reduced Hilbert space. The generalised Ritz theorem still holds within this subspace. Since an arbitrary state in the subspace can be expressed as $\Phi = \sum_{i=1}^{n} c_i\phi$, an arbitrary perturbation of the state can be expressed as a perturbation in the expansion coefficients c_i. Therefore subspace eigenstates can be found by setting $\delta E/\delta c_i = 0$ for all i i.e.

$$\begin{aligned} 0 &= \frac{\delta E}{\delta c_i} \\ &= \frac{\delta}{\delta c_i}\left[\frac{\langle\Phi|H|\Phi\rangle}{\langle\Phi|\Phi\rangle}\right] \\ &= \frac{\delta}{\delta c_i}\left[\frac{\sum_{k,l} c_k c_l H_{kl}}{\sum_{k,l} c_k c_l S_{kl}}\right] \\ &= \frac{\sum_l c_l H_{il} + \sum_k c_k H_{ki}}{\sum_{k,l} c_k c_l S_{kl}} - \frac{\left(\sum_{k,l} c_k c_l H_{kl}\right)\left(\sum_l c_l S_{il} + \sum_k c_k S_{ki}\right)}{\left[\sum_{k,l} c_k c_l S_{kl}\right]^2} \\ \therefore \quad 0 &= \sum_k (c_i H_{ik} - E c_i S_{ik}), \end{aligned} \tag{3.5}$$

where overlap and Hamiltonian matrix elements are defined as

$$S_{ij} = \langle \phi_i | \phi_j \rangle \tag{3.6}$$

and

$$H_{ij} = \langle \phi_i | H | \phi_j \rangle. \tag{3.7}$$

Later, analytic expressions for these elements will be determined, as their rapid computation is essential to the efficient use of these methods. Equation (3.5) applies for any δc_i, and is the natural equivalent of the energy eigenvalue problem in the subspace defined by the set of basis vectors, in that it defines eigenstates that satisfy the generalised Ritz theorem within the subspace. This can be written more concisely as a generalised eigenvalue problem for two matrices $\mathbf{H}$ and $\mathbf{S}$ with elements H_{ij} and S_{ij}:

$$\mathbf{Hc} = \epsilon \mathbf{Sc}, \tag{3.8}$$

where ϵ is an eigenvalue and $\mathbf{c}$ an eigenvector. As $\mathbf{H}$ and $\mathbf{S}$ are $n \times n$ matrices, this generalised eigenvalue problem yields n eigenvalues. Extending the concept of the original formulation of the Ritz theorem, the mini-max theorem states that these n trial eigenvalues provide upper bounds on the first n true eigenvalues of the system.

3.3 Coordinate Choice

In the case of a quantum mechanical N-body problem, there are generally $3N$ spatial coordinates in the Hamiltonian, and so one expects that $3N$-dimensional trial functions will be required. However, the problem becomes more numerically tractable if the system is first transformed to Jacobi coordinates, which are a generalisation of the familiar relative and centre of mass coordinates. The most important simplification this provides is allowing one of the coordinates to be the interparticle distance $r = |\mathbf{r}_1 - \mathbf{r}_2|$, which allows a simple expression for the matrix element to be found when two-body interactions are included. Throughout this thesis, the following general coordinate transformation will be used for an arbitrary

number of particles N with masses m_i:

$$U = \begin{pmatrix} 1 & -1 & 0 & \cdots & 0 \\ \frac{m_1}{m_{12}} & \frac{m_2}{m_{12}} & -1 & \cdots & 0 \\ \vdots & \vdots & & & \vdots \\ \frac{m_1}{m_{12\cdots N-1}} & \frac{m_2}{m_{12\cdots N-1}} & \cdots & \cdots & -1 \\ \frac{m_1}{m_{12\cdots N}} & \frac{m_2}{m_{12\cdots N}} & \cdots & \cdots & \frac{m_N}{m_{12\cdots N}} \end{pmatrix}, \tag{3.9}$$

where $m_{12\cdots N} = m_1 + \cdots + m_N$. In the two- and three-particle cases, this reduces respectively to

$$U = \begin{pmatrix} 1 & -1 \\ \frac{m_1}{m_1+m_2} & \frac{m_2}{m_1+m_2} \end{pmatrix} \tag{3.10}$$

and

$$U = \begin{pmatrix} 1 & -1 & 0 \\ \frac{m_1}{m_1+m_2} & \frac{m_2}{m_1+m_2} & -1 \\ \frac{m_1}{m_1+m_2+m_3} & \frac{m_2}{m_1+m_2+m_3} & \frac{m_3}{m_1+m_2+m_3} \end{pmatrix}. \tag{3.11}$$

The first transformed coordinate is generally referred to as $\mathbf{r}$, the second as $\boldsymbol{\rho}$ and the third as $\mathbf{R}$, which is the centre of mass coordinate. In many cases, this transformation decouples the centre of mass from the rest of the Hamiltonian, which effectively reduces the number of coordinates by 3 (also noting that no complications will arise from permutations of particles, since $\mathbf{R}$ is invariant under such permutations). However, in the case of trap-imbalanced systems, non-removable couplings appear in the Hamiltonian between all coordinates, which are discussed in detail in Chapter 7. Therefore, the full set of Jacobi coordinates will always be discussed, rather than ignoring the centre of mass, as would be appropriate in many contexts. It will be convenient to work in spherical coordinates, meaning that each coordinate vector (such as $\mathbf{r}$, $\boldsymbol{\rho}$ or $\mathbf{R}$) is expressed as a radial coordinate and two angles, for instance $\boldsymbol{\rho} = (\rho, \theta_\rho, \phi_\rho)$.

These transformations generally give a Hamiltonian with the kinetic and trapping terms similar to the untransformed Hamiltonian, but potentially with dot product terms of the form $\mathbf{r}\cdot\boldsymbol{\rho}$, $\nabla_{\mathbf{r}}\cdot\nabla_{\boldsymbol{\rho}}$, etc. In most cases, these dot product terms do not appear (i.e. their coefficients are zero), but in the case of trap imbalanced systems,

dot product terms between all coordinates in the transformed trapping Hamiltonian will be encountered. Generally, for a system of N particles with masses m_i and trapping frequencies ω_i, and an arbitrary coordinate transformation with elements U_{ij}, the coefficients of the various transformed kinetic and trapping terms are given respectively by

$$\Lambda_{ij} = \sum_{k=1}^{N} \frac{1}{m_k} U_{ik} U_{jk} \tag{3.12}$$

and

$$\Omega_{ij} = \sum_{k=1}^{N} m_k \omega_k^2 U_{ki}^{-1} U_{kj}^{-1}. \tag{3.13}$$

3.4 Radial Basis Functions: Gaussians

To proceed with the variational method, an appropriate set of basis functions is needed. These functions must:

1. Provide the required variation at appropriate length scales, as discussed above
2. Allow for efficient computation of the elements of **H** and **S**.

For the radial coordinates, a basis of Gaussians of the form $e^{-\frac{r^2}{w^2}}$, where w is the width of the Gaussian, has been shown to provide excellent convergence in many few-body systems [91], suggesting that it will fulfil the first criterion. As will be seen, Gaussians also permit the derivation of analytic expressions of all the terms of the trap-imbalanced system's Hamiltonian, removing any need for numerical integration and fulfilling the second criterion.

3.5 Angular Basis Functions: Spherical Harmonics

Gaussians are not appropriate for the angular coordinates e.g. θ_ρ and ϕ_ρ, since they do not satisfy periodic boundary conditions. A set of functions that satisfy the same criteria of convergence and ease of integrability, while also being periodic, is needed. Solid spherical harmonics are the natural choice. In order to allow coupling to the system's physical angular momenta, coupled spherical harmonics

are used, rather than simply using arbitrary spherical harmonics in each coordinate. For two particles, these functions are quite simple: a basis function is defined by its angular momentum in the two coordinates, coupled to the system's total angular momentum (L, M):

$$\begin{aligned} |l_r, l_R\rangle &= [\mathcal{Y}_{l_r} \times \mathcal{Y}_{l_R}]_{LM} \\ &= \sum_{m_r m_R} \langle l_r m_r l_R m_R | LM \rangle \mathcal{Y}_{l_r m_r}(\hat{\mathbf{r}}) \mathcal{Y}_{l_R m_R}(\hat{\mathbf{R}}), \end{aligned} \tag{3.14}$$

where $\langle l_1 m_1 l_2 m_2 | LM \rangle$ is a Clebsch-Gordan coefficient, $\mathcal{Y}_{lm}(\hat{\mathbf{r}}) = r^l \mathrm{Y}^l_m(\hat{\mathbf{r}})$ is a solid spherical harmonic, and Y^l_m is the standard spherical harmonic. With three particles, the coupling becomes more complicated, and an intermediate coupling angular momentum l_{coup} is required to fully describe the system:

$$\begin{aligned} |l_r, l_\rho, l_{\text{coup}}, l_R\rangle &= \left[\left[\mathcal{Y}_{l_r} \times \mathcal{Y}_{l_\rho} \right]_{l_{\text{coup}}} \times \mathcal{Y}_{l_R} \right]_{LM} \\ &= \sum_{m_r,\, m_\rho,\, m_{\text{coup}},\, m_R} \langle l_r m_r l_\rho m_\rho | l_{\text{coup}} m_{\text{coup}} \rangle \\ &\qquad \times \langle l_{\text{coup}} m_{\text{coup}} l_R m_R | LM \rangle \\ &\qquad \times \mathcal{Y}^{l_r}_{m_r}(\hat{\mathbf{r}}) \mathcal{Y}^{l_\rho}_{m_\rho}(\hat{\boldsymbol{\rho}}) \mathcal{Y}^{l_R}_{m_R}(\hat{\mathbf{R}}). \end{aligned} \tag{3.15}$$

Generalisations to higher numbers of coordinates are possible, but the matrix elements would become prohibitively complicated. Suzuki and Varga [115] detail another approach using a so-called global angular momentum vector, which has better scalability. These explicitly coupled states were chosen as they allow a more immediate understanding of how the system's behaviour relates to the physical angular momenta, since one can specify precisely which angular momentum states will make up the basis. This is useful given the non-trivial angular structure of the trap-imbalanced Hamiltonian.

3.6 Definition of an Arbitrary Basis State

In this section, the parameters present in an arbitrary basis state in the variational scheme will be precisely enumerated. For generality, additional parameters arising from the application of $\mathcal{P}_{13}$ will be included. In the three-body case, the following parameters are present:

- Three Gaussian widths: a in the coordinate $\mathbf{r}$, b in the coordinate $\boldsymbol{\rho}$ and c in the coordinate $\mathbf{R}$.
- Angular momenta: l_r in the coordinate $\mathbf{r}$, l_ρ in the coordinate $\boldsymbol{\rho}$, l_R in the coordinate $\mathbf{R}$, and a coupling angular momentum l_{coup}.
- Extra even powers of r and ρ defined by the integers n_r and n_ρ, arising from the transformation Eq. (3.26), in the form of a factor $r^{2n_r}\rho^{2n_\rho}$. These are assumed to be zero in an untransformed ket.
- The quantity δ appearing in the factor $e^{-\delta\mathbf{r}\cdot\boldsymbol{\rho}}$, which also only arises from the transformation Eq. (3.26).

Thus an arbitrary basis state can be written in the following form:

$$|\beta\rangle = (a, b, c, \delta, l_r, n_r, l_\rho, n_\rho, l_{\text{coup}}, l_R). \tag{3.16}$$

3.7 Selection of Basis Functions

Thus far, the basis functions have been defined in terms of free parameters such as Gaussian widths and angular momenta, and described how a set of these functions can give an approximate solution to Schrödinger's equation. However, the way in which these parameters will be chosen, such that a good approximation of the system's true energy can be reached, has not yet been described. Generally, convergence to the true eigenvalues requires a variety of basis functions that vary at the same radial length scales as the true eigenfunction, while also including the same angular momentum components.

The Hamiltonian has two important length scales in each radial coordinate: the trapping length, and the interaction length r_0. Initially, I used an approach in which basis functions were generated over these length scales in a simple geometric progression of Gaussian widths, ranging from slightly below r_0 to slightly above the appropriate trapping length for each coordinate. The number of basis functions was then gradually increased, increasing the number of terms in this geometric progression without changing its limits, until adequate convergence was achieved. To demonstrate, if a geometric progression of N Gaussians in a coordinate r is required, ranging from a lower width of w_{lower} to an upper width of w_{upper}, the

following widths w_i would be included:

$$w_i = w_{\text{lower}} * \kappa^i, \tag{3.17}$$

where $\kappa = (w_{\text{upper}}/w_{\text{lower}})^{\frac{1}{N-1}}$. However, this approach has a number of limitations. Most importantly, it requires a restrictively high number of basis functions to achieve convergence in many cases. Furthermore, it is difficult to demonstrate that adequate convergence has been reached, especially as the number of basis functions becomes large and additional simulations expensive. Therefore, I eventually adopted a stochastic approach, in which basis functions are determined randomly, then tested to see which ones are most helpful to achieving convergence.

3.7.1 Random Basis Functions

As per Eq. (3.16), a basis function is determined by its Gaussian widths and angular momenta. Therefore, to generate a new random basis function, random values of these parameters are chosen. The Gaussian widths are generated within predetermined ranges, typically from just below r_0 to just above the trapping length of the corresponding coordinate. To randomise the angular momenta, a list of the angular states allowed by the system's total angular momentum and parity is created, with some upper limit placed on the value of each component. Then, one of these states is selected at random.

Most randomly generated states are unhelpful, in that they have little impact on the system's eigenvalues when added to the basis. Therefore, it is desirable to test each state's contribution before deciding whether to permanently add it to the basis. The obvious way to do this is to simply solve the generalised eigenvalue problem with the newly generated function included, and look at the new eigenvalues. However, this becomes computationally expensive as the basis grows larger, as the eigenvalue routines have scaling of the order N^3. Fortunately, Chapter 3 of Suzuki and Varga describes a more efficient method [115]. Starting with a basis of k functions $\{|\beta_i\rangle\}$, with eigenvalues $\{\epsilon_i\}$ and eigenvectors $\{|\phi_i\rangle\}$, the goal is to determine the effect of a newly generated function $|\beta_{k+1}\rangle$ on the system. To do this efficiently, the eigenvalue problem is re-expressed in a basis containing the first k eigenvectors, and a function $|\phi_{k+1}\rangle$ created from β_{k+1} by removing the components

parallel to each $|\phi_i\rangle$ (the Gram-Schmidt process):

$$|\phi_{k+1}\rangle = \left(\langle\beta_{k+1}|\beta_{k+1}\rangle - \sum_{i=1}^{k} |\langle\phi_i|\beta_{k+1}\rangle|^2\right)^{-\frac{1}{2}} \times\left\{|\beta_{k+1}\rangle - \sum_{i=1}^{k}\langle\phi_i|\beta_{k+1}\rangle\right\}. \tag{3.18}$$

Now, using the basis $\{|\phi_1\rangle, \cdots, |\phi_{k+1}\rangle\}$, the eigenvalue problem becomes:

$$\begin{pmatrix} \epsilon_1 & 0 & \cdots & 0 & h_1 \\ 0 & \epsilon_2 & \cdots & 0 & h_2 \\ \vdots & \vdots & & \vdots & \vdots \\ 0 & 0 & \cdots & \epsilon_k & h_k \\ h_1 & h_2 & \cdots & h_k & h_{k+1} \end{pmatrix} \begin{pmatrix} c_1 \\ c_2 \\ \vdots \\ c_k \\ c_{k+1} \end{pmatrix} = E \begin{pmatrix} c_1 \\ c_2 \\ \vdots \\ c_k \\ c_{k+1} \end{pmatrix}, \tag{3.19}$$

where $h_i = \langle\phi_i|H|\phi_{k+1}\rangle$, E is an eigenvalue, and $\{c_i\}$ are the undetermined coefficients of the new eigenvectors. Because of the nearly-diagonal form of the above matrix, the eigenvalues are the roots of the following characteristic equation:

$$0 = \left(\prod_{i=1}^{k}(\epsilon_i - E)\right)\left(h_{k+1} - E - \sum_{j=1}^{k}\frac{|h_j|^2}{\epsilon_j - E}\right). \tag{3.20}$$

For large bases, computing the roots of this equation is much faster than rediagonalising, allowing randomly generated functions to be sampled with minimal computational effort. The following scheme of *competitive selection* is used to determine which sampled functions are permanently added to the basis:

1. Generate n new basis functions, as described above. (Typically n is in the hundreds or thousands.)

2. Determine each function's contribution to the eigenvalues as per Eq. (3.20).

3. Keep the function that produces the lowest eigenvalue, provided its difference from the old eigenvalue is sufficiently large, as determined by some predefined tolerance.

4. If no significant contribution was found, stop. Otherwise, go to step 1.

3.8 Antisymmetrisation

In the three-body case, since particles 1 and 3 are identical fermions, the problem must be antisymmetrised. Instead of computing the matrix elements H_{ij} and S_{ij} as defined above, the antisymmetrisation operator $1 - \mathcal{P}_{13}$ is applied to every state vector:

$$H_{ij} = \langle (1 - \mathcal{P}_{13})\phi_i | \hat{\mathrm{H}} | (1 - \mathcal{P}_{13})\phi_j \rangle. \tag{3.21}$$

This expression can be simplified by noting that $\mathcal{P}_{13}$ trivially commutes with $\hat{\mathrm{H}}$, since particles 1 and 3 necessarily contribute identical terms to the Hamiltonian. Also noting that $\mathcal{P}_{13}^{\dagger} = \mathcal{P}_{13}$, and $\mathcal{P}_{13}^2 = \hat{1}$, Eq. (3.21) can be rewritten as:

$$H_{ij} = 2\langle \phi_i | \hat{\mathrm{H}} | \phi_j \rangle - 2\langle \phi_i | \hat{\mathrm{H}} | \mathcal{P}_{13}\phi_j \rangle. \tag{3.22}$$

A similar expression applies for S_{ij}. An overall factor of 2 can be removed, as it will not affect the generalised eigenvalues of $\mathbf{H}$ and $\mathbf{S}$ as per Eq. (3.8), giving:

$$H_{ij} = \langle \phi_i | \hat{\mathrm{H}} | \phi_j \rangle - \langle \phi_i | \hat{\mathrm{H}} | \mathcal{P}_{13}\phi_j \rangle \tag{3.23}$$

and

$$S_{ij} = \langle \phi_i | \phi_j \rangle - \langle \phi_i | \hat{\mathrm{H}} | \mathcal{P}_{13}\phi_j \rangle. \tag{3.24}$$

3.8.1 Applying $\mathcal{P}_{13}$

To evaluate the above antisymmetrised matrix elements, the action of $\mathcal{P}_{13}$ on an arbitrary state in the basis must be understood. In fact, this permutation is equivalent to a coordinate transformation, since the system is expressed entirely in coordinate-space (i.e. there are no spin couplings or similar complications). This transformation is simple in single-particle coordinates (it just swaps the first and third coordinates), but will need to be expressed in terms of Jacobi coordinates. Therefore, the system is first transformed back to single-particle coordinates, then the permutation is applied, then the system is returned to Jacobi coordinates, giving:

$$\begin{aligned} \mathcal{P}_{13} &= U \begin{pmatrix} 0 & 0 & 1 \\ 0 & 1 & 0 \\ 1 & 0 & 0 \end{pmatrix} U^{-1} \\ &= \begin{pmatrix} \frac{m_1}{m_1+m_2} & -1 & 0 \\ -\frac{m_2(m_2+2m_1)}{(m_1+m_2)^2} & -\frac{m_1}{m_1+m_2} & 0 \\ 0 & 0 & 1 \end{pmatrix}. \end{aligned} \tag{3.25}$$

3.8.2 General Basis Permutations

Ultimately, an arbitrary permuted basis function $\mathcal{P}_{13}|\beta\rangle$ must be expressed as a sum of unpermuted basis functions, in the following form:

$$\mathcal{P}_{13}|\beta\rangle = \sum_{\bar{\beta}} \mathcal{B}(\beta,\bar{\beta})|\bar{\beta}\rangle, \tag{3.26}$$

for some transformation coefficients $\mathcal{B}(\beta,\bar{\beta})$. This is essential, as overlaps can't be directly computed between permuted and unpermuted functions. In fact, Suzuki and Varga [115] determine these coefficients for an arbitrary linear coordinate transformation not including the centre of mass, rather than just $\mathcal{P}_{13}$:

$$\begin{aligned}\mathcal{B}_L(\beta,\bar{\beta}) = \sum_{\substack{\nu_1\ \lambda_1\ \nu_2\ \lambda_2\\ n_1\ l_1\ n_2\ l_2}} & D^{n_r l_r}_{\nu_1\lambda_1\nu_2\lambda_2} D^{n_\rho l_\rho}_{n_1 l_1 n_2 l_2} E^{\lambda_1\lambda_2 l_r l_1 l_2 l_\rho L}_{\bar{l}_r \bar{l}_\rho} \\ & \times (T_{11})^{2\nu_1+\lambda_1} (T_{12})^{2\nu_2+\lambda_2} \\ & \times (T_{21})^{2n_1+l_1} (T_{22})^{2n_2+l_2}\,,\end{aligned} \tag{3.27}$$

where the summation indices are constrained as follows:

$$\begin{aligned} 2\nu_1 + \lambda_1 + 2\nu_2 + \lambda_2 &= 2n_r + l_r, \\ 2n_1 + l_1 + 2n_2 + l_2 &= 2n_\rho + l_\rho, \\ 2\nu_1 + \lambda_1 + 2n_1 + l_1 &= 2\bar{n}_r + \bar{l}_r, \\ 2\nu_2 + \lambda_2 + 2n_2 + l_2 &= 2\bar{n}_\rho + \bar{l}_\rho, \end{aligned} \tag{3.28}$$

and where T is any linear transformation of the form

$$\begin{pmatrix} T_{11} & T_{12} & 0 \\ T_{21} & T_{22} & 0 \\ 0 & 0 & 1 \end{pmatrix}. \tag{3.29}$$

The D-coefficient is defined as:

$$D^{KL}_{k_1 l_1 k_2 l_2} = \frac{(2K+L)!}{(2k_1+l_1)!(2k_2+l_2)!} \frac{B_{k_1 l_1} B_{k_2 l_2}}{B_{KL}} C(l_1 l_2; L), \tag{3.30}$$

where

$$B_{kl} = \frac{4\pi(2k+l)!}{2^k k!(2k+2l+1)!!} \tag{3.31}$$

and

$$C(ll';L) = \sqrt{\frac{(2l+1)(2l'+1)}{4\pi(2L+1)}} \langle l0l'0|L0\rangle, \tag{3.32}$$

and finally the E-coefficient, which is a recoupling coefficient between the solid spherical harmonic basis states, is defined as:

$$E^{l_1 l_2 l_{12} l_3 l_4 l_{34} L}_{l_{13} l_{24}} = \sqrt{(2l_{12}+1)(2l_{34}+1)(2l_{13}+1)(2l_{24}+1)} \times C(l_1, l_3; l_{13}) C(l_2 l_4; l_{24}) \begin{Bmatrix} l_1 & l_2 & l_{12} \\ l_3 & l_4 & l_{34} \\ l_{13} & l24 & L \end{Bmatrix} \tag{3.33}$$

where the braced expression is a $9j$-symbol. To reiterate, Eq. (3.27) describes the transformation coefficient from state $|\beta\rangle$ to $|\bar{\beta}\rangle$ under some transformation T. This transformation introduces some minor complications, so $|\bar{\beta}\rangle$ must be slightly more general than the definition of a basis state in Eq. (3.16):

1. $|\bar{\beta}\rangle$ may contain additional even powers of the radial coordinates r, ρ and R.

2. $|\bar{\beta}\rangle$ may contain off-diagonal elements in the Gaussian matrix, even if $|\beta\rangle$ does not. Since the transformation does not affect the CoM coordinate $\mathbf{R}$, this only happens with $\mathbf{r}$ and $\boldsymbol{\rho}$, giving factors of the form $\exp(\mathbf{r} \cdot \boldsymbol{\rho})$.

The first point is easily accommodated as the various integrals generalise with extra radial powers. The second point is more difficult. It is necessary to expand the off-diagonal part of the Gaussian using

$$e^{-\delta \mathbf{x} \cdot \mathbf{y}} = 4\pi \sum_{\kappa} \epsilon(\kappa, \delta) i_l(|\delta| xy) \mathrm{Y}^{(\kappa\kappa)}_{00}(\hat{\mathbf{x}}, \hat{\mathbf{y}}), \tag{3.34}$$

where $i_l(x)$ is the modified spherical Bessel function of the first kind, and $\epsilon(\kappa, \delta) = 1$ for $\delta > 0$ and $(-1)^\kappa$ for $\delta \leq 0$. Combined with the complicated Eq. (3.27), this gives an extremely lengthy expression for the transformed state, which will not be written out in full. Nonetheless, the transformed state has been expressed in terms of known functions as well as various algebraic factors.

3.9 Matrix Elements

Having defined and expounded the various basis functions that will be used, the next step is to calculate the basis elements H_{ij} and S_{ij}, as defined in Eqs. (3.6) and (3.7). The calculation of these elements for many different basis functions is where

most of the computer's resources are spent when carrying out this method. Therefore, deriving simple analytic expressions for these matrix elements wherever possible will heavily reduce computation time. The calculation of the simplest matrix element, the two-body overlap, and of the three-body overlap with an arbitrarily transformed state, are produced here as they demonstrate the general techniques used. All other necessary matrix elements for are listed in Appendix A.

3.9.1 Two-Body Overlap

In the two-body case, the width b, as well as l_ρ, l_{coup}, n_r, n_ρ and δ are excluded, as there are only two coordinates and the B-coefficients of Eq. (3.27) are not required. The following integral identity will be used:

$$\mathcal{I}(a,n) = \int_0^\infty r^n \exp\left(-\frac{1}{2}ar^2\right) dr = \frac{\Gamma(\frac{n+1}{2})}{2\left(\frac{a}{3}\right)^{\frac{n+1}{2}}}, \tag{3.35}$$

giving the following expression for the overlap element:

$$\begin{aligned}\langle\beta'|\beta\rangle &= \int_0^\infty d\mathbf{r}\, d\mathbf{R}\, r^{l_r+l'_r} R^{l_R+l'_R} \exp(-\frac{1}{2}[a+a']r^2) \exp(-\frac{1}{2}[c+c']R^2) \\ &\qquad \times \mathrm{Y}^{l_r}_{m_r}(\hat{\mathbf{r}})\mathrm{Y}^{l'_r}_{m'_r}(\hat{\mathbf{r}})\mathrm{Y}^{l_R}_{m_R}(\hat{\mathbf{R}})\mathrm{Y}^{l'_R}_{m'_R}(\hat{\mathbf{R}}) \\ &= \mathcal{I}(2l_r+2, a+a')\mathcal{I}(2l_R+2, b+b')\delta_{l_r l'_r}\,\delta_{l_R l'_R}\end{aligned} \tag{3.36}$$

3.9.2 Three-Body Overlap

As discussed, the three-body case is complicated considerably by the requirement of antisymmetry. The permuted state $\mathcal{P}_{13}|\beta\rangle$ can be expressed as a sum of unpermuted states as per Eq. (3.26), with the transformation coefficients given by Eq. (3.27). The transformed states can then be integrated with an unpermuted bra $\langle\beta'|$ in coordinate space, in the same manner as the above two-body integral. However, this is complicated somewhat by the off-diagonal Gaussian factors (proportional to $e^{\delta\mathbf{r}\cdot\boldsymbol{\rho}}$ etc.). The following identity is used to expand this off-diagonal Gaussian:

$$e^{-\delta\mathbf{r}\cdot\boldsymbol{\rho}} = 4\pi \sum_l \sqrt{2l+1}\epsilon(l,\delta) i_l(|\delta| r\rho) Y_{00}^{(ll)}(\hat{\mathbf{r}}\hat{\boldsymbol{\rho}}) \tag{3.37}$$

This leads to integrals of the following general form:

$$\begin{aligned}\mathcal{K}(\nu,n,l,u,v,\delta) &= \int_0^\infty\int_0^\infty x^{2\nu+l+2}y^{2n+l+2}e^{-\frac{1}{2}ux^2-\frac{1}{2}vy^2}i_l(|w|xy)dx\,dy \\ &= \sqrt{\frac{\pi}{8}}(2n)!!\Gamma\left(n+l+\frac{3}{2}\right)\frac{|\delta|^l}{u^{n+l+\frac{3}{2}}} \\ &\quad\times\sum_{k=0}\frac{\Gamma(k+\nu+l+\frac{3}{2}}{k!(n-k_!\Gamma(k+l+\frac{3}{2})}\end{aligned} \tag{3.38}$$

Combining this with the $\mathcal{B}$-coefficient expansion of Eq. (3.26), this gives the following expression for the three-body overlap:

$$\begin{aligned}S_{ij} &= \langle\beta'|\beta\rangle \\ &= 4\pi\,\mathcal{I}(2l_R+2,c+c')\delta_{l_Rl'_R} \\ &\quad\times\sum_{\bar\beta}\mathcal{B}(\beta,\bar\beta)\sum_\kappa\sqrt{2\kappa+1}\epsilon(\kappa,\omega)E^{\kappa\kappa0l'_rl'_\rho LL}_{\bar l_r\bar l_\rho} \\ &\quad\times\mathcal{K}\Bigg(\bar n_r+n'_r+\frac{\bar l_r+l'_r-\kappa}{2}, \\ &\qquad\qquad \bar n_\rho+n'_\rho+\frac{\bar l_\rho+l'_\rho-\kappa}{2},\kappa,\bar a+a',\bar b+b',\bar c+c'\Bigg)\end{aligned} \tag{3.39}$$

3.10 Structure Factors

An essential tool in the interpretation of few-body numerical results is the structure factor, which is essentially the probability density of the state with all but a single coordinate integrated out. This may be any coordinate, whether single-particle, Jacobi or the hyperradius. Thus the definition of a general structure factor is

$$P(y') = \langle\Phi|\delta[y(\vec{x})-y']|\Phi\rangle, \tag{3.40}$$

where $y(\vec{x})$ is the coordinate of the structure factor, which is a function of (potentially) the full set of the systems coordinates, contained in the vector $\vec{x}$, and the structure factor is evaluated at some particular value y'. The most common structure factor is where y is simply the first Jacobi radius, r, which is often referred to as the *pair-correlation*. Expanding $|\Phi\rangle$ as per Eq. (3.1) reveals that Eq. (3.40) is in fact a sum over a matrix with elements delta-function kernels, which are evaluated in a manner similar to the above examples (see Appendix A). Throughout the

remaining chapters, examples of structure factors will frequently be shown and interpreted. These structure factors are sometimes rescaled by factors of y^2, to ensure good behaviour near the origin.

3.11 Conclusion

In this Chapter, the theoretical basis of the stochastic variational method has been established. This method can yield solutions to a wide variety of few-body problems efficiently and accurately. The details of my implementation of the method, which will be used throughout the remainder of this thesis, have been specified. In particular, the basis functions which will be used in Eq. (3.16) have been described. Finally, the derivations of some of the matrix elements H_{ij} and S_{ij} have been shown, the calculation of which is the most demanding part of the method's implementation. Expressions for more matrix elements can be found in Appendix A. In subsequent Chapters, this method will be used to verify existing analytic and numeric results, and to provide new results on trap-imbalanced systems in Chapter 7.

Chapter 4

The Two-Body Problem

4.1 Introduction

The simplest non-trivial problem in cold atom physics is that of two interacting particles of equal mass in a harmonic trap. In fact, there exists a complete analytic solution to this problem, derived by Busch et al. [24], which is reproduced and discussed in this Chapter. The methods of Chapter 3 are then applied to produce equivalent results, providing a simple test of the numerical methods.

4.2 Analytic Solution

To reach the solution of Busch et al., the zero-range pseudopotential discussed in Chapter 2 is used, giving rise to the following Hamiltonian:

$$H = -\frac{1}{2m}\nabla_1^2 - \frac{1}{2m}\nabla_2^2 + \frac{1}{2}m\omega^2 r_1^2 + \frac{1}{2}m\omega^2 r_2^2 + \frac{4\pi\hbar^2 a_s}{m}\delta(\mathbf{r}_{12})\frac{\partial}{\partial r_{12}}r_{12}, \qquad (4.1)$$

where $\mathbf{r}_1$ and $\mathbf{r}_2$ are the coordinates of the two particles, m is the mass, ω is the trapping frequency, a_s is the scattering length, and $r_{12} = |\mathbf{r}_1 - \mathbf{r}_2|$. Note that the problem can equivalently be solved by replacing the interaction with a Bethe-Peierls boundary condition [11] and formulating the solution as an irregular Green's function [12]. The system is now re-expressed in coordinates with the system's natural length scale (equivalent to setting $\hbar = m = \omega = 1$), and transformed to the Jacobi coordinates $\mathbf{r} = \frac{1}{\sqrt{2}}(\mathbf{r}_1 - \mathbf{r}_2)$ and $\mathbf{R} = \frac{1}{\sqrt{2}}(\mathbf{r}_1 + \mathbf{r}_2)$. These definitions follow Busch et al.'s convention [24], but in subsequent Chapters a slightly different definition will

be used. This transformation separates the Hamiltonian into relative and centre of mass parts:

$$\begin{aligned} H &= H_{\text{com}} + H_{\text{rel}} \\ &= -\frac{1}{2}\nabla_R^2 + \frac{1}{2}R^2 - \frac{1}{2}\nabla_r^2 + \frac{1}{4}r^2 + \sqrt{2}\pi a_s \delta^{(3)}(\mathbf{r})\frac{\partial}{\partial r}r. \end{aligned} \tag{4.2}$$

Thus the two-body problem is reduced to two one-body problems. The centre of mass part is a simple three-dimensional harmonic oscillator, with well-known solutions. The following eigenvalue problem defines the relative part of the solution:

$$E\Psi(\mathbf{r}) = H_{\text{rel}}\Psi(\mathbf{r}), \tag{4.3}$$

where Ψ(r) is the coordinate space representation of an eigenstate of the relative Hamiltonian. Ψ(r) is then expanded in the complete set of harmonic oscillator eigenstates:

$$\Psi(\mathbf{r}) = \sum_{n=0}^{\infty} c_n \phi_n(\mathbf{r}). \tag{4.4}$$

Note that the $l \neq 0$ states are not included in the sum. This is because they are unaffected by the delta function potential, since in all cases these states vanish at $r = 0$, thus remaining eigenstates of the system even after the introduction of the interaction. The unknown perturbed $l = 0$ eigenstates do not contain any components proportional to these $l \neq 0$ eigenstates, as all the system's eigenstates must be orthogonal. Inserting the expansion into Eq. (4.3), it is found that

$$\sum_{n=0}^{\infty} c_n(E_n - E)\phi_n(\mathbf{r}) + \sqrt{(2)}\pi a_s \delta^{(3)}(\mathbf{r})\frac{\partial}{\partial r}r\sum_{m=0}^{\infty} c_m \phi_m(\mathbf{r}) = 0. \tag{4.5}$$

Projecting on to ϕ_n^*:

$$c_n(E_n - E) + \sqrt{2}\pi a_s \phi_n^*(0)\left[\frac{\partial}{\partial r}\left(r\sum_{m=0}^{\infty} c_m \phi_m(\mathbf{r})\right)\right]_{r\to\infty} = -\frac{1}{a_s}. \tag{4.6}$$

Noting that the sum over m depends only on the normalisation of Ψ, it is found that the expansion coefficients are of the form:

$$c_n = A\frac{\phi_n^*(0)}{E_n - E}, \tag{4.7}$$

for some constant A that depends on the normalisation. Inserting Eq. (4.7) into Eq. (4.6),

$$\sqrt{2}\pi\left[\frac{\partial}{\partial r}\left(r\sum_{n=0}^{\infty}\frac{\phi_n^*(0)\phi_n(\mathbf{r})}{E_n - E}\right)\right]_{r\to\infty} = -\frac{1}{a_s}. \tag{4.8}$$

Thus an equation that determines the desired eigenvalues E_n has been found. However, further simplification is possible. First, a representation of the harmonic oscillator wavefunctions is inserted:

$$\phi_n(\mathbf{r}) = \pi^{-\frac{3}{4}}[L_n^{(1/2)}(0)]^{-\frac{1}{2}} e^{-r^2/2} L_n^{(1/2)}(r^2), \tag{4.9}$$

giving:

$$\frac{1}{\sqrt{2\pi}}\left[\frac{\partial}{\partial r}\left(re^{-r^2/2}\sum_{n=0}^{\infty}\frac{L_n^{(1/2)}(r^2)}{n-\nu}\right)\right]_{r\to\infty} = -\frac{1}{a_s}, \tag{4.10}$$

where $\nu = \frac{1}{2}E - \frac{3}{4}$ is the non-integer quantum number of the oscillator. To further simplify the expression, the following integral representation is used:

$$\frac{1}{n-\nu} = \int_0^{\infty}\frac{dy}{(1+y)^2}\left(\frac{y}{1+y}\right)^{n-\nu-1}, \tag{4.11}$$

valid for $n - \nu > 0$, which gives:

$$\sum_{n=0}^{\infty}\frac{L_n^{(1/2)}(r^2)}{n-\nu} = \sum_{n=0}^{\infty}\int_0^{\infty}\frac{dy}{(1+y)^2}\left(\frac{y}{1+y}\right)^{n-\nu-1} L_n^{(1/2)}(r^2). \tag{4.12}$$

The summation variable n now only appears in the exponent and in the degree of the Laguerre polynomial, so the expression can be simplified using a generating function of the Laguerre polynomials:

$$\sum_{n=0}^{\infty} L_n^{(1/2)}(x)z^n = (1-z)^{-3/2}\exp\left(\frac{xz}{z-1}\right), \tag{4.13}$$

which gives

$$\begin{aligned}\sum_{n=0}^{\infty}\frac{L_n^{(1/2)}(r^2)}{n-\nu} &= \int_0^{\infty}\frac{dy}{\sqrt{1+y}}e^{-yr^2}\left(\frac{y}{1+y}\right)^{-\nu-1} \\ &= \Gamma(-\nu)U(-\nu,\frac{3}{2},r^2)\end{aligned} \tag{4.14}$$

Using the short-range behaviour of U, the following is reached:

$$\Gamma(-\nu)U(-\nu,\frac{2}{3},r^2) = -\sqrt{\pi}\left(\frac{2\Gamma(-\nu)}{\Gamma(-\nu-\frac{1}{2})} - \frac{1}{r} + O(r)\right). \tag{4.15}$$

Finally,

$$\sqrt{2}\frac{\Gamma(-E/2+3/4)}{\Gamma(-E/2+1/4)} = \frac{1}{a_s}, \tag{4.16}$$

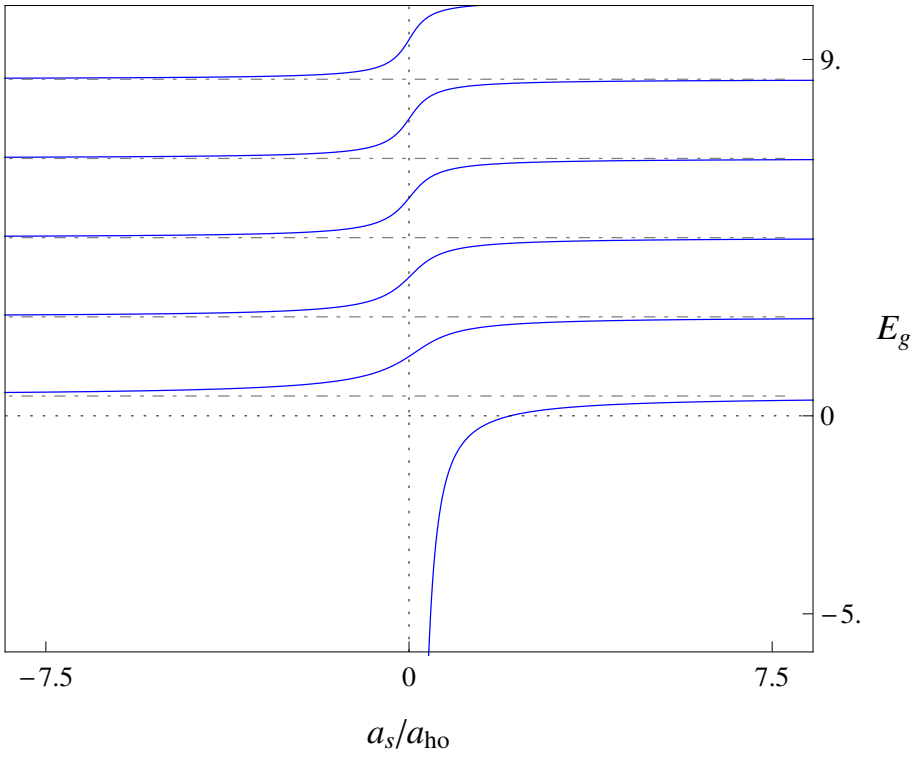

Figure 4.1: Spectrum of the $l = 0$ states of the interacting two-particle system, given by Eq. (4.16).

which is a transcendental equation whose solutions are the eigenvalues of the system.

This immediately allows the energy eigenvalues to be examined as a function of the scattering length a_s, as shown in Fig. 4.1. Thus a repulsive interaction, corresponding to a positive scattering length, induces a positive shift in the energy levels. The difference between successive energy levels, $\Delta E = 1$, approaches unity at large values of $|a_s|$. Conversely, a repulsive interaction ($a_s < 0$) experiences a negative shift, saturating at $\Delta E = -1$. Of immediate interest is the presence of a bound state on the $a_s > 0$ side, with the energy diverging to $-\infty$ as $a_s \to 0^+$. This bound state also occurs in the absence of the trapping potential, as can be seen by taking the limit $-E \gg 1$ in Eq. (4.16), which corresponds to the oscillator length diverging to $+\infty$.

Equation (4.16), combined with Eqs. (4.4), (4.7) and (4.9), gives the following

expression for the coordinate space wavefunction:

$$\Psi(\mathbf{r}) = \frac{1}{2}\pi^{-3/2}Ae^{-r^2/2}\Gamma(-\nu)U(-\nu, \frac{3}{2}, r^2), \tag{4.17}$$

where as before A is some constant depending on the normalisation. This expression will allow the three-body problem to be solved in Chapter 5.

4.3 Numerical Results

The balanced two-body system can now be used as the first test of the numerical methods described in Chapter 3. The obvious initial test is to reproduce the ground state energy of Eq. (4.16) at unitarity. As discussed in Chapter 3, this requires an examination of a range of finite values of the interaction range r_0, and extrapolate back to the zero-range case which corresponds directly to Eq. (4.16). The result of these calculations is shown in Fig. 4.2; a linear fit of the data allows extrapolation to $E_g = 0.49998$ at $r_0 = 0$, very close to the known value of 0.5 obtained from Eq. (4.16).

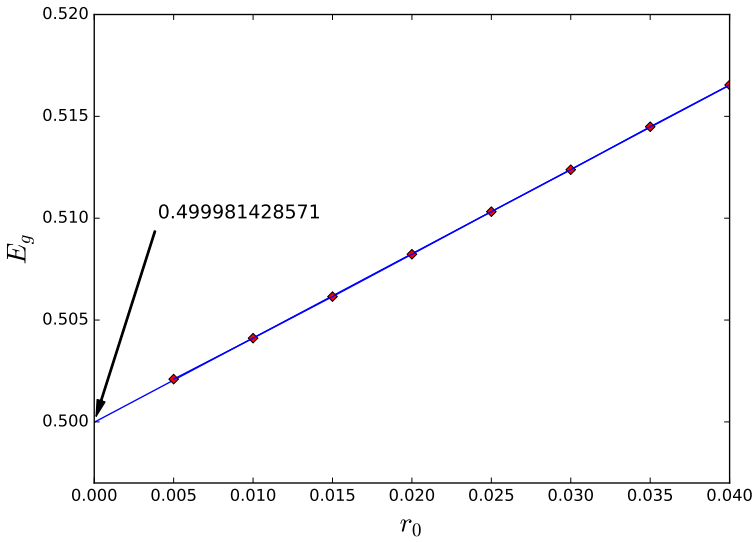

Figure 4.2: Stochastic variational ground state energies for a $l = 0$ two-body system with $a_s \approx 10^8$, and various values of the interaction range r_0. The blue line shows a linear fit.

The spectrum of Fig. 4.1 can also be compared to a numerical calculation.

Figure 4.3 shows the ground state spectrum produced by my code, which compares well with the analytic result.

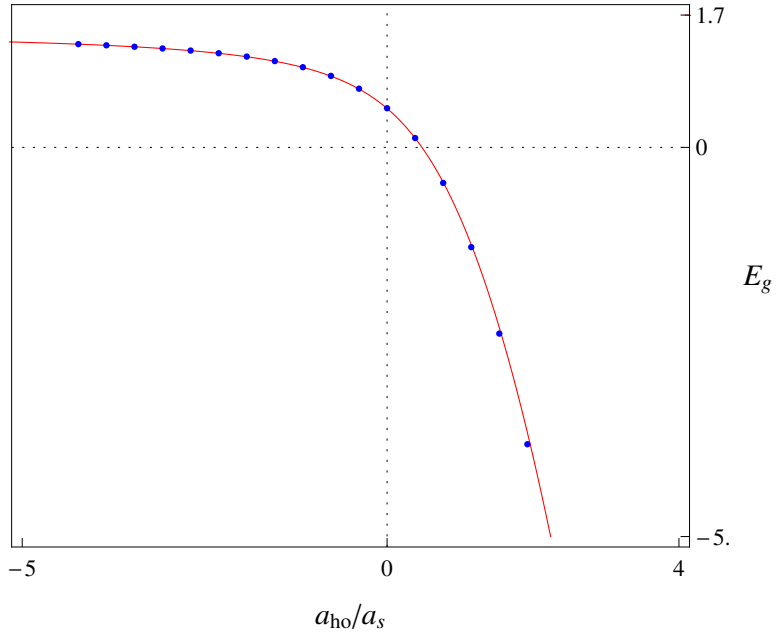

Figure 4.3: Stochastic variational spectrum for a two-body system with $r_0 = 0.01a_{\mathrm{ho}}$, and $a_s \approx 10^8$. The red line shows the exact solution given by Eq. (4.16).

4.4 Conclusion

In this Chapter, the analytic solution of two strongly interacting atoms in a harmonic trap has been rederived, leading to the energy eigenvalue equation Eq. (4.16). The stochastic variational method has been applied to solve this system numerically with a high degree of accuracy, as discussed in Chapter 3.

Chapter 5

The Three-Body Problem

5.1 Introduction

In this Chapter, the problem of three trapped fermions of equal masses is examined. This problem has proven to be analytically tractable [73, 85, 129]. In this Chapter, the analytic solution formulated by Liu et al. [85] is reproduced. Secondly, the application of the stochastic variational method to this system is discussed, and important numerical results are reproduced.

5.2 Analytic Solution

The starting point for the analytic solution to this problem is the solution to the two-body problem, plus the observation that the three-body problem is essentially identical to the two-body, once the centre-of-mass coordinate is separated. The one complication is the requirement of antisymmetry. The system has the following Hamiltonian, with all masses and trapping frequencies being unity:

$$H = \sum_{i=1}^{3} \left[\frac{1}{2} \nabla_{\mathbf{r}_i}^2 + \frac{1}{2} r_i^2 \right]. \tag{5.1}$$

Instead of including the interaction in the Hamiltonian explicitly, Bethe-Peierls boundary conditions will be used. These conditions ensure the wavefunction has the required short-range behaviour that would be induced by a delta-function pseudopotential, and make the analytics more straightforward. The boundary condi-

tions takes the form:

$$\lim_{r_{ij}\to 0} \frac{\partial(r_{ij}\psi)}{\partial r_{ij}} = -\frac{r_{ij}\psi}{a_s}, \tag{5.2}$$

with one such boundary condition for each pair of interacting particles; in this case, this gives two conditions, for $i = 1, j = 2$ and $i = 1, j = 3$. To separate the centre of mass, the system is transformed to the following Jacobi coordinates:

$$\mathbf{r} = \mathbf{r}_1 - \mathbf{r}_2, \tag{5.3}$$

$$\boldsymbol{\rho} = \frac{2}{\sqrt{3}}(\mathbf{r}_3 - \frac{1}{2}\mathbf{r}_2 - \frac{1}{2}\mathbf{r}_1), \tag{5.4}$$

$$\mathbf{R} = \frac{1}{3}(\mathbf{r}_1 + \mathbf{r}_2 + \mathbf{r}_3). \tag{5.5}$$

This reduces the Hamiltonian to the usual centre-of-mass harmonic oscillator, and a relative Hamiltonian which is also simple harmonic oscillators, but which must satisfy antisymmetry and the boundary conditions:

$$H_{\mathrm{CoM}} = -\frac{1}{2M}\nabla^2_{\mathbf{R}} + \frac{1}{2}MR^2, \tag{5.6}$$

$$H_{\mathrm{rel}} = -\frac{1}{2\mu}\nabla^2_{\mathbf{r}} + \frac{1}{2}\mu r^2 - \frac{1}{2\mu}\nabla^2_{\boldsymbol{\rho}} + \frac{1}{2}\mu\rho^2, \tag{5.7}$$

where $M = 3m$ and $\mu = \frac{m}{2}$. The centre-of-mass part has trivial harmonic oscillator eigenstates (noting that the permutation, which swaps $\mathbf{r}_1$ and $\mathbf{r}_3$, has no effect on the centre-of-mass coordinate $\mathbf{R}$). The relative part of the wavefunction is now expanded in the complete set of solutions to the two-body interacting problem [24], i.e. the $\Psi(\mathbf{r})$ of Eq. (4.17), which are now renamed $\psi^{\mathrm{rel}}_{\mathrm{2b}}(\mathbf{r})$. Furthermore, antisymmetry is enforced using the operator $(1 - \mathcal{P}_{13})$, giving the following ansatz for the relative wavefunction:

$$\psi^{\mathrm{rel}}_{3b}(\mathbf{r}, \boldsymbol{\rho}) = (1 - \mathcal{P}_{13})\chi(\mathbf{r}, \boldsymbol{\rho}), \tag{5.8}$$

where

$$\chi(\mathbf{r}, \boldsymbol{\rho}) = \sum_n a_n \psi^{\mathrm{rel}}_{2b}(r; \nu_{l,n}) R_{nl}(\rho) Y^m_l(\hat{\rho}). \tag{5.9}$$

Here $R_{nl}(\rho)Y^m_l(\hat{\rho})$ is the standard 3D harmonic oscillator wavefunction with principal quantum number n and angular momentum (l, m), with energy $2n + l + \frac{3}{2}$. The operator $\mathcal{P}_{13}$ swaps the single-particle coordinates $\mathbf{r}_1$ and $\mathbf{r}_3$, giving:

$$\mathcal{P}_{13}\chi(\mathbf{r}, \boldsymbol{\rho}) = \chi(\mathbf{r}/2 + \sqrt{3}\boldsymbol{\rho}/2,\ \sqrt{3}\mathbf{r}/2 - \boldsymbol{\rho}/2). \tag{5.10}$$

The first Bethe-Peierls boundary condition reads as follows, noting that $r = r_{12}$:

$$\lim_{r\to 0} \frac{\partial}{\partial r}[r\psi_{3b}^{\text{rel}}(\mathbf{r},\boldsymbol{\rho})] = -\frac{1}{a} r\psi_{3b}^{\text{rel}}(\mathbf{r},\boldsymbol{\rho}). \tag{5.11}$$

Since Eq. (5.8) requires that ψ_{3b}^{rel} is antisymmetric under the interchange of particles 1 and 3, the second boundary condition (with r_{23} replacing $r_{12} = r$) is automatically satisfied given Eq. (5.11), since it can be reached by applying $\mathcal{P}_{13}$ to both sides of Eq. (5.11). Now, writing $\chi(\mathbf{r},\boldsymbol{\rho}) = \phi(r,\rho)Y_l^m(\hat{\rho})$, and using the asymptotic behaviour of the hypergeometric function gives:

$$\lim_{r\to 0} -\frac{1}{a_s}[r\phi(r,\rho)] = -\frac{\sqrt{\pi}}{a_s}\sum_n a_n R_{nl}(\rho), \tag{5.12}$$

and

$$\lim_{r\to 0} \frac{\partial[r\phi(r,\rho)]}{\partial r} = -\sqrt{\pi}\sum_n a_n R_{nl}(\rho)\frac{2\Gamma(-\nu_{l,n})}{\Gamma(-\nu_{l,n}-1/2)}. \tag{5.13}$$

This allows the boundary condition to be rewritten as:

$$\sum_n a_n \left[B_n R_{nl}(\rho) - R_{nl}\left(\frac{\rho}{2}\right)\psi_{2b}^{\text{rel}}\left(\frac{\sqrt{3}\rho}{2};\nu_{l,n}\right)\right] = 0, \tag{5.14}$$

where

$$B_n = (-1)^l\sqrt{\pi}\left[\frac{d}{a} - \frac{2\Gamma(-\nu_{l,n})}{\Gamma(-\nu_{l,n}-1/2)}\right]. \tag{5.15}$$

Then, projecting onto $R_{nl}(\rho)$ gives:

$$\frac{2\Gamma(-\nu_{l,n})}{\Gamma(-\nu_{l,n}-1/2)}a_n + \frac{(-1)^l}{\sqrt{\pi}}\sum_{n'} C_{nn'}a_{n'} = \left(\frac{d}{a_s}\right)a_n, \tag{5.16}$$

where

$$C_{nn'} = \int_0^\infty \rho^2 d\rho R_{nl}(\rho)R_{n'l}\left(\frac{\rho}{2}\right)\psi_{2b}^{\text{rel}}\left(\frac{\sqrt{3}\rho}{2};\nu_{l,n'}\right). \tag{5.17}$$

Equations (5.16) and (5.17) tell us, in principle, the energy eigenvalues of the system, since $E_{\text{rel}} = [(2\nu_{l,n}+3/2)+(2n+l+3/2)]\omega$. However, there is no way to reach a simple expression for E_{rel} from Eq. (5.16), so a numerical approach is necessary. The simplest approach would be to use a root finding algorithm on E_{rel} to satisfy Eq. (5.16). However, Liu et al. [85] suggest that a faster approach is to diagonalise the matrix with elements given by

$$A_{nn'} = \frac{2\Gamma(-\nu_{l,n})}{\Gamma(-\nu_{l,n}-1/2)}\delta_{nn'} + \frac{(-1)^l}{\sqrt{\pi}}C_{nn'}, \tag{5.18}$$

for a given value of E_{rel}. It is interesting to note that the term containing $C_{nn'}$ in Eq. (5.16) arises only due to the action of the permutation operator $\mathcal{P}_{13}$. Without this term, the equation reduces to Eq. (4.16), the solution of the two-body problem. This is to be expected, since the relative Hamiltonian Eq. (5.7) is identical to that of the two-body problem, and the only difference is the requirement of antisymmetrisation.

5.3 Numerical Solutions

As in the two-body case, the methods described in Chapter 2 are easily applied to this system. In fact, because the Hamiltonian Eq. (5.1) depends only on the radii, there is no need to include spherical harmonics in the basis (or, to be precise, only a single harmonic is included). Figure 5.1 shows the ground state energy of the system for a range of r_0 values, which interpolate to $E_g \approx 2.773$ at $r_0 = 0$. This ground state energy does not include the centre of mass energy $E_{\text{com}} = 1.5$, as is the convention when discussing systems in which the centre of mass decouples.

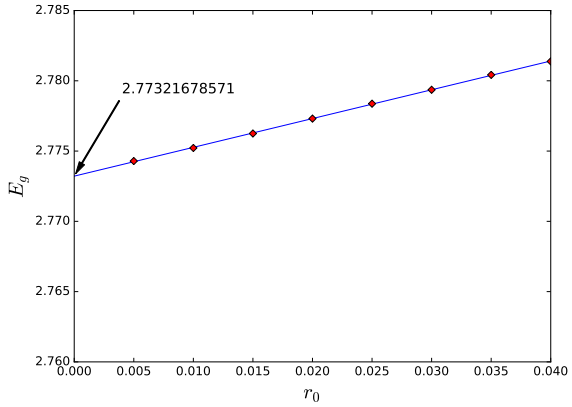

Figure 5.1: Stochastic variational energies for $L_{\text{total}} = 1$ three-body systems, with $a_s \approx 10^8$, and various values of the interaction range $r0$, showing convergence to $E_g \approx 2.773$. The blue line is a linear fit.

5.3.1 The Atom-Dimer System

The ground state of the three-body system is known as an atom-dimer state. Loosely speaking, this means that two of the atoms form a relatively tight dimer, while the

third sits further away. To better understand this, a good definition of what constitutes an atom-dimer state is needed. To this end, the notion of the *atom-dimer system* is introduced, as described by Daily et al. [32]. This is the three-body system explicitly split into two subsystems: the dimer and the lone atom, with the interaction between the atom and the dimer being switched off, and the two like particles made distinguishable. Atom-dimer states are then characterised as those states whose energies converge to the energy of the atom-dimer system as the scattering length becomes positive. Physically, this corresponds to the dimer becoming so tightly bound that its overlap with the remaining atom becomes negligible, meaning that the antisymmetry and second interaction term can be ignored. Figure 5.2 reflects this: the energy of the three-body system approaches that of the atom-dimer system as $a_s^{-1}/a_{\text{ho}} \to \infty$.

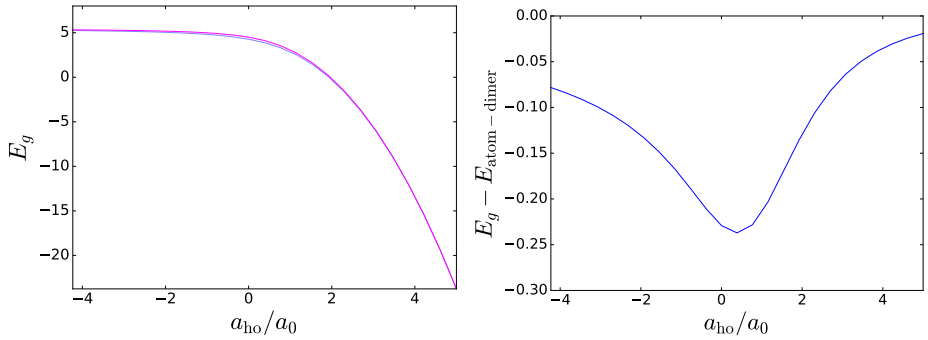

Figure 5.2: Stochastic variational spectrum for a $L_{\text{total}} = 1$ three-body system (blue) and the corresponding atom-dimer system (pink), with $a_s \approx 10^8$, $r_0 = 0.01$ (left), and the difference of the two energies (right).

The nature of the atom-dimer three-body ground state can be examined in more detail by inspecting the pair-correlation function, as defined in Eq. (3.40) and shown in Fig. 5.3. Loosely speaking, this function shows the probability density of different values of the distance between the two species, and in this case is characteristic of an atom-dimer state. This can be thought of in terms of placing an atom of either species at the origin, and examining how likely it is to find the other species at different radii. With two spin-up atoms and one spin-down, it is most helpful to imagine the lone spin-down at the origin. This allows the atom-dimer state to be recognised qualitatively, by noting the two-peaked structure. The first peak corresponds to the dimer i.e. the first spin-up atom sitting close to the spin-

down, at values of r considerably less than the trapping length. The second "spare" spin-down atom sits further away. Of course, this picture is slightly misleading as the two spin-down atoms are in fact indistinguishable and therefore in the same quantum state. However, the general picture remains accurate.

It is noted that the pair-correlation decays to nearly zero in a small region near the origin. This is a consequence of using a finite-range interaction, as the wave-function must necessarily decay exponentially as the interaction term (proportional to $e^{-r^2/2r_0^2}$) becomes significant. Hence the width of this near-zero region is approximately the interaction length r_0.

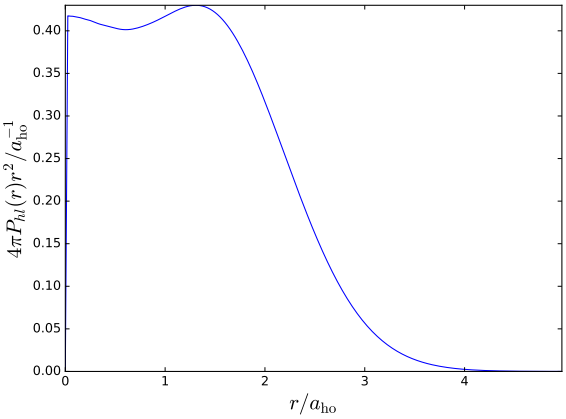

Figure 5.3: Pair-correlation for a $L_{\mathrm{total}} = 1$ three-body system with $r_0 = 0.001$, and $a_s \approx 10^8$.

5.4 Conclusion

In this Chapter, a mostly analytic solution of the balanced three-body problem by Hiu et al. [85] has been rederived and discussed. The ground state energy of this system, as well as the corresponding pair-correlation function, have been reproduced using my code. Some important physics of this solution has been discussed: in particular, why and how this solution can be classified as an atom-dimer state.

Chapter 6

Efimov States and Mass-Imbalanced Systems

6.1 Introduction

Thus far, the background theory and the simplest examples of few-body strongly-interacting systems have been discussed, as well as a numerical method of finding solutions to such systems. These methods will now be applied to the more exotic class of heteronuclear systems, where two species of atom are present, which may have different masses and trapping potentials. In this Chapter, only heteronuclear systems with unequal masses are considered, which have been relatively widely studied [8, 10, 17, 18, 35, 37, 40, 58, 59, 66, 77, 78, 78, 86, 92, 99–101, 107, 126, 128, 130, 134].

The Efimov effect is one of the most surprising properties of few-body quantum systems, in which three bosons (of any masses), or three mass-imbalanced fermions, may form deeply-bound states known as Efimov states, which have various unusual properties. In this Chapter, established physics of these systems is reviewed, and my code is applied to systems of three fermions of various mass ratios to reproduce key results.

6.2 Heteronuclear Systems

The few-body heteronuclear systems studied here contain two neutral species with different masses m_1 and m_1. All members of a particular species are assumed to be identical, and to be in identical internal states. The two species may also experience different trapping frequencies ω_1 and ω_2 from the confining harmonic potential, but in this Chapter it is assumed $\omega_1/\omega_2 = 1$. Thus far, there have been a variety of experiments observing diatomic heteronuclear molecules in optically trapped cold gases with bosons [37, 77, 101, 128] and fermions [126]. There have also been a number of experiments in optical lattices [35, 99]. Optical lattices offer the advantage of more easily producing isolated few-body systems, as well as offering potentially greater control of the trapping potential.

Only heteronuclear systems containing two species are considered, as adding additional species is either theoretically difficult, or trivial in the case of three bodies, and is of little current interest to experimentalists. The two species are categorised by the ratio of their masses $\kappa = m_1/m_2$, and the ratio of their trapping frequencies $\eta = \omega_1/\omega_2$, with $\eta = 1$ until the next Chapter.

6.3 Efimov States

The Efimov effect is, in fact, a general scenario that is not confined to the field of ultracold atoms. Therefore, the general case is first outlined, and the ultracold atom case is described later.

6.3.1 Overview

The general Efimov scenario [40] is as follows: three spinless neutral bosons of equal mass interact through some potential $gV(r)$, with the first two-body bound state appearing at some $g = g_0$. The interaction is resonant, i.e. its range r_0 is much less than the scattering length a_s, at least in the region of the bound state at $g = g_0$. Given these conditions, Efimov predicts that as $g \to g_0$ and $a_s \to \infty$, three-body bound states appear sequentially, becoming more and more frequent, and approaching an infinite number as $g \to g_0$. As g exceeds g_0, these states sequentially disappear into the atom-dimer continuum. Efimov gives the following

expression for the number of such states:

$$N \approx \frac{1}{\pi}\log(|a_s|/r_0), \tag{6.1}$$

where N is the number of Efimov states. These states have binding energies much greater than $1/r_0^2$, and their ranges are much greater than r_0. As such, they are often described as *loosely-bound*, since their spatial extent considerably exceeds the range of the binding interaction. This series of states has an additional interesting property: each state appears at a value of a_s approximately 22.7 times larger than the previous state. Furthermore, the new state has a length scale 22.7 times larger, and an energy 22.7^2 times smaller than the existing state. This geometric scaling law brings to mind a fractal-like procession of self-similar states as the resonance is approached. Figure 6.1 demonstrates the appearance of Efimov states below the triatomic threshold for $a_s^{-1} < 0$, followed by their disappearance into the atom-dimer continuum for $a_s^{-1} > 0$.

6.3.2 The Three-Body Parameter

The preceding discussion does not mention the actual energies of the Efimov states. In fact, these cannot be determined solely from the current assumptions. Physically, it depends on the details of the potential where the three bodies are close. Fundamentally, this arises from the fact that the scattering theory from Chapter 2 only gives universality for two-body scattering events. Therefore, when three-body effects become important, one or more additional parameters may be needed to describe the system. It is noted that this is not a concern in the cases discussed in previous Chapters, as the states involved always exhibit large separations of at least two of the particles.

Efimov showed [41] that only a single additional parameter is necessary, which is generally referred to as a *three-body parameter*. While he doesn't use this term, Efimov notes that the three-body system's energies can be determined by fixing the logarithmic derivative of the hyperradial wavefunction at a particular point, or equivalently by specifying the energy of the first Efimov state. In practice, either of these two quantities, or an equivalent one, might be referred to as a three-body parameter. It makes sense that the second method should be a complete description, since the scaling law will then determine the remaining energies.

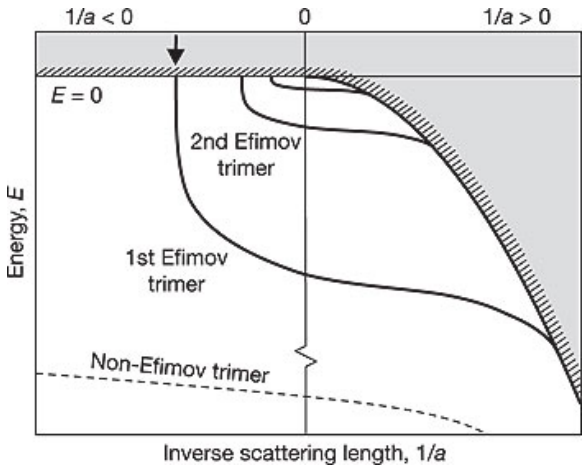

Figure 6.1: Figure from [78] outlining Efimov's scenario, showing the ground state energy of three identical bosons as a function of the inverse scattering length a_s^{-1}. The grey region is the atom-dimer and atom-atom-atom continuum, while the white region is where discrete Efimov states may exist, shown as solid lines. As $1/a_s \to 0$, an unbounded number of Efimov states appear (only three are shown). Points where an Efimov state intersects the continuum may lead to observable resonances.

There is no *a priori* reason why such a three-body parameter should be universal. In other words, two interaction potentials may both give infinite scattering lengths, but different three-body parameters. Surprisingly to many, the three-body parameter was nonetheless found to be universal in various experiments [8, 10, 59, 66, 86, 100, 107, 130, 134]. This is not true in general, however: some experiments see deviations [107]. As will also be seen, systems of three or four trapped mass-imbalanced fermions may exhibit three-body bound states that are not universal.

6.3.3 Summary

The general features of the three-body Efimov effect can be summarised as follows:

- Trimer states appear near a resonance in the interaction, with energies lying below the atom-atom-atom and atom-dimer thresholds
- As the resonance is approached, the number of trimer states increases, approaching an infinite number on resonance

- The states follow a geometric scaling law, in which each new state appears at a value of a_s^{-1} approximately 22.7 times larger than the last, while having an energy 22.7^2 times smaller and a width 22.7 times larger

6.3.4 Coulomb Forces

Efimov's work was inspired by Thomas' study of the triton [122], which showed that at least one three-body bound state exists near an atomic resonance. In fact, nuclear systems like the triton were the only systems of immediate experimental interest to Efimov and his contemporaries. As such, he was immediately concerned with the effect of atomic charges, as there are no nuclear systems containing only neutral particles. Noting that the Coulomb force will dominate for distances larger than the Bohr radius $a_C = 1/e^2$, where e is here the electron charge, and that the resonant interaction will dominate as smaller radii, Efimov approximates the maximum number of levels for three equally charged particles as [40]:

$$N_{\max} \approx \frac{1}{\pi}\log(a_C/r_0). \tag{6.2}$$

This is further complicated by spin-dependent forces, and the imperfect nature of the resonances in nuclear systems (i.e. a_s is large but not overwhelmingly so). This expression typically evaluates to numbers of the order of unity, indicating that Coulomb forces have the potential to interfere with, drown out, or otherwise obscure Efimov physics.

6.4 Initial Reactions

Since its publication, the Efimov effect has been the subject of academic interest in a variety of forms. There was considerable initial excitement in the nuclear physics community, due to the prospect of observing these states in nature, and due to their potential explanatory power in existing physics. The Helium trimer is the most natural candidate system, and was discussed almost immediately [83], and subsequently in more than 50 papers [47]. Nuclear physicists were very interested to know if the helium trimer, one of the most fundamental nuclear systems, resembled an Efimov state. Despite continued interest, there has still been no observation of the Efimov effect in a nuclear system. Due to its unusual nature, the Efimov effect was subject to immediate theoretical scrutiny. One early paper validating the

theory was sardonically titled “Efimov’s effect: A new pathology of three-particle systems” [4].

6.4.1 Observation

Eventually, the advances of the 90s and 00s in trapping and cooling technology [57] allowed the realisation of highly controllable ultracold atomic systems, which have of course bloomed into the field which now encompasses this thesis. It was in these systems that the Efimov effect was finally observed, in a gas of ultracold Cesium in 2005 [78], more than 35 years after Efimov’s original paper. The possibility of observing Efimov states in ultracold gases was well-established [21], and it is now believed that an earlier experiment [127] saw evidence of them, which was too uncertain to interpret definitively at the time. Since then, Efimov states have been observed in many different ultracold gas experiments [8, 10, 58, 59, 66, 78, 86, 92, 100, 107, 130, 134].

6.4.2 Three-Body Losses

The first observation of Efimov physics was achieved by the somewhat indirect means of observing an enhancement of the three-body loss rate in the Cesium gas. Three-body recombination is a process in which three atoms collide, allowing two of them to form a bound dimer state, with the associated binding energy being released as kinetic energy in the third atom. In the case of an ultracold gas, the third atom is then immediately ejected from the system, as it now has a kinetic energy far exceeding the rest of the cloud. This is largely an unavoidable process and is the leading cause of atom loss in most experiments [43, 46, 94]. The three-body loss coefficient L_3 is defined by:

$$\dot{n} = -L_3 n^3, \tag{6.3}$$

where n is the number density of the atomic cloud. Usually, L_3 is largely determined by the kinetics of the available dimer states in the atomic gas. However, if the three-body subsystem supports an Efimov state (or other trimer state) with energy close to the atom-dimer energy, the trimer state provides a different pathway by which the three-body system can reach an atom-dimer state and thus cause

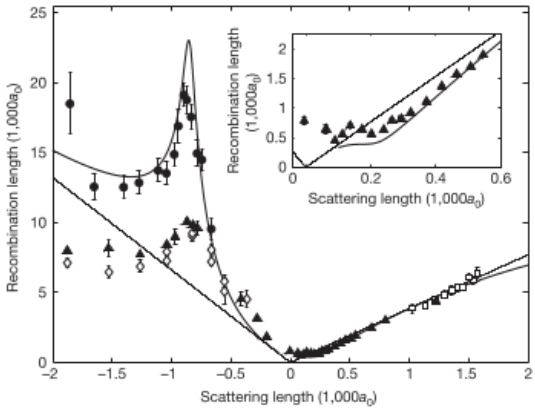

Figure 6.2: Experimental results from [78], showing enhanced three-body loss due to resonance with an Efimov state at around $a_s = -0.8/1000$, where $\rho \propto L_3^{1/4}$ is the recombination length. Filled circles are data taken at 10nK, while other data are between 200 and 400nK. The inset highlights a destructive interference effect.

three-body recombination. This kinematic picture is demonstrated in Fig. 6.1. Experimentally, this means a large enhancement to the three-body loss rate L_3 can be observed at particular values of the scattering length where a trimer state reaches the atom-atom-atom or atom-dimer threshold. Feshbach resonances are used to facilitate the required sweep of scattering lengths. In this way, the nominally undesirable phenomenon of three-body recombination was used to observe Efimov physics for the first time [78]. Figure 6.2 shows key data from that experiment, exhibiting a peak in three-body loss which corresponds to a trimer resonance.

6.5 Efimov States with Fermions

Thus far, only the case of three bosons with $L = 0^+$ has been considered. Naturally, the Efimov effect does not occur with three identical fermions, as any short-range interaction will have no effect due to the statistics. Things become much more interesting in the case of two identical fermions with a third particle, with potentially unequal masses specified by the ratio $\kappa = m_1/m_2$, where $m_1 = m_3$. For $\kappa = 1$, the Efimov effect does not occur. This can be viewed as a consequence of the centripetal barrier i.e. the fermionic statistics make the interaction in the hyperradial coordinate effectively repulsive. However, the coefficient of the centripetal term

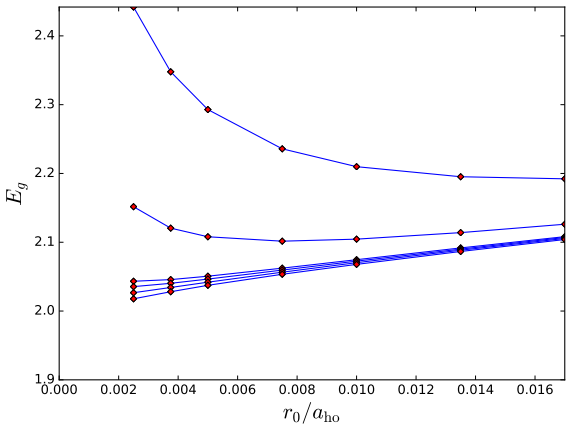

Figure 6.3: Ground state energies for 2+1 $L_{\mathrm{total}} = 1^-$ fermions with $a_s \approx 10^8$, mass imbalances $\kappa = 12.25, 12.3, 12.3131, 12.314, 12.315$ and 12.316 (top to bottom), and various interaction lengths r_0.

decreases as κ increases, eventually changing sign and allowing the Efimov effect to occur for mass ratios higher than 13.6 [103].

6.6 Non-Universality

Blume and Daily [17, 18] explore the bound states of trapped few-body fermionic systems in considerable detail. In the three-body case, they focus on an intermediate regime $12.314(2) < \kappa < 13.6$, where the system exhibits *non-universal* bound states.

6.6.1 Numerical Results

Blume and Daily carefully show the onset of these non-universal bound states with increasing κ. To test my code, some of these results are reproduced here. The same techniques will be applied in the next Chapter to examine non-universal bound states in trap-imbalanced systems. Figure 6.3 shows the dependence of the ground state energy E_g on the interaction range r_0 for various mass ratios near the critical ratio $\kappa \approx 12.314$. When κ exceeds the critical value, the energy begins to decrease non-linearly as r_0 becomes small. The energy's trajectory in these cases is well-fitted by a function of the form $c_{-2}/r_0^2 + c_{-1}/r_0 + c_0$, indicating a much lower energy

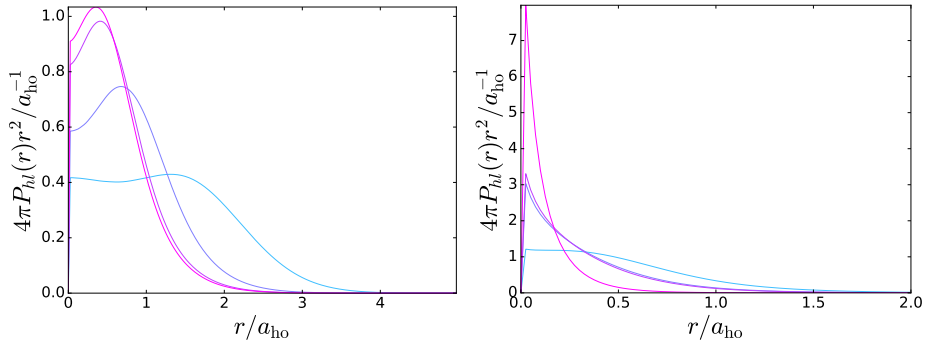

Figure 6.4: Pair-correlations for three fermions with $r_0 = 0.003$, $a_s \approx 10^8$, mass imbalances $\kappa = 1.0, 6.7, 11.0, 11.5$ (left) and $12.0, 12.3, 12.314, 12.5$ (right). Greater values of κ correspond to graphs with higher peaks.

in the true $r_0 \to 0$ limit, and constituting a three-body bound state. At higher values of κ, E_g quickly decreases further, becoming large and negative even at high values of r_0.

Figure 6.4 shows the pair-correlations of a range of systems from $\kappa = 1$ to $\kappa = 12.5$, well above the critical ratio. A transition takes place from the $\kappa = 1$ two-peaked atom-dimer structure (also shown in Fig. 5.3) to a sharply-peaked structure close to the origin, characteristic of a relatively deeply-bound state.

6.7 Four Bosons

Having examined the Efimov states of three particles in detail, it is natural to ask whether similar physics exists for higher numbers of particles. In fact, it was confirmed almost immediately after Efimov's initial publication that no *true* Efimov effect exists in four-body systems [3]. This means that a single three-body bound state cannot give rise to an infinite progression of four-body bound states.

However, this does not preclude the existence of universal four-body states which may be related to Efimov trimers. Such states were predicted to exist in cold gases for years [63, 105, 119, 133], eventually leading to the result that each Efimov trimer should give rise to two universal tetramers [62, 113]. These predictions were eventually confirmed experimentally [39, 48, 113].

6.8 Continued Interest

Since the first observation in 2006, Efimov states have been observed in a variety of cold atom systems. They were observed in 2009 in atom-dimer scattering events [75], which was discussed earlier from a theoretical point of view [95]. Groups at Heidelberg and Penn State tested Efimov physics in three-component ^{6}Li, which shows much more rapid decay than two-component ^{6}Li [66, 100, 131]. This is related to the absence of Efimov physics in 2 + 1 equal mass fermions. Efimov states have also been found in heteronuclear systems: the first such system was bosonic ^{41}K and ^{87}Rb [8].

There has also been continued and renewed interest in finding Efimov physics in nuclear systems [52, 69], despite the lack of direct observation. Neutron-rich systems are of particular interest [88, 132]. The role of finite effective ranges in the interaction is the subject of much recent theoretical work [61, 70, 72, 106, 120, 121].

6.9 Conclusion

In this Chapter, the history and physics of Efimov states, which are of fundamental importance to few-body quantum systems, has been examined. Notably, in three-body fermionic systems, Efimov states only appear above a critical mass ratio of $\kappa = 13.6$. Furthermore, non-universal bound states appear in trapped systems above $\kappa = 12.314$. Using the numerical methods of Chapter 3, the appearance of these non-universal states near the critical ratio has been reproduced.

Chapter 7

Trap-Imbalanced Systems

7.1 Introduction

In this Chapter, the trap-imbalanced two- and three-body systems are discussed, which are the focus of this research. Other than an excellent paper by Blume [14] and some mention of the two-body case in a more experimental context [126], these systems have been investigated very little. To begin, trap-imbalanced Hamiltonians are examined. The trap imbalance introduces additional dot-product terms in Jacobi coordinates, which create distinct physical differences from balanced systems. A variety of new numerical results in two- and three-body trap-imbalanced systems are then explored.

This Chapter also seeks to answer questions concerning three-body bound states, and how they can be influenced by trap imbalances. This includes both deeply-bound Efimovian and non-universal states, as discussed in Chapter 6, and weakly-bound atom-dimer states. It will be shown that trap imbalances have little effect on the physics of deeply-bound states, but can produce a variety of effects in weakly-bound systems, including those on the cusp of Efimov state formation. As in previous Chapters, all numerical calculations are performed at scattering lengths of $a_s \approx 10^8 a_{\text{ho}}$, i.e. essentially at unitarity, otherwise specified. Some quantities are also scaled by the oscillator length a_{ho}, as described in the Definitions Section.

7.2 General Definitions

The general trap-imbalanced system that will be considered contains two distinct fermionic species, with masses m_1 and m_2, and trapping frequencies ω_1 and ω_2. Systems with more than two species are not considered, as these offer little new theoretical interest for low numbers of particles, and furthermore are beyond the scope of current experimental work. As in the previous Chapter, the mass and trap imbalances are characterised by the ratios $\kappa = m_1/m_2$ and $\eta = \omega_1/\omega_2$. These ratios, rather than to the masses and trapping frequencies themselves, are used to specify the particular system under consideration,

7.2.1 Scaling Conventions

Clearly, specifying the ratios κ and η is not sufficient to determine the Hamiltonian. However, these ratios are sufficient to determine H up to an arbitrary rescaling of the coordinates. For two-body systems, the convention of Blume [14] is followed to determine m_1, m_2, ω_1 and ω_2 from κ and η:

$$\begin{aligned} m_1 &= \frac{2}{1+\kappa}, \\ m_2 &= \frac{2\kappa}{1+\kappa}, \\ \omega_1 &= \frac{2}{1+\eta}, \\ \omega_2 &= \frac{2\eta}{1+\eta}. \end{aligned} \tag{7.1}$$

A different convention, which provides a more natural scaling of the energy with different values of η, will be used for three-body systems:

$$\begin{aligned} m_1 &= \frac{3}{1+2\kappa}, \\ m_2 &= \frac{3\kappa}{1+2\kappa}, \\ \omega_1 &= \frac{3}{1+2\eta}, \\ \omega_2 &= \frac{3\eta}{1+2\eta}. \end{aligned} \tag{7.2}$$

As mentioned in the Definitions section, the pair correlations in this chapter are scaled to a_{ho}, which is taken as the oscillator length of the first Jacobi coordinate of the relevant system i.e. $a_{\text{ho}} = (m_r\omega_r)^{-1/2}$.

7.2.2 Centre of Mass Energies

In previous Chapters, ground state energies E_g are quoted that do not include the centre of mass energy, as is conventional when dealing with systems where the centre of mass can be decoupled, and hence where $E_{\text{com}} = 1.5$ in all cases. This is not true for trap-imbalanced systems. As such, energies quoted in this Chapter always explicitly include the centre of mass energy.

7.3 Two-Body Trap-Imbalanced Systems

Two-body trap-imbalanced systems are considered first, which have the following general Hamiltonian:

$$H = -\frac{1}{2m_1}\nabla_1^2 - \frac{1}{2m_2}\nabla_2^2 + \frac{1}{2}m_1\omega_1^2 r_1^2 + \frac{1}{2}m_2\omega_2^2 r_2^2 + V(|r_1 - r_2|), \tag{7.3}$$

where $\mathbf{r_1}$ and $\mathbf{r_2}$ are the positions of the two particles. One naturally wonders whether the method of Busch et al. [24] can still be applied to give an analytic solution. In the case of a mass imbalance but no trap imbalance, i.e. $\omega_1 = \omega_2$, the above general Hamiltonian can be reduced to the original Hamiltonian of Eq. (4.1) by rescaling to $\mathbf{r_1}' = \sqrt{m_1}\mathbf{r_1}$ and $\mathbf{r_2}' = \sqrt{m_2}\mathbf{r_2}$, but this approach no longer works when $\omega_1 \neq \omega_2$. The next step is to try the usual transformation to Jacobi coordinates:

$$\begin{pmatrix}\mathbf{r}\\ \mathbf{R}\end{pmatrix} = \begin{pmatrix}1 & -1\\ 1/2 & 1/2\end{pmatrix}\begin{pmatrix}\mathbf{r_1}\\ \mathbf{r_2}\end{pmatrix}. \tag{7.4}$$

Applied to to Eq. (7.3), this gives:

$$H = -\frac{1}{2}\nabla_{\mathbf{r}}^2 - \frac{1}{2}\nabla_{\mathbf{R}}^2 + \frac{1}{8}(\omega_1^2+\omega_2^2)r^2 + (\omega_1^2+\omega_2^2)R^2 + \frac{1}{2}(\omega_1^2-\omega_2^2)\mathbf{r}\cdot\mathbf{R} + V(r). \tag{7.5}$$

Unlike in Eq. (4.2), a term proportional to $\mathbf{r}\cdot\mathbf{R}$ is present. This term arises naturally from any linear transformation of the Hamiltonian, but in the trap-balanced case the contributions cancel when transforming to Jacobi coordinates. This dot product term complicates the Hamiltonian significantly. Firstly, the two coordinates are no

longer separable, so the centre of mass must be included explicitly in the problem. Secondly, the dot product introduces angular structure to the problem, whereas previously the Hamiltonian depended purely on the radii r and R. This angular structure can be better understood by examining the following expansion of the dot product:

$$\mathbf{r} \cdot \mathbf{R} = \frac{4\pi}{3} rR \sum_{m=-1}^{1} \mathrm{Y}_{1m}(\hat{\mathbf{r}}) \mathrm{Y}^{*}_{1m}(\hat{\mathbf{R}}). \tag{7.6}$$

The products of spherical harmonics with $l = 1$ have the effect of coupling angular states differing by a single quantum in l_r or l_R. This angular coupling can have many effects on the physics of the system. The immediate question to ask is whether some other choice of coordinates can alleviate the problem. However, a brief examination of a general coordinate transformation reveals that any choice of coordinates that removes the dot product term will necessary introduce a term proportional to $\nabla_{\mathbf{r}} \cdot \nabla_{\mathbf{R}}$, which is equally bad or worse. Therefore, the usual Jacobi coordinates remain the most efficient choice, and ways must be found to deal with the additional complexity introduced by the dot product term.

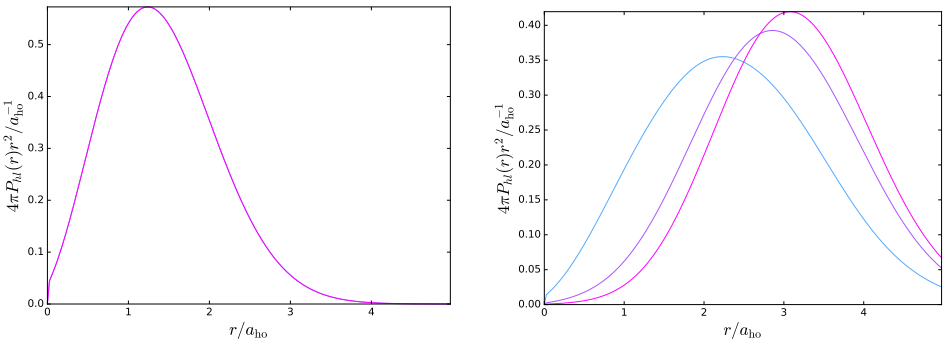

Figure 7.1: Pair correlations for two-body systems with $\kappa = 1$, $r_0 = 0.003$, $a_s \approx 10^8$ and $L_{\mathrm{total}} = 1$ (blue), 2 (purple) and 3 (pink), with $\eta = 1$ (left), and $\eta = 60.44$ (right). Note that this value of η was chosen arbitrarily from the range of values sampled. Other values exhibit the same effect but to a greater or lesser degree.

7.4 Numerical Results for Two-Body Systems

While the above dot product term makes theoretical approaches difficult, they are handled easily enough by the stochastic variational method of Chapter 3. It is these

terms that make the inclusion of different angular momentum states in the basis of Eq. (3.16) necessary. The application of the methods of Chapter 3 to this system requires the computation of some nontrivial integrals, but is ultimately manageable. The various necessary integral expressions are listed in Appendix A. It is noted that there are four key parameters that describe a two-body system, as per Eq. (7.5):

- The mass ratio κ
- The trap ratio η
- The interaction range r_0
- The total angular momentum L_{total}

In both the two- and three-body cases, these four quantities define the full parameter space which will be explored.

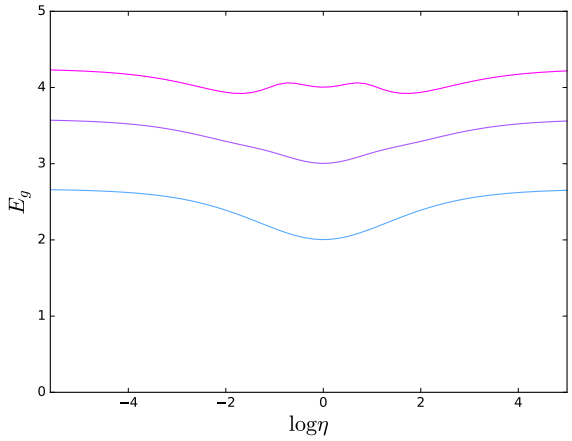

Figure 7.2: Ground state energies for a range of trap-imbalanced two-body systems with $\kappa = 1$, $r_0 = 0.003$, $a_s \approx 10^8$, and $L_{\text{total}} = 0$ (blue), 1 (purple) and 2 (pink).

7.4.1 Angular Momentum Degeneracies

As discussed, Eq. (7.6) indicates that the introduction of a trap imbalance will couple previously uncoupled angular momentum states. This is easily observed by examining the pair correlations of systems of various angular momenta and trap imbalances, as shown in Fig. 7.1. In the trap-balanced case, extra angular momentum is always placed in the centre of mass coordinate **R**, giving an energy increase

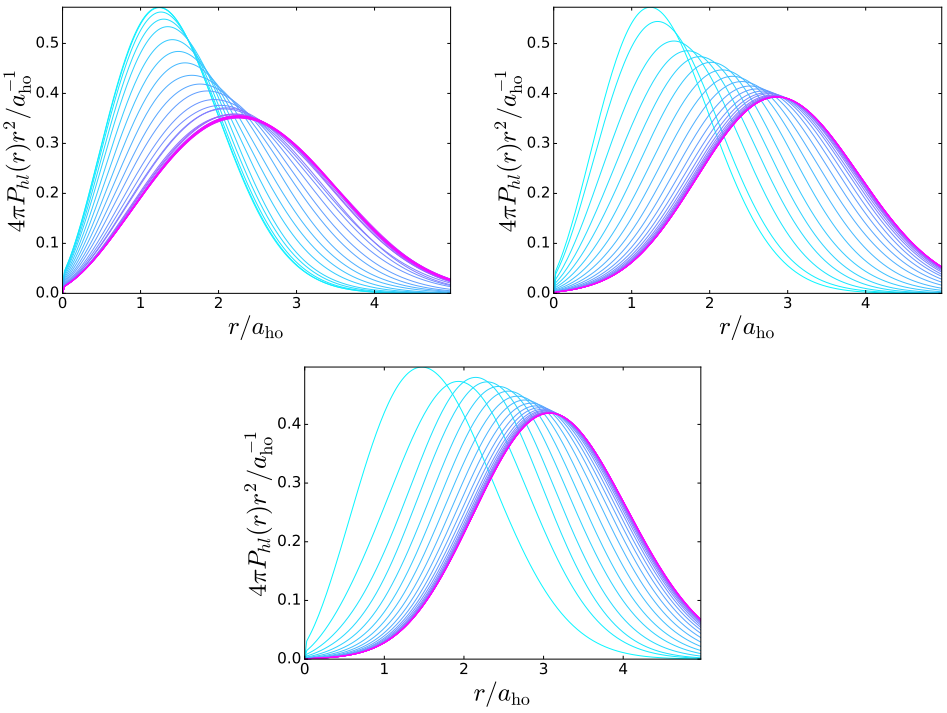

Figure 7.3: Pair correlation functions for trap-imbalanced two-body systems with $\kappa = 1$, $r_0 = 0.003$, $a_s \approx 10^8$, and $L_{\rm total} = 0$ (left), 1 (right) and 2 (bottom), with η ranging from 1.0 (light blue) to 148.4 (pink).

of unity and having no effect on the relative coordinate $\mathbf{r}$. In other words, there exists a degeneracy in the relative part of the problem, with respect to changing the total angular momentum. This is no longer the case once a trap imbalance is introduced, as the angular coupling shifts the eigenstate to some superposition of various angular states. This is difficult to quantify by examination of only the energy, as the concept of a simple angular momentum "ladder" with unity energy intervals no longer applies once a trap imbalance is included. However, the removal of the degeneracy is clearly seen when the changes in the pair correlations shown in Fig. 7.1 are examined. Whereas all three are degenerate in the $\eta = 1$ case, the trap imbalance alters them. This provides the simplest demonstration of the ability of a trap imbalance to introduce new physics to the system.

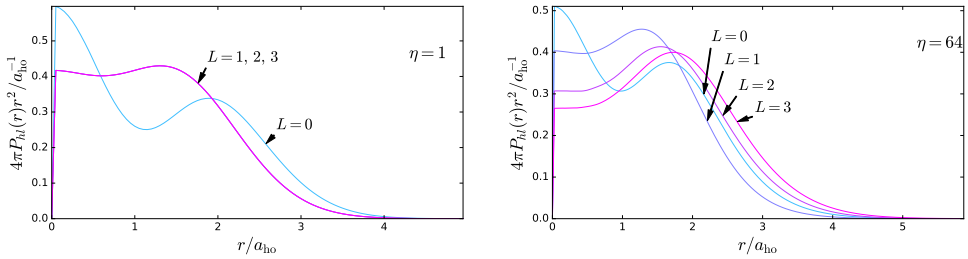

Figure 7.4: Scaled pair correlation functions for three-body systems with $\kappa = 1$, $r_0 = 0.003$, $a_s \approx 10^8$, $\eta = 1$ (left), $\eta = 64.0$ (right), and $L_{\text{total}} = 0$, 1, 2 and 3.

7.4.2 Two-Body Energy Shifts and Saturation

In this section, the energies of a large range of $\kappa = 1$ trap-imbalanced systems are examined, which are shown in Fig. 7.2. Notably, the energy saturates at extreme values of the trap imbalance. Once this limit is reached, any interplay between the interaction and trapping terms is fixed and will not change significantly with further changes in η. This is reflected in the pair correlation shown in Fig. 7.3: as the trap imbalance is turned on, the pair correlation "spreads out", before saturating, like the energy, at large values of η. This spreading of the pair correlation makes sense physically, as for large η, one atom will be trapped close to the origin, while the other will be free to move in a relatively weak trap, leading to a large mean value of the interparticle distance r. Note that Fig. 7.2 is symmetrical, as there is only a single atom of each species. In other words, for a two-body system, a trap imbalance of $\eta > 1$ is entirely equivalent to $1/\eta$. The $L_{\text{total}} = 0$ and 1 cases show a simple monotonic energy increase as the trap imbalance is turned on (see Fig. 7.2), while $L_{\text{total}} = 2$ shows a more interesting structure with an additional peak near $\eta = 1$, and an energy minimum at some finite η.

7.5 Numerical Results for Three-Body Systems

Three-body trap-imbalanced systems require similar considerations to the two-body case. As discussed, only fermionic systems in which particles 1 and 3 are identical are considered. As such, the parameter space remains the same as described in Section 7.4, except that the $\eta < 1$ cases will now be distinct, since there will be two weakly-trapped and one strongly-trapped particle, or vice-versa. The

three-body case has the following general Hamiltonian:

$$H = \sum_{i=1}^{3}\left(-\frac{1}{2m_i}\nabla_i^2 + \frac{1}{2}m_i\omega_i^2 r_i^2\right) + V(|r_1 - r_2|) + V(|r_2 - r_3|), \tag{7.7}$$

where m_i and ω_i are the ith particle's mass and trapping frequency, and the first and third particles are identical ($m_1 = m_3$, $\omega_1 = \omega_3$). The system is transformed to Jacobi coordinates using:

$$U = \begin{pmatrix} 1 & -1 & 0 & \cdots & 0 \\ \frac{m_1}{m_{12}} & \frac{m_2}{m_{12}} & -1 & \cdots & 0 \\ \vdots & \vdots & & & \vdots \\ \frac{m_1}{m_{12\cdots N-1}} & \frac{m_2}{m_{12\cdots N-1}} & \cdots & \cdots & -1 \\ \frac{m_1}{m_{12\cdots N}} & \frac{m_2}{m_{12\cdots N}} & \cdots & \cdots & \frac{m_N}{m_{12\cdots N}} \end{pmatrix}, \tag{7.8}$$

giving:

$$\begin{aligned} H = \; & -\tfrac{1}{2m_r}\nabla_r^2 + \tfrac{1}{2}m_r\omega_r^2 r^2 - \tfrac{1}{2m_\rho}\nabla_\rho^2 + \tfrac{1}{2}m_\rho\omega_\rho^2\rho^2 + \\ & \tfrac{1}{2m_R}\nabla_R^2 + \tfrac{1}{2}m_R\omega_R^2 R^2 + V(r) + V(\mathcal{P}_{13}r) + \\ & k_1\mathbf{r}\cdot\boldsymbol{\rho} + k_2\boldsymbol{\rho}\cdot\mathbf{R} + k_3\mathbf{r}\cdot\mathbf{R}, \end{aligned} \tag{7.9}$$

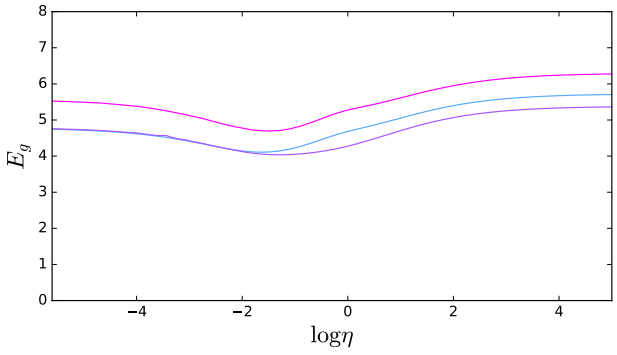

Figure 7.5: Ground state energies for a range of trap-imbalanced three-body systems ($\kappa = 1$), with $L_{\text{total}} = 0$ (blue), $L_{\text{total}} = 1$ (purple), and $L_{\text{total}} = 2$ (pink).

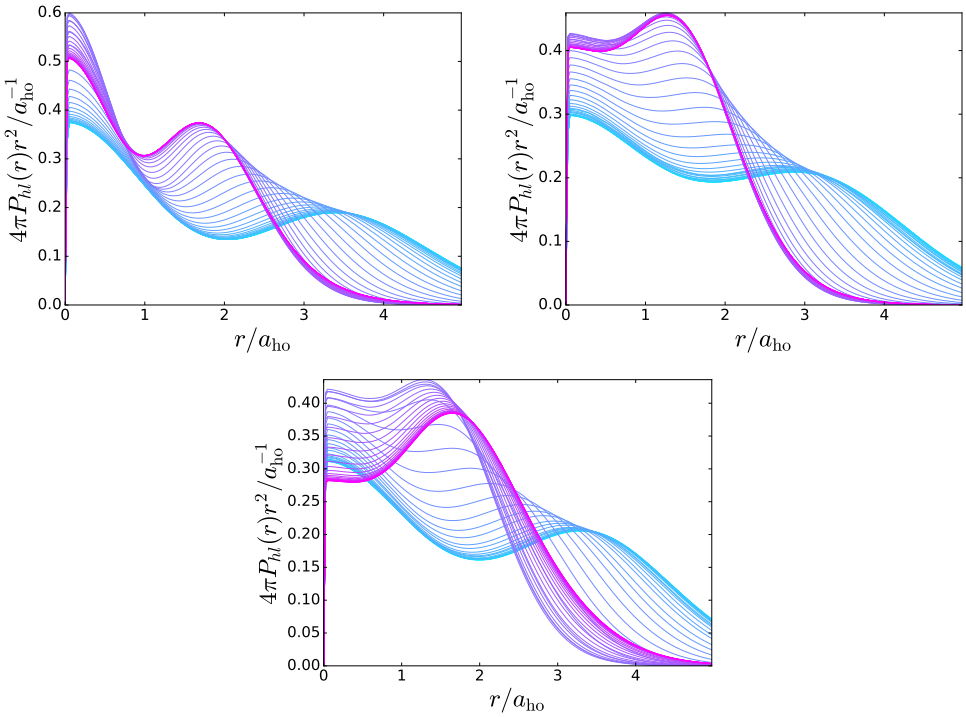

Figure 7.6: Pair correlations for a range of trap-imbalanced three-body systems with $\kappa = 1$, $r_0 = 0.003$ and $a_s \approx 10^8$. Trap imbalances range from $\eta = 0.0037$ (light blue) to $\eta = 148.4$ (pink). $L_{\rm total} = 0$ (top left), 1 (top right), and 2 (bottom centre).

where m_r, m_ρ, m_R, ω_r, ω_ρ, ω_R, k_1, k_2 and k_3 are as follows:

$$\begin{aligned}
m_r &= \frac{m_1 m_2}{m_1 + m_2}, \\
m_\rho &= \frac{m_1(m_1 + m_2)}{2m_1 + m_2}, \\
m_R &= 2m_1 + m_2, \\
\omega_r &= \sqrt{\frac{m_1\omega_1^2 + m_2\omega_2^2}{2m_1 + m_2}}, \\
\omega_R &= \sqrt{\frac{m_2\omega_1^2 + m_1\omega_2^2}{2m_1 + m_2}}, \\
k_1 &= \frac{m_1 m_2(m_1\omega_2^2 + m_2\omega_1^2)}{(m_1 + m_2)^2}, \\
k_2 &= \frac{m_1 m_2(\omega_1^2 - \omega_2^2)}{m_1 + m_2}, \\
k_3 &= \frac{m_1 m_2(\omega_1^2 - \omega_2^2)}{2m_1 + m_2}.
\end{aligned} \tag{7.10}$$

As before, the introduction of these dot products cannot be avoided by any change in coordinates.

7.5.1 Three-Body Angular Degeneracies and Saturation

As in the two-body case, the angular coupling lifts degeneracies between values of the total angular momentum L_{total}, demonstrated in Fig. 7.4. In the three-body case, the $L_{\text{total}} = 0$ state is distinct even for $\eta = 1$, so the degeneracy is only lifted for $L_{\text{total}} > 0$. A similar energy saturation effect is seen, shown in Fig. 7.5, now with the energy saturating to a low value for $\eta \ll 1$, and a much higher value for $\eta \gg 1$. Figure 7.5 is of course not symmetric like Fig. 7.2, as there are now more atoms of one species than the other.

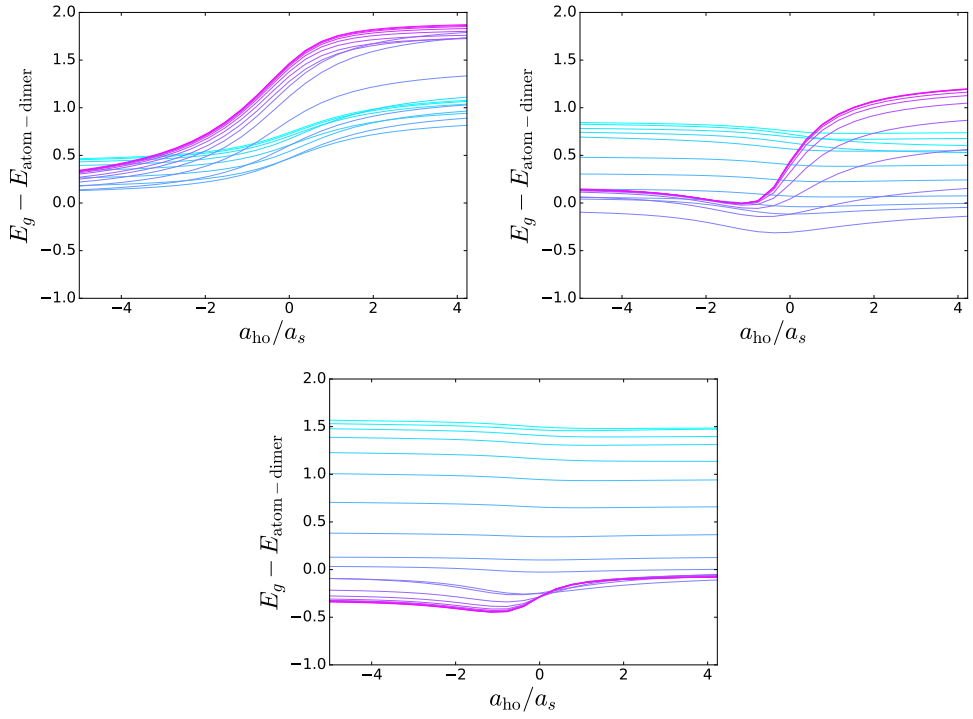

Figure 7.7: Difference between the ground state energy and atom-dimer energy spectra as a function of the inverse scattering length a_s^{-1}, for various trap imbalances and angular momenta, with $\kappa = 1$, $r_0 = 0.003$ and $a_s \approx 10^8$. Trap imbalances range from $\eta = 0.0037$ (light blue) to $\eta = 148.4$ (pink). $L_{\text{total}} = 0$ (top left), 1 (top right), and 2 (bottom centre).

Figure 7.5 has two more interesting features: firstly, there is some minimum in the energy at approximately $\log(\eta) = -1.5$. This is distinct from the two-body case, in which the trap imbalance increases the energy monotonically when $L_{\text{total}} < 2$. Secondly, the energy of the $L_{\text{total}} = 0$ and $L_{\text{total}} = 1$ become degenerate as $\log(\eta) \to -\infty$.

7.5.2 Three-Body Structural Changes

Figure 7.6 shows the pair correlations for a variety of trap imbalances, with saturation occurring for extreme values of η, as with the energy. For all values of L_{total}, there is a distinct change in the form of the pair correlation when $\eta \ll 1$, while it remains similar to the balanced case when $\eta \gg 1$. This change in the spatial structure of the wavefunction is of interest, as it indicates a physical effect beyond a shift in the energy. As discussed in Chapter 5, the ground state of the balanced three-body system can be classified as an atom-dimer state, which is reflected in the particular form of the pair correlation. Therefore, the $\eta \ll 1$ system is evidently something other than an atom-dimer state, given its noticeably different pair correlation, whereas $\eta \gg 1$ system maintains the atom-dimer state structure.

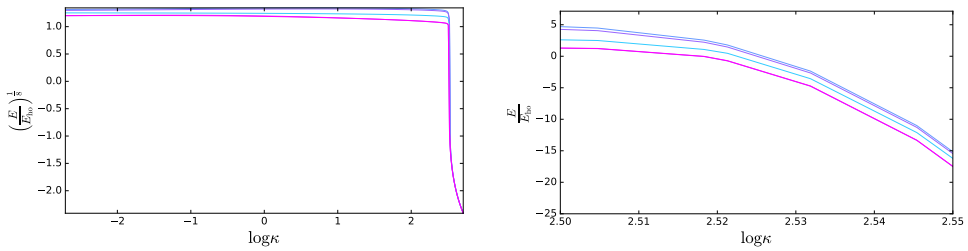

Figure 7.8: Ground state energies of three fermions ($L_{\text{total}} = 1$, $r_0 = 0.003$, $a_s \approx 10^8$), for a range of mass imbalances, and trap imbalances $\eta = \frac{1}{64}$ (blue), $\frac{1}{8}$, 1, 8, and 64 (pink). The lower graph shows a small rescaled section of the upper graph.

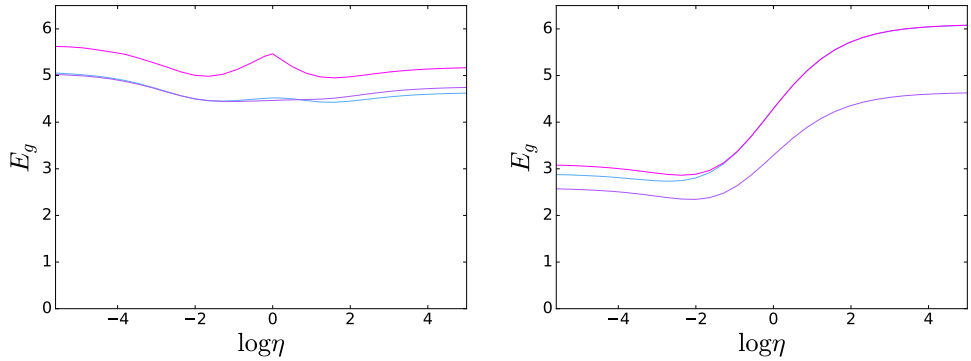

Figure 7.9: Ground state energies for a range of three-body systems ($r_0 = 0.003$, $a_s \approx 10^8$), with trap imbalances η, and mass imbalances (left) $\kappa = 0.1$ and (right) $\kappa = 10.0$. Different values of L_{total} are shown: $L_{\text{total}} = 0$ (blue), $L_{\text{total}} = 1$ (purple), and $L_{\text{total}} = 2$ (pink).

The $\eta = 1$ atom-dimer state also has a characteristic spectrum (see Fig. 5.2), in which the three-body energy is very close to the atom-dimer energy for all values of the inverse scattering length, and the two energies converge away from unitarity. Figure 7.7 shows the difference between the ground state and atom-dimer energies for various trap imbalances and different total angular momenta. In all cases, there is a significant departure from what was seen in Fig. 5.2. High values of η produce differences in the spectrum which change by a large amount across unitarity ($1/a_s = 0$), a feature which is not seen at all in the balanced cases. As $1/a_s \to -\infty$, $E_{\text{atom-dimer}}$ returns to a value close to the ground state energy. This is a fundamental similarity to the balanced case, in which a deeply-bound dimer forms in this limit, meaning that the three-body and atom-dimer states become essentially identical. $\eta < 1$ systems show distinctly different behaviour, in which a significant energy difference is maintained across the entire spectrum. This indicates a departure from atom-dimer physics that mirrors what was observed in the pair correlations of Fig. 7.6. In other words, the ground states are no longer well-approximated by the product of a dimer state and the state of an isolated atom. Instead, all three atoms are involved in a non-separable manner.

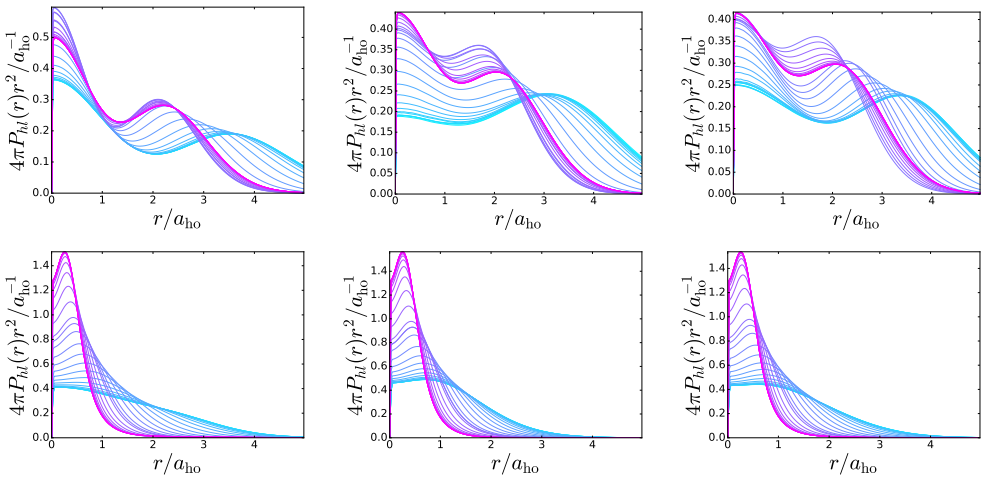

Figure 7.10: Scaled pair correlation functions with $r_0 = 0.003$ and $a_s \approx 10^8$ for a range of trap imbalances from $\eta = 0.0037$ (light blue) to $\eta = 148.4$ (pink), with mass imbalances $\kappa = 0.1$ (top row) and $\kappa = 10.0$ (bottom row), and angular momenta $L_{\rm total} = 0$ (left), $L_{\rm total} = 1$ (middle) and $L_{\rm total} = 2$ (right).

7.6 Trap-Imbalances and Deeply-Bound States

As discussed in Chapter 6, three fermions do not experience the Efimov effect and form universal bound states, except above a critical mass ratio of $\kappa \approx 13.6$. They also form non-universal bound states in the trapped case above $\kappa \approx 12.314$. Figure 7.8 demonstrates that this critical ratio has no strong dependence on the trapping ratio η. Specifically, the energy differences between different values of η do not change dramatically across the critical ratio, and that each value of η gives the same trajectory of energies with increasing κ.

This independence is to be expected for two reasons. Firstly, the deeply bound states which form above the critical ratio have very narrow spatial extents, as shown in Fig. 6.4. This means that they will not be particularly affected by a change in the shape of the trapping potential, as the state only has appreciable amplitude near the centre of the trap, where the trapping potential is small. Secondly, the Efimov effect is primarily a consequence of the kinetic energy operator, as demonstrated by its existence in the continuum case as well as the trapped one. As such, one expects the nature of the trap to have little effect. Although these two arguments suggest that bound state formation will be independent of η, they are not entirely

conclusive. Particularly, it is conceivable that the angular structure bestowed on the Hamiltonian by the trap imbalance could have some influence on borderline cases near the critical ratio. Furthermore, the trapped case exhibits non-universal bound states above the first critical ratio $\kappa = 12.314$ (see Chapter 6), which necessarily rely in some way on the trapping potential, as they do not exist in the continuum case. Therefore it remains pertinent to demonstrate this η-independence numerically in Fig. 6.4.

7.7 Trap Imbalances With Small Mass Imbalances

In the previous section, it was found that a trap imbalance has little influence on the appearance of deeply-bound trimer states above the critical ratio $\kappa \approx 12.314$. However, there are still many combinations of mass and trap imbalances outside this regime which may yield interesting physics. In this section, systems with mass imbalances $1/10 < \kappa < 10$ are examined over many values of η. The goal is to see whether the breakdown of atom-dimer physics demonstrated in Figs. 7.5, 7.6 and 7.7 occurs in a similar fashion in mass-imbalanced systems, and generally to examine whatever structural effects arise from the combination of mass and trap imbalances.

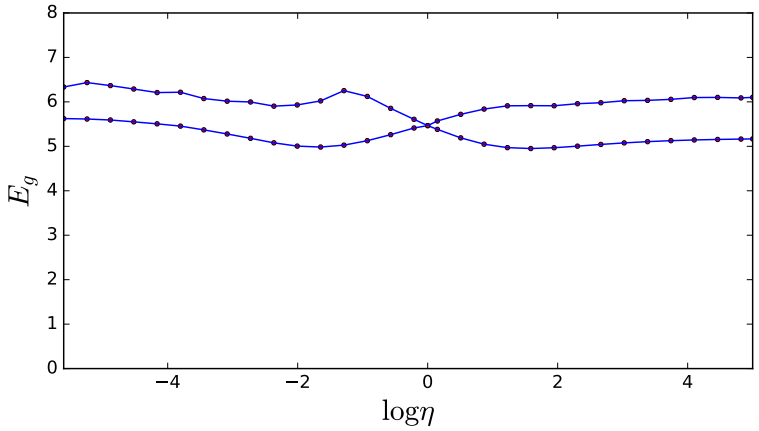

Figure 7.11: Ground and first excited state energies for three fermions with $L_{\text{total}} = 2$, $\kappa = 0.1$, $r_0 = 0.003$ and $a_s \approx 10^8$, with a range of trap imbalances. Excited states are not well-converged and serve only to demonstrate a change in which state is the ground state across $\log(\eta) = 0$.

7.7.1 Energy Shifts

In this section, energy spectra over many values of η are examined for various mass imbalances, as shown in Fig. 7.9. Large differences the mass-balanced case of Fig. 7.5 are immediately seen, with different mass imbalances giving very distinct behaviour. With mass imbalances $\kappa < 1$, the original convergence of the $L_{\text{total}} = 0$ and $L_{\text{total}} = 1$ states as $\eta \to -\infty$ is preserved, at least approximately. In other aspects, differences from the balanced case appear. Most notably, the $L_{\text{total}} = 2$ state exhibits a sharp peak in energy near $\eta = 0$. This is in fact the result of a crossing between two angular states that are degenerate at $\eta = 1$, which is demonstrated in Fig. 7.11. Secondly, the $L_{\text{total}} = 0$ state becomes the ground state as $\eta \to \infty$, unlike the balanced case where $L_{\text{total}} = 1$ remains the ground state. The $\kappa > 1$ case has less dramatic effects, with each L_{total} state showing a smooth transition from a low energy at $\eta \ll 1$ to a high energy at $\eta \gg 1$, with an additional slight dip in between. This is similar to a vertically stretched version of the original Fig. 7.5. However, the $L_{\text{total}} = 0$ and $L_{\text{total}} = 2$ now become degenerate for $\eta \gg 1$, an entirely different degeneracy to the balanced case.

These effects are reflected in the pair correlation. Figure 7.10 shows all pair correlations taking roughly the same shape for the $\kappa > 1$ case. This indicates a relative homogeneity in their response to trap imbalances, as seen in Fig. 7.9

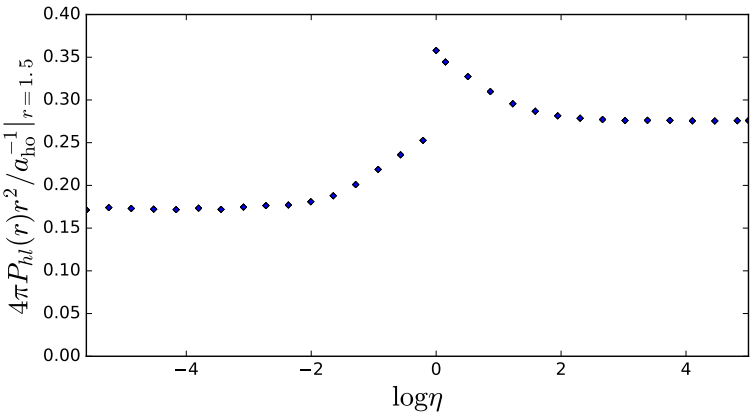

Figure 7.12: Value of the pair correlation at the specific point $r = 1.5$ with $\kappa = 0.1$, $r_0 = 0.003$ and $a_s \approx 10^8$, for various trap imbalances η, showing a sharp discontinuity near $\eta = 1$.

i.e. the radial wavefunctions are highly similar, with differences arising only in the angular structure. This idea fits with the expectation that as $\kappa \to 12.314$, the system necessarily approaches the same deeply-bound (Efimovian or otherwise) state in all cases, as argued in the previous section. Conversely, there are much greater structural differences for $\kappa < 1$. The $L_{\text{total}} = 2$ case is of the most interest. Corresponding to the sharp energy peak at $L_{\text{total}} = 0$ seen in Fig. 7.9, a very rapid transition appears between two radial structures. This can be inferred by noting the "gap" between lines as one moves from purple to blue in the top right of Fig. 7.9, whereas in other sub-figures there is a relatively homogeneous distribution of lines. Figure 7.12 highlights this by showing the discontinuous change in the value of the pair correlation at a specific value of r across $\eta = 1$.

7.8 Conclusion

In this Chapter, a variety of new results for trap and mass-imbalanced two- and three-fermion systems have been explored. It has been demonstrated that trap imbalances remove angular degeneracies, both structural and energetic, in the relative wavefunction. The dependence of the ground state energy on the trap imbalance has been examined extensively, revealing an energy minimum at a non-unity value of η for three equal-mass fermions. It has also been shown that a trap imbalance can significantly change the structural properties of the ground state. In particular, it can change the usual three-body atom-dimer state into a distinctly different loosely-bound trimer state. Finally, it has been found that trap imbalances have little influence on the formation of non-universal deeply-bound trimers above the critical mass ratio $\kappa = 12.314$. This makes sense physically, as these states are concentrated at the centre of the trap, where changes in the trapping potential will have little influence. These results indicate that trap imbalances can significantly change the few-body physics of a system, both energetically and structurally, which could offer new means to tune and control heteronuclear experiments.

Chapter 8

Conclusion

In this thesis, the fundamentals as well as various specific areas of few-body interactions in trapped ultracold atomic gases have been explored. The particular focus has been heteronuclear systems, in which the different masses and/or trapping frequencies of two atomic species can give rise to profound changes in few-body scattering, as exemplified by Efimov states and other deeply-bound states.

In Chapter 2, the theory of low-energy scattering processes, which are fundamental to most ultracold atomic systems, was reviewed. For the low-energy scattering processes found in ultracold gases, this theory leads to the concept of universality, in which the scattering length a_s becomes the only parameter necessary to describe the system's interaction. Feshbach resonances were also reviewed, which allow a_s to be tuned experimentally to virtually any desired value.

In Chapter 3, an implementation of the stochastic variational method was developed, which is a powerful numerical technique that has been used extensively in nuclear, atomic and molecular quantum systems. Unlike most, my implementation explicitly includes the centre of mass, as well as arbitrary angular basis states specified by coupled spherical harmonics. These extensions allow the method to be used on trap-imbalanced systems, which couple the centre of mass to the other Jacobi coordinates — an effect not found in most few-body systems.

In Chapters 4 and 5, based on the theory of Chapter 2, existing analytic results on homonuclear two- and three-body scattering were explored. These are the most fundamental few-body systems, and were used as a testing ground for my code.

In Chapter 6, the history and physics of the Efimov state were explored. The

Efimov effect occurs naturally in homonuclear bosonic systems, but not in fermionic ones. However, heteronuclear fermionic systems with a mass ratio above the critical 13.316 experience the full effect of Efimov physics. Efimov states have a variety of remarkable properties. In principle, they become unbounded in number as the system approaches unitarity. Furthermore, they form a curious geometric progression, with each successive state having a binding energy approximately 22.7^2 times smaller than the last, while having an identical geometry rescaled by the same (unsquared) factor of 22.7. In the harmonically trapped case, the three-Fermion system also exhibits the formation of non-universal bound states above a lower critical mass ratio of approximately 12.314. Known results on this phenomenon were used to provide a more rigourous test of the numerical methods of Chapter 3.

In Chapter 7, various new results on the relatively unexplored few-body scattering of trap-imbalanced systems were presented. In trap-imbalanced systems, two atomic species experience different harmonic trapping frequencies, as well as potentially different masses. The original premise of this research was to examine how a trap-imbalance could effect the formation of deeply-bound states in a three-Fermion system — in particular, whether the imbalance would have an effect on the critical mass ratio 12.314. It was ultimately demonstrated that the trap imbalance has no discernible effect on the critical ratio. These results build on earlier work by Blume and Daily, which examined trap-imbalanced systems below the critical ratio [14], as well as trap-balanced systems above and below the critical ratio [15, 16, 18, 32]. This thesis contains the first examination of trap imbalances above the critical ratio, in addition to a number of other new results.

Following this, other structural and energetic changes that arise from trap imbalances were explored extensively. Firstly, the imbalance lifts degeneracies between various angular states of the system, due to its introduction of an anisotropy to the Hamiltonian in Jacobi coordinates. Furthermore, the effect of the imbalance saturates above trapping ratios in the region of 150, meaning that further increasing the imbalance has no additional effect on the system.

In the homonuclear case, a two-component three-Fermion system typically forms an atom-dimer state, in which two unlike atoms form a deeply-bound dimer, while the third exists as a discrete atom (more accurately, the two like atoms exist in a superposition of these two scenarios, due to antisymmetry). It was demonstrated that the trap imbalance can significantly change this picture, leading to

loosely-bound trimer states in which all three atoms play a significant role. The effects of various combinations of trap and mass imbalances were also examined. In some cases, this leads to the interesting effect of two different states serving as the ground state, depending on the direction of the trap imbalance (i.e. whether the two like particles are strongly trapped or weakly trapped relative to the unlike particle). This effect is not seen in any trap-balanced system.

These results hint at exciting new possibilites in heteronuclear and other exotic cold gas experiments. Trap imbalances have a strong effect on the energetic and structural properties of few-body systems, while leaving some aspects (i.e. the formation of deeply-bound states) unaffected. Since trapping potentials can readily be tuned in real time in an experiment, there is the possibility of using the trap imbalance as a means of tuning and controlling a heteronuclear system, in addition to the various techniques that are already available. These results could also be realised in future few-body experiments, as well as in optical lattices (whether in isolated sites, or in many-body dynamics across the lattice). In these cases, the results provide a fundamental description of the types of behaviour that may occur in these experiments.

Appendix A: Integral Formulae

Here various integral formulae are listed, the purpose of which is to reduce the matrix elements of Eq. (3.6) Eq. (3.7) from integrals over coordinate space to algebraic expressions that can easily be calculated by a computer. In all cases, S_{ij} and H_{ij} can be expressed as linear combinations of these formulae.

Definitions

- $\langle l_1 m_1 l_2 m_2 | l_3 m_3 \rangle$ denotes a Clebsch-Gordan coefficient
- $i_l(r)$ is the modified spherical Bessel function of the first kind
- $E^{l_1 l_2 l_{12} l_3 l_4 l_{34} L}_{l_{13} l_{24}}$ is defined as per Eq. (3.33).

Basis States

As detailed in Chapter 3 and Eq. (3.16), a general basis state $|\beta\rangle$ in the variational scheme can be specified as

$$|\beta\rangle = (a, b, c, \delta, l_r, n_r, l_\rho, n_\rho, l_{\text{coup}}, l_R), \tag{8.1}$$

where a, b and c are the Gaussian widths of the three Jacobi coordinates, δ is the off-diagonal Gaussian coefficient of $\mathbf{r} \cdot \boldsymbol{\rho}$, and the remaining quantities specify the angular state. Similarly, an arbitrary two-body basis state $|\beta\rangle$ is specified by

$$|\beta\rangle = (a, c, l_r, l_R), \tag{8.2}$$

where the centre of mass width continues to be labelled as c. All states are coupled to the system's total angular momentum L_{total}, which is shortened to L in this

Appendix. The system's total magnetic quantum number M_{total} is taken to be zero in all cases, as it has no effect on the system's physics. The following integrals are also defined for brevity:

$$\mathcal{I}(a,n) = \int_0^\infty r^n \exp\left(-\frac{1}{2}ar^2\right)dr = \frac{\Gamma(\frac{n+1}{2})}{2\left(\frac{a}{3}\right)^{\frac{n+1}{2}}}, \tag{8.3}$$

$$\begin{aligned}\mathcal{K}(\nu,n,l,u,v,w) &= \int_0^\infty\int_0^\infty x^{2\nu+l+2}y^{2n+l+2}e^{-\frac{1}{2}ux^2-\frac{1}{2}vy^2}i_l(|w|xy)dx\,dy \\ &= \sqrt{\frac{\pi}{8}}(2n)!!\Gamma\left(n+l+\frac{3}{2}\right)\frac{|w|^l}{u^{n+l+\frac{3}{2}}} \\ &\quad\times\sum_{k=0}\frac{\Gamma(k+\nu+l+\frac{3}{2}}{k!(n-k_1\Gamma(k+l+\frac{3}{2})}\end{aligned} \tag{8.4}$$

$$\begin{aligned}&\mathcal{Z}(l_1,m_1,l_2,m_2,a,m_a,b,m_b) \\ &\quad= \sum_m\frac{4\pi}{3}(-1)^{m_a+m_b+m} \\ &\quad\times\int_1 \mathrm{Y}_{l_1m_1}\mathrm{Y}_{am_a}\mathrm{Y}_{1m}d\hat{\mathbf{r}}\int\mathrm{Y}_{l_2m_2}\mathrm{Y}_{bm_b}\mathrm{Y}_{1\text{-}m}d\hat{\boldsymbol{\rho}} \\ &\quad= \sum_m(-1)^m\langle a\ 0\ 1\ 0|l_1\ 0\rangle\langle b\ 0\ 1\ 0|l_2\ 0\rangle \\ &\quad\times\langle l_1\ m_1\ 1\ m|a\ m_a\rangle\langle l_2\ m_2\ 1\ \text{-}m|b\ m_b\rangle\end{aligned} \tag{8.5}$$

Two-Body Integrals

Overlap

$$S_{ij} = \langle\beta'|\beta\rangle = \mathcal{I}(2l_r+2,a+a')\,\mathcal{I}(2l_R+2,c+c')\delta_{l_rl_r'}\delta_{l_Rl_R'} \tag{8.6}$$

Hamiltonian Components

$$\langle\beta'|r^2|\beta\rangle = \mathcal{I}(2l_r+4,a+a')\,\mathcal{I}(2l_R+2,c+c')\delta_{l_rl_r'}\delta_{l_Rl_R'} \tag{8.7}$$

$$\langle\beta'|R^2|\beta\rangle = \mathcal{I}(2l_r+2,a+a')\,\mathcal{I}(2l_R+4,c+c')\delta_{l_rl_r'}\delta_{l_Rl_R'} \tag{8.8}$$

$$\begin{aligned}\langle\beta'|\nabla_r^2|\beta\rangle &= a[a\mathcal{I}(2l_r+4,a+a') - (2l_r+3)\mathcal{I}(2l_r+2,a+a')] \\ &\quad \times \mathcal{I}(2l_R+2,c+c')\delta_{l_r l_r'}\delta_{l_R l_R'} \end{aligned} \tag{8.9}$$

$$\begin{aligned}\langle\beta'|\nabla_R^2|\beta\rangle &= \mathcal{I}(2l_r+2,a+a')\times c[c\mathcal{I}(2l_R+4,c+c') \\ &\quad -(2l_R+3)\mathcal{I}(2l_R+2,c+c')]\delta_{l_r l_r'}\delta_{l_R l_R'} \end{aligned} \tag{8.10}$$

$$\begin{aligned}\langle\beta'|\mathbf{r}\cdot\mathbf{R}|\beta\rangle &= \mathcal{I}(l_r+l_r'+3,a+a')\ \mathcal{I}(l_R+l_R'+3,c+c') \\ &\quad \times \mathcal{Z}(l_r,m_r,l_R,m_R,l_r',m_r',l_R',m_R') \end{aligned} \tag{8.11}$$

$$\langle\beta'|\exp(-r^2/2r_0^2)|\beta\rangle = \mathcal{I}(2l_r+2,a+a'+1/r_0^2)\ \mathcal{I}(2l_R+2,c+c')\delta_{l_R l_R'} \tag{8.12}$$

Three-Body Integrals

Overlap

$$\begin{aligned} S_{ij} &= \langle\beta'|\beta\rangle \\ &= 4\pi\ \mathcal{I}(2l_R+2,c+c')\delta_{l_R l_R'} \\ &\quad \times \sum_{\bar\alpha}\mathcal{B}(\alpha,\bar\alpha)\sum_{\kappa}\sqrt{2\kappa+1}\epsilon(\kappa,\omega)E^{\kappa\kappa 0 l_r' l_\rho' LL}_{\bar l_r \bar l_\rho} \\ &\quad \times \mathcal{K}\left(\bar n_r + n_r' + \frac{\bar l_r + l_r' - \kappa}{2},\right. \\ &\qquad \left. \bar n_\rho + n_\rho' + \frac{\bar l_\rho + l_\rho' - \kappa}{2}, \kappa, \bar a + a', \bar b + b', \bar c + c'\right) \end{aligned} \tag{8.13}$$

Hamiltonian Elements

$$\begin{aligned}\langle\beta'|e^{-\frac{r^2}{2r_0^2}}|\beta\rangle &= \langle\beta'|\beta\rangle \\ &= 4\pi\ \mathcal{I}(2l_R+2,c+c')\delta_{l_R l'_R} \\ &\quad\times\sum_{\bar\alpha}\mathcal{B}(\alpha,\bar\alpha)\sum_{\kappa}\sqrt{2\kappa+1}\epsilon(\kappa,\omega)E^{\kappa\kappa 0 l'_r l'_\rho LL}_{\bar l_r \bar l_\rho} \\ &\quad\times\mathcal{K}\Bigg(\bar n_r+n'_r+\frac{\bar l_r+l'_r-\kappa}{2}, \\ &\qquad\bar n_\rho+n'_\rho+\frac{\bar l_\rho+l'_\rho-\kappa}{2},\kappa,\bar a+a'+\frac{1}{r_0^2},\bar b+b',\bar c+c'\Bigg)\end{aligned} \tag{8.14}$$

$$\begin{aligned}\langle\beta'|\nabla_r^2|\beta\rangle &= -a'(3+2l_r)\langle\beta'|\beta\rangle \\ &\quad+4\pi a'^2\ \mathcal{I}(2l_R+2,c+c')\delta_{l_R l'_R} \\ &\quad\times\sum_{\bar\alpha}\mathcal{B}(\alpha,\bar\alpha)\sum_{\kappa}\sqrt{2\kappa+1}\epsilon(\kappa,\omega)E^{\kappa\kappa 0 l'_r l'_\rho LL}_{\bar l_r \bar l_\rho} \\ &\quad\times\mathcal{K}\Bigg(\bar n_r+n'_r+\frac{\bar l_r+l'_r-\kappa}{2}+2, \\ &\qquad\bar n_\rho+n'_\rho+\frac{\bar l_\rho+l'_\rho-\kappa}{2},\kappa,\bar a+a',\bar b+b',\bar c+c'\Bigg)\end{aligned} \tag{8.15}$$

$$\begin{aligned}\langle\beta'|\nabla_\rho^2|\beta\rangle &= -b'(3+2l_\rho)\langle\beta'|\beta\rangle \\ &\quad+4\pi b'^2\ \mathcal{I}(2l_R+2,c+c')\delta_{l_R l'_R} \\ &\quad\times\sum_{\bar\alpha}\mathcal{B}(\alpha,\bar\alpha)\sum_{\kappa}\sqrt{2\kappa+1}\epsilon(\kappa,\omega)E^{\kappa\kappa 0 l'_r l'_\rho LL}_{\bar l_r \bar l_\rho} \\ &\quad\times\mathcal{K}\Bigg(\bar n_r+n'_r+\frac{\bar l_r+l'_r-\kappa}{2}, \\ &\qquad\bar n_\rho+n'_\rho+\frac{\bar l_\rho+l'_\rho-\kappa}{2}+2,\kappa,\bar a+a',\bar b+b',\bar c+c'\Bigg)\end{aligned} \tag{8.16}$$

$$\begin{aligned}\langle\beta'|\nabla_R^2|\beta\rangle &= -c'(3+2l_R)\langle\beta'|\beta\rangle \\ &\quad + 4\pi {c'}^2\ \mathcal{I}(2l_R+4, c+c')\delta_{l_R l'_R} \\ &\quad \times \sum_{\bar\alpha}\mathcal{B}(\alpha,\bar\alpha)\sum_{\kappa}\sqrt{2\kappa+1}\epsilon(\kappa,\omega)E^{\kappa\kappa 0 l'_r l'_\rho LL}_{\bar l_r \bar l_\rho} \\ &\quad \times \mathcal{K}\Bigg(\bar n_r + n'_r + \frac{\bar l_r + l'_r - \kappa}{2}, \\ &\qquad \bar n_\rho + n'_\rho + \frac{\bar l_\rho + l'_\rho - \kappa}{2}, \kappa, \bar a + a', \bar b + b', \bar c + c'\Bigg) \end{aligned} \tag{8.17}$$

$$\begin{aligned}\langle\beta'|r^x\rho^y R^z|\beta\rangle &= 4\pi\ \mathcal{I}(z+2l_R+2, c+c')\delta_{l_R l'_R} \\ &\quad \times \sum_{\bar\alpha}\mathcal{B}(\alpha,\bar\alpha)\sum_{\kappa}\sqrt{2\kappa+1}\epsilon(\kappa,\omega)E^{\kappa\kappa 0 l'_r l'_\rho LL}_{\bar l_r \bar l_\rho} \\ &\quad \times \mathcal{K}\Bigg(\frac{x}{2} + \bar n_r + n'_r + \frac{\bar l_r + l'_r - \kappa}{2}, \\ &\qquad \frac{y}{2} + \bar n_\rho + n'_\rho + \frac{\bar l_\rho + l'_\rho - \kappa}{2}, \kappa, \bar a + a', \bar b + b', \bar c + c'\Bigg) \end{aligned} \tag{8.18}$$

$$\begin{aligned}\langle\beta'|\mathbf{r}\cdot\boldsymbol{\rho}|\beta\rangle &= 4\pi\ \mathcal{I}(2l_R+2, c+c')\delta_{l_R l'_R} \\ &\quad \times \sum_{\bar\alpha}\mathcal{B}(\alpha,\bar\alpha)\sum_{\kappa}\sqrt{2\kappa+1}\epsilon(\kappa,\omega) \\ &\quad \times \sum_{a\ b}\sum_{\substack{\bar m_r\ \bar m_\rho \\ m_a\ m_b}} E^{\kappa\kappa 0 l'_r l'_\rho LL}_{ab}\langle \bar l_r\ \bar m_r\ \bar l_\rho\ \bar m_\rho | l_{\rm coup}\ m_{\rm coup}\rangle\langle a\ m_a\ b\ m_b | l_{\rm coup}\ m_{\rm coup}\rangle \\ &\quad \times \mathcal{Z}(\bar l_r, \bar m_r, \bar l_\rho, \bar m_\rho, a, m_a, b, m_b) \\ &\quad \times \mathcal{K}\Bigg(\bar n_r + n'_r + \frac{\bar l_r + l'_r - \kappa + 1}{2}, \\ &\qquad \bar n_\rho + n'_\rho + \frac{\bar l_\rho + l'_\rho - \kappa + 1}{2}, \kappa, \bar a + a', \bar b + b', \bar c + c'\Bigg) \end{aligned} \tag{8.19}$$

$$
\begin{aligned}
\langle\beta'|\mathbf{r}\cdot\mathbf{R}|\beta\rangle \;=\;& 4\pi\,\mathcal{I}(2l_R+3,c+c') \\
&\times\sum_{\bar\alpha}\mathcal{B}(\alpha,\bar\alpha)\sum_{\kappa}\sqrt{2\kappa+1}\epsilon(\kappa,\omega) \\
&\times\sum_{a}\sum_{\substack{\bar m_r\,\bar m_a\\ m_R\,m'_R}} E^{\kappa\kappa 0 l'_r l'_\rho LL}_{a\bar l_\rho} \\
&\times\langle\bar l_r\;\bar m_r\;\bar l_\rho\;\text{-}(m_R+\bar m_r)|l_{\text{coup}}\;\text{-}m_r\rangle\langle a\;m_a\;\bar l_\rho\;\text{-}(m'_r+m_a)|l'_{\text{coup}}\;\text{-}m'_r\rangle \\
&\times\langle l_{\text{coup}}\;\text{-}m_R\;l_R\;m_R|L\;0\rangle\langle l'_{\text{coup}}\;\text{-}m'_r\;l'_R\;m'_R|L\;0\rangle \\
&\times\mathcal{Z}(\bar l_r,\bar m_r,l_R,m_R,a,m_a,l'_R,m'_R) \\
&\times\mathcal{K}\Bigg(\bar n_r+n'_r+\frac{\bar l_r+l'_r-\kappa+1}{2}, \\
&\qquad\bar n_\rho+n'_\rho+\frac{\bar l_\rho+l'_\rho-\kappa}{2},\kappa,\bar a+a',\bar b+b',\bar c+c'\Bigg)
\end{aligned}
\tag{8.20}
$$

$$
\begin{aligned}
\langle\beta'|\boldsymbol{\rho}\cdot\mathbf{R}|\beta\rangle \;=\;& 4\pi\,\mathcal{I}(2l_R+3,c+c') \\
&\times\sum_{\bar\alpha}\mathcal{B}(\alpha,\bar\alpha)\sum_{\kappa}\sqrt{2\kappa+1}\epsilon(\kappa,\omega) \\
&\times\sum_{a}\sum_{\substack{\bar m_r\,\bar m_a\\ m_R\,m'_R}} E^{\kappa\kappa 0 l'_r l'_\rho LL}_{a\bar l_\rho} \\
&\times\langle\bar l_r\;\text{-}(m_R+\bar m_r)\;\bar l_\rho\;\bar m_\rho|l_{\text{coup}}\;\text{-}m_r\rangle\langle\bar l_r\;\text{-}(m_R+\bar m_r)\;b\;m_b|l'_{\text{coup}}\;\text{-}m'_r\rangle \\
&\times\langle l_{\text{coup}}\;\text{-}m_R\;l_R\;m_R|L\;0\rangle\langle l'_{\text{coup}}\;\text{-}m'_r\;l'_R\;m'_R|L\;0\rangle \\
&\times\mathcal{Z}(\bar l_\rho,\bar m_\rho,l_R,m_R,b,m_b,l'_R,m'_R) \\
&\times\mathcal{K}\Bigg(\bar n_r+n'_r+\frac{\bar l_r+l'_r-\kappa}{2}, \\
&\qquad\bar n_\rho+n'_\rho+\frac{\bar l_\rho+l'_\rho-\kappa+1}{2},\kappa,\bar a+a',\bar b+b',\bar c+c'\Bigg)
\end{aligned}
\tag{8.21}
$$

Bibliography

[1] J. Abo-Shaeer, C. Raman, J. Vogels and W. Ketterle, 'Observation of vortex lattices in bose-einstein condensates,' *Science* **292**, 476 (2001).

[2] M. Abramowitz and I. A. Stegun, *Handbook of mathematical functions: with formulas, graphs, and mathematical tables*, 55 (Courier Corporation, 1964).

[3] R. Amado and F. Greenwood, 'There is no efimov effect for four or more particles,' *Physical Review D* **7**, 2517 (1973).

[4] R. Amado and J. Noble, 'Efimov's effect: A new pathology of three-particle systems. ii,' *Physical Review D* **5**, 1992 (1972).

[5] M. H. Anderson, J. R. Ensher, M. R. Matthews, C. E. Wieman and E. A. Cornell, 'Observation of bose-einstein condensation in a dilute atomic vapor,' *science* **269**, 198 (1995).

[6] M. Baranov, M. Dalmonte, G. Pupillo and P. Zoller, 'Condensed matter theory of dipolar quantum gases,' *Chemical Reviews* **112**, 5012 (2012).

[7] J. Bardeen, L. N. Cooper and J. R. Schrieffer, 'Theory of superconductivity,' *Physical Review* **108**, 1175 (1957).

[8] G. Barontini, C. Weber, F. Rabatti, J. Catani, G. Thalhammer, M. Inguscio and F. Minardi, 'Observation of heteronuclear atomic efimov resonances,' *Physical review letters* **103**, 043201 (2009).

[9] P. F. Bedaque, E. Braaten and H.-W. Hammer, 'Three-body recombination in bose gases with large scattering length,' *Physical Review Letters* **85**, 908 (2000).

[10] M. Berninger, A. Zenesini, B. Huang, W. Harm, H.-C. Nägerl, F. Ferlaino, R. Grimm, P. Julienne and J. Hutson, 'Universality of the three-body parameter for efimov states in ultracold cesium,' *Physical Review Letters* **107**, 120401 (2011).

[11] H. Bethe and R. Peierls, 'Quantum theory of the diplon,' *Proceedings of the Royal Society of London. Series A, Mathematical and Physical Sciences* **148**, 146 (1935).

[12] S. Blinder, 'Propagators from integral representations of greens functions for the n-dimensional free-particle, harmonic oscillator and coulomb problems,' *Journal of mathematical physics* **25**, 905 (1984).

[13] I. Bloch, J. Dalibard and S. Nascimbène, 'Quantum simulations with ultracold quantum gases,' *Nature Physics* **8**, 267 (2012).

[14] D. Blume, 'Small mass-and trap-imbalanced two-component fermi systems,' *Physical Review A* **78**, 013613 (2008).

[15] D. Blume, 'Few-body physics with ultracold atomic and molecular systems in traps,' *Reports on Progress in Physics* **75**, 046401 (2012).

[16] D. Blume, 'Efimov physics and the three-body parameter for shallow van der waals potentials,' *Few-Body Systems* pp. 1–9 (2015).

[17] D. Blume and K. Daily, 'Breakdown of universality for unequal-mass fermi gases with infinite scattering length,' *Physical review letters* **105**, 170403 (2010).

[18] D. Blume and K. Daily, 'Few-body resonances of unequal-mass systems with infinite interspecies two-body s-wave scattering length,' *Physical Review A* **82**, 063612 (2010).

[19] S. N. Bose, 'Plancks gesetz und lichtquantenhypothese,' *Z. phys* **26**, 178 (1924).

[20] T. Bourdel, J. Cubizolles, L. Khaykovich, K. Magalhaes, S. Kokkelmans, G. Shlyapnikov and C. Salomon, 'Measurement of the interaction energy

near a feshbach resonance in a l i 6 fermi gas,' *Physical review letters* **91**, 020402 (2003).

[21] E. Braaten and H.-W. Hammer, 'Three-body recombination into deep bound states in a bose gas with large scattering length,' *Physical Review Letters* **87**, 160407 (2001).

[22] C. C. Bradley, C. Sackett, J. Tollett and R. G. Hulet, 'Evidence of bose-einstein condensation in an atomic gas with attractive interactions,' *Physical Review Letters* **75**, 1687 (1995).

[23] S. Burger, K. Bongs, S. Dettmer, W. Ertmer, K. Sengstock, A. Sanpera, G. Shlyapnikov and M. Lewenstein, 'Dark solitons in bose-einstein condensates,' *Physical Review Letters* **83**, 5198 (1999).

[24] T. Busch, B.-G. Englert, K. Rzażewski and M. Wilkens, 'Two cold atoms in a harmonic trap,' *Foundations of Physics* **28**, 549 (1998).

[25] Q. Chen, J. Stajic, S. Tan and K. Levin, 'Bcs–bec crossover: From high temperature superconductors to ultracold superfluids,' *Physics Reports* **412**, 1 (2005).

[26] C. Chin, R. Grimm, P. Julienne and E. Tiesinga, 'Feshbach resonances in ultracold gases,' *Reviews of Modern Physics* **82**, 1225 (2010).

[27] S. Chu, 'Laser manipulation of atoms and particles,' *Science* **253**, 861 (1991).

[28] S. Chu, C. Cohen-Tannoudji and W. Phillips, 'Nobel lectures in physics 1997,' *Rev. Mod. Phys* **70**, 685 (1998).

[29] N. R. Cooper, 'Rapidly rotating atomic gases,' *Advances in Physics* **57**, 539 (2008).

[30] E. A. Cornell and C. E. Wieman, 'Nobel lecture: Bose-einstein condensation in a dilute gas, the first 70 years and some recent experiments,' *Reviews of Modern Physics* **74**, 875 (2002).

[31] S. L. Cornish, N. R. Claussen, J. L. Roberts, E. A. Cornell and C. E. Wieman, 'Stable 85 rb bose-einstein condensates with widely tunable interactions,' *Physical Review Letters* **85**, 1795 (2000).

[32] K. Daily and D. Blume, 'Energy spectrum of harmonically trapped two-component fermi gases: Three-and four-particle problem,' *Physical Review A* **81**, 053615 (2010).

[33] K. B. Davis, M.-O. Mewes, M. R. Andrews, N. Van Druten, D. Durfee, D. Kurn and W. Ketterle, 'Bose-einstein condensation in a gas of sodium atoms,' *Physical review letters* **75**, 3969 (1995).

[34] B. DeMarco and D. S. Jin, 'Onset of fermi degeneracy in a trapped atomic gas,' *Science* **285**, 1703 (1999).

[35] F. Deuretzbacher, K. Plassmeier, D. Pfannkuche, F. Werner, C. Ospelkaus, S. Ospelkaus, K. Sengstock and K. Bongs, 'Heteronuclear molecules in an optical lattice: Theory and experiment,' *Phys. Rev. A* **77**, 032726 (2008).

[36] M. Drechsler and W. Zwerger, 'Crossover from bcs-superconductivity to bose-condensation,' *Annalen der Physik* **504**, 15 (1992).

[37] S. Dutta, J. Lorenz, A. Altaf, D. S. Elliott and Y. P. Chen, 'Photoassociation of ultracold lirb* molecules: Observation of high efficiency and unitarity-limited rate saturation,' *Phys. Rev. A* **89**, 020702 (2014).

[38] P. Dyke, E. Kuhnle, S. Whitlock, H. Hu, M. Mark, S. Hoinka, M. Lingham, P. Hannaford and C. Vale, 'Crossover from 2d to 3d in a weakly interacting fermi gas,' *Physical review letters* **106**, 105304 (2011).

[39] J. DIncao, J. Von Stecher and C. H. Greene, 'Universal four-boson states in ultracold molecular gases: Resonant effects in dimer-dimer collisions,' *Physical review letters* **103**, 033004 (2009).

[40] V. Efimov, 'Energy levels arising from resonant two-body forces in a three-body system,' *Physics Letters B* **33**, 563 (1970).

[41] V. Efimov, 'Low-energy properties of three resonantly interacting particles,' *Sov. J. Nucl. Phys* **29**, 546 (1979).

[42] A. Einstein, *Einheitliche Feldtheorie von Gravitation und Elektrizität* (Wiley Online Library, 1925).

[43] B. Esry, C. H. Greene and J. P. Burke Jr, 'Recombination of three atoms in the ultracold limit,' *Physical Review Letters* **83**, 1751 (1999).

[44] U. Fano, 'Sullo spettro di assorbimento dei gas nobili presso il limite dello spettro darco,' *Il Nuovo Cimento (1924-1942)* **12**, 154 (1935).

[45] U. Fano, 'Effects of configuration interaction on intensities and phase shifts,' *Physical Review* **124**, 1866 (1961).

[46] P. Fedichev, M. Reynolds and G. Shlyapnikov, 'Three-body recombination of ultracold atoms to a weakly bound s level,' *Physical review letters* **77**, 2921 (1996).

[47] F. Ferlaino and R. Grimm, 'Trend: Forty years of efimov physics: How a bizarre prediction turned into a hot topic,' *Physics* **3**, 9 (2010).

[48] F. Ferlaino, S. Knoop, M. Berninger, W. Harm, J. Dincao, H.-C. Nägerl and R. Grimm, 'Evidence for universal four-body states tied to an efimov trimer,' *Physical review letters* **102**, 140401 (2009).

[49] H. Feshbach, 'Unified theory of nuclear reactions,' *Annals of Physics* **5**, 357 (1958).

[50] A. L. Fetter, 'Lowest-landau-level description of a bose-einstein condensate in a rapidly rotating anisotropic trap,' *Physical Review A* **75**, 013620 (2007).

[51] M. P. Fisher, P. B. Weichman, G. Grinstein and D. S. Fisher, 'Boson localization and the superfluid-insulator transition,' *Physical Review B* **40**, 546 (1989).

[52] T. Frederico, A. Delfino, L. Tomio and M. T. Yamashita, 'Universal aspects of light halo nuclei,' *Progress in Particle and Nuclear Physics* **67**, 939 (2012).

[53] S. Giorgini, L. P. Pitaevskii and S. Stringari, 'Theory of ultracold atomic fermi gases,' *Reviews of Modern Physics* **80**, 1215 (2008).

[54] A. Görlitz, J. Vogels, A. Leanhardt, C. Raman, T. Gustavson, J. Abo-Shaeer, A. Chikkatur, S. Gupta, S. Inouye, T. Rosenband *et al.*, 'Realization of bose-einstein condensates in lower dimensions,' *Physical Review Letters* **87**, 130402 (2001).

[55] M. Greiner, O. Mandel, T. Esslinger, T. W. Hänsch and I. Bloch, 'Quantum phase transition from a superfluid to a mott insulator in a gas of ultracold atoms,' *nature* **415**, 39 (2002).

[56] M. Greiner, C. A. Regal and D. S. Jin, 'Emergence of a molecular bose–einstein condensate from a fermi gas,' *Nature* **426**, 537 (2003).

[57] R. Grimm, M. Weidemüller and Y. B. Ovchinnikov, 'Optical dipole traps for neutral atoms,' *Advances in Atomic Molecular and Optical Physics* **42**, 95 (2000).

[58] N. Gross, Z. Shotan, S. Kokkelmans and L. Khaykovich, 'Observation of universality in ultracold li 7 three-body recombination,' *Physical review letters* **103**, 163202 (2009).

[59] N. Gross, Z. Shotan, S. Kokkelmans and L. Khaykovich, 'Nuclear-spin-independent short-range three-body physics in ultracold atoms,' *Physical review letters* **105**, 103203 (2010).

[60] Z. Hadzibabic, P. Krüger, M. Cheneau, B. Battelier and J. Dalibard, 'Berezinskii–kosterlitz–thouless crossover in a trapped atomic gas,' *Nature* **441**, 1118 (2006).

[61] H.-W. Hammer, T. A. Lähde and L. Platter, 'Effective-range corrections to three-body recombination for atoms with large scattering length,' *Physical Review A* **75**, 032715 (2007).

[62] H.-W. Hammer and L. Platter, 'Universal properties of the four-body system with large scattering length,' *The European Physical Journal A* **32**, 113 (2007).

[63] G. Hanna and D. Blume, 'Energetics and structural properties of three-dimensional bosonic clusters near threshold,' *Physical Review A* **74**, 063604 (2006).

[64] M. Holland, S. Kokkelmans, M. Chiofalo and R. Walser, 'Resonance superfluidity in a quantum degenerate fermi gas,' *Physical review letters* **87**, 120406 (2001).

[65] K. Huang, 'Statistical mechanics,' (1963).

[66] J. Huckans, J. Williams, E. Hazlett, R. Stites and K. OHara, 'Three-body recombination in a three-state fermi gas with widely tunable interactions,' *Physical review letters* **102**, 165302 (2009).

[67] S. Inouye, M. Andrews, J. Stenger, H.-J. Miesner, D. Stamper-Kurn and W. Ketterle, 'Observation of feshbach resonances in a bose–einstein condensate,' *Nature* **392**, 151 (1998).

[68] D. Jaksch, C. Bruder, J. I. Cirac, C. W. Gardiner and P. Zoller, 'Cold bosonic atoms in optical lattices,' *Physical Review Letters* **81**, 3108 (1998).

[69] A. Jensen, K. Riisager, D. V. Fedorov and E. Garrido, 'Structure and reactions of quantum halos,' *Reviews of modern physics* **76**, 215 (2004).

[70] C. Ji, E. Braaten, D. R. Phillips and L. Platter, 'Universal relations for range corrections to efimov features,' *Physical Review A* **92**, 030702 (2015).

[71] S. Jochim, M. Bartenstein, A. Altmeyer, G. Hendl, S. Riedl, C. Chin, J. H. Denschlag and R. Grimm, 'Bose-einstein condensation of molecules,' *Science* **302**, 2101 (2003).

[72] M. Jona-Lasinio and L. Pricoupenko, 'Three resonant ultracold bosons: Off-resonance effects,' *Physical review letters* **104**, 023201 (2010).

[73] J. Kestner and L.-M. Duan, 'Level crossing in the three-body problem for strongly interacting fermions in a harmonic trap,' *Physical Review A* **76**, 033611 (2007).

[74] L. Khaykovich, F. Schreck, G. Ferrari, T. Bourdel, J. Cubizolles, L. Carr, Y. Castin and C. Salomon, 'Formation of a matter-wave bright soliton,' *Science* **296**, 1290 (2002).

[75] S. Knoop, F. Ferlaino, M. Mark, M. Berninger, H. Schöbel, H.-C. Nägerl and R. Grimm, 'Observation of an efimov-like trimer resonance in ultracold atom–dimer scattering,' *Nature Physics* **5**, 227 (2009).

[76] T. Köhler, K. Góral and P. S. Julienne, 'Production of cold molecules via magnetically tunable feshbach resonances,' *Reviews of modern physics* **78**, 1311 (2006).

[77] M. P. Köppinger, D. J. McCarron, D. L. Jenkin, P. K. Molony, H.-W. Cho, S. L. Cornish, C. R. Le Sueur, C. L. Blackley and J. M. Hutson, 'Production of optically trapped ^{87}RbCs feshbach molecules,' *Phys. Rev. A* **89**, 033604 (2014).

[78] T. Kraemer, M. Mark, P. Waldburger, J. Danzl, C. Chin, B. Engeser, A. Lange, K. Pilch, A. Jaakkola, H.-C. Nägerl *et al.*, 'Evidence for efimov quantum states in an ultracold gas of caesium atoms,' *Nature* **440**, 315 (2006).

[79] T. Lahaye, C. Menotti, L. Santos, M. Lewenstein and T. Pfau, 'The physics of dipolar bosonic quantum gases,' *Reports on Progress in Physics* **72**, 126401 (2009).

[80] P. A. Lee, N. Nagaosa and X.-G. Wen, 'Doping a mott insulator: Physics of high-temperature superconductivity,' *Reviews of modern physics* **78**, 17 (2006).

[81] A. J. Leggett, 'Diatomic molecules and cooper pairs,' in 'Modern trends in the theory of condensed matter,' pp. 13–27 (Springer, 1980).

[82] W. Li, T. Pohl, J. Rost, S. T. Rittenhouse, H. Sadeghpour, J. Nipper, B. Butscher, J. Balewski, V. Bendkowsky, R. Löw *et al.*, 'A homonuclear molecule with a permanent electric dipole moment,' *Science* **334**, 1110 (2011).

[83] T. Lim, S. K. Duffy and W. C. Damer, 'Efimov state in the he 4 trimer,' *Physical Review Letters* **38**, 341 (1977).

[84] X.-J. Liu, H. Hu and P. D. Drummond, 'Virial expansion for a strongly correlated fermi gas,' *Physical review letters* **102**, 160401 (2009).

[85] X.-J. Liu, H. Hu and P. D. Drummond, 'Three attractively interacting fermions in a harmonic trap: Exact solution, ferromagnetism, and high-temperature thermodynamics,' *Physical Review A* **82**, 023619 (2010).

[86] T. Lompe, T. Ottenstein, F. Serwane, K. Viering, A. Wenz, G. Zürn and S. Jochim, 'Atom-dimer scattering in a three-component fermi gas,' *Physical review letters* **105**, 103201 (2010).

[87] K. Madison, F. Chevy, W. Wohlleben and J. Dalibard, 'Vortex formation in a stirred bose-einstein condensate,' *Physical Review Letters* **84**, 806 (2000).

[88] I. Mazumdar, A. Rau and V. Bhasin, 'Efimov states and their fano resonances in a neutron-rich nucleus,' *Physical review letters* **97**, 062503 (2006).

[89] H. J. Metcalf and P. Straten, *Laser cooling and trapping of neutral atoms* (Wiley Online Library, 2007).

[90] A. Micheli, G. Brennen and P. Zoller, 'A toolbox for lattice-spin models with polar molecules,' *Nature Physics* **2**, 341 (2006).

[91] J. Mitroy, S. Bubin, W. Horiuchi, Y. Suzuki, L. Adamowicz, W. Cencek, K. Szalewicz, J. Komasa, D. Blume and K. Varga, 'Theory and application of explicitly correlated gaussians,' *Reviews of Modern Physics* **85**, 693 (2013).

[92] S. Nakajima, M. Horikoshi, T. Mukaiyama, P. Naidon and M. Ueda, 'Measurement of an efimov trimer binding energy in a three-component mixture of li 6,' *Physical review letters* **106**, 143201 (2011).

[93] S. Nascimbene, N. Navon, K. Jiang, F. Chevy and C. Salomon, 'Exploring the thermodynamics of a universal fermi gas,' *Nature* **463**, 1057 (2010).

[94] E. Nielsen and J. Macek, 'Low-energy recombination of identical bosons by three-body collisions,' *Physical Review Letters* **83**, 1566 (1999).

[95] E. Nielsen, H. Suno and B. Esry, 'Efimov resonances in atom-diatom scattering,' *Physical Review A* **66**, 012705 (2002).

[96] P. Nozieres and S. Schmitt-Rink, 'Bose condensation in an attractive fermion gas: From weak to strong coupling superconductivity,' *Journal of Low Temperature Physics* **59**, 195 (1985).

[97] K. O'hara, S. Hemmer, M. Gehm, S. Granade and J. Thomas, 'Observation of a strongly interacting degenerate fermi gas of atoms,' *Science* **298**, 2179 (2002).

[98] C. Orzel, A. Tuchman, M. Fenselau, M. Yasuda and M. Kasevich, 'Squeezed states in a bose-einstein condensate,' *Science* **291**, 2386 (2001).

[99] C. Ospelkaus, S. Ospelkaus, L. Humbert, P. Ernst, K. Sengstock and K. Bongs, 'Ultracold heteronuclear molecules in a 3d optical lattice,' *Phys. Rev. Lett.* **97**, 120402 (2006).

[100] T. B. Ottenstein, T. Lompe, M. Kohnen, A. Wenz and S. Jochim, 'Collisional stability of a three-component degenerate fermi gas,' *Physical review letters* **101**, 203202 (2008).

[101] S. B. Papp and C. E. Wieman, 'Observation of heteronuclear feshbach molecules from a ^{85}Rb$^{\smile 87}$Rb gas,' *Phys. Rev. Lett.* **97**, 180404 (2006).

[102] C. Pethick and D. Ravenhall, 'Matter at large neutron excess and the physics of neutron-star crusts,' *Annual Review of Nuclear and Particle Science* **45**, 429 (1995).

[103] D. Petrov, 'Three-body problem in fermi gases with short-range interparticle interaction,' *Physical Review A* **67**, 010703 (2003).

[104] D. Petrov, C. Salomon and G. V. Shlyapnikov, 'Weakly bound dimers of fermionic atoms,' *Physical Review Letters* **93**, 090404 (2004).

[105] L. Platter, H.-W. Hammer and U.-G. Meißner, 'Four-boson system with short-range interactions,' *Physical Review A* **70**, 052101 (2004).

[106] L. Platter, C. Ji and D. R. Phillips, 'Range corrections to three-body observables near a feshbach resonance,' *Physical Review A* **79**, 022702 (2009).

[107] S. E. Pollack, D. Dries and R. G. Hulet, 'Universality in three-and four-body bound states of ultracold atoms,' *Science* **326**, 1683 (2009).

[108] C. Regal, M. Greiner and D. S. Jin, 'Observation of resonance condensation of fermionic atom pairs,' *Physical Review Letters* **92**, 040403 (2004).

[109] J. J. Sakurai and J. Napolitano, *Modern quantum mechanics* (Addison-Wesley, 2011).

[110] F. Schreck, L. Khaykovich, K. Corwin, G. Ferrari, T. Bourdel, J. Cubizolles and C. Salomon, 'Quasipure bose-einstein condensate immersed in a fermi sea,' *Physical Review Letters* **87**, 080403 (2001).

[111] V. Schweikhard, I. Coddington, P. Engels, V. Mogendorff and E. A. Cornell, 'Rapidly rotating bose-einstein condensates in and near the lowest landau level,' *Physical review letters* **92**, 040404 (2004).

[112] F. Serwane, G. Zürn, T. Lompe, T. Ottenstein, A. Wenz and S. Jochim, 'Deterministic preparation of a tunable few-fermion system,' *Science* **332**, 336 (2011).

[113] J. von Stecher, J. P. DIncao and C. H. Greene, 'Signatures of universal four-body phenomena and their relation to the efimov effect,' *Nature Physics* **5**, 417 (2009).

[114] K. E. Strecker, G. B. Partridge, A. G. Truscott and R. G. Hulet, 'Formation and propagation of matter-wave soliton trains,' *Nature* **417**, 150 (2002).

[115] Y. Suzuki and K. Varga, *Stochastic variational approach to quantum-mechanical few-body problems*, vol. 54 (Springer Science & Business Media, 1998).

[116] S. Tan, 'Energetics of a strongly correlated fermi gas,' *Annals of Physics* **323**, 2952 (2008).

[117] S. Tan, 'Generalized virial theorem and pressure relation for a strongly correlated fermi gas,' *Annals of Physics* **323**, 2987 (2008).

[118] S. Tan, 'Large momentum part of a strongly correlated fermi gas,' *Annals of Physics* **323**, 2971 (2008).

[119] M. Thøgersen, D. V. Fedorov and A. S. Jensen, 'N-body efimov states of trapped bosons,' *EPL (Europhysics Letters)* **83**, 30012 (2008).

[120] M. Thøgersen, D. V. Fedorov and A. S. Jensen, 'Universal properties of efimov physics beyond the scattering length approximation,' *Physical Review A* **78**, 020501 (2008).

[121] M. Thøgersen, D. V. Fedorov, A. S. Jensen, B. Esry and Y. Wang, 'Conditions for efimov physics for finite-range potentials,' *Physical Review A* **80**, 013608 (2009).

[122] L. H. Thomas, 'The interaction between a neutron and a proton and the structure of h^3,' *Phys. Rev.* **47**, 903 (1935).

[123] E. Tiesinga, B. Verhaar and H. Stoof, 'Threshold and resonance phenomena in ultracold ground-state collisions,' *Physical Review A* **47**, 4114 (1993).

[124] A. G. Truscott, K. E. Strecker, W. I. McAlexander, G. B. Partridge and R. G. Hulet, 'Observation of fermi pressure in a gas of trapped atoms,' *Science* **291**, 2570 (2001).

[125] N. Van Kampen, 'A simplified cluster expansion for the classical real gas,' *Physica* **27**, 783 (1961).

[126] A.-C. Voigt, M. Taglieber, L. Costa, T. Aoki, W. Wieser, T. W. Hänsch and K. Dieckmann, 'Ultracold heteronuclear fermi-fermi molecules,' *Phys. Rev. Lett.* **102**, 020405 (2009).

[127] V. Vuletić, A. J. Kerman, C. Chin and S. Chu, 'Observation of low-field feshbach resonances in collisions of cesium atoms,' *Physical review letters* **82**, 1406 (1999).

[128] C. Weber, G. Barontini, J. Catani, G. Thalhammer, M. Inguscio and F. Minardi, 'Association of ultracold double-species bosonic molecules,' *Phys. Rev. A* **78**, 061601 (2008).

[129] F. Werner and Y. Castin, 'Unitary gas in an isotropic harmonic trap: Symmetry properties and applications,' *Physical Review A* **74**, 053604 (2006).

[130] R. Wild, P. Makotyn, J. Pino, E. Cornell and D. Jin, 'Measurements of tans contact in an atomic bose-einstein condensate,' *Physical review letters* **108**, 145305 (2012).

[131] J. Williams, E. Hazlett, J. Huckans, R. Stites, Y. Zhang and K. OHara, 'Evidence for an excited-state efimov trimer in a three-component fermi gas,' *Physical review letters* **103**, 130404 (2009).

[132] M. T. Yamashita, T. Frederico and L. Tomio, 'Trajectory of neutron–neutron–18 c excited three-body state,' *Physics Letters B* **660**, 339 (2008).

[133] M. T. Yamashita, L. Tomio, A. Delfino and T. Frederico, 'Four-boson scale near a feshbach resonance,' *EPL (Europhysics Letters)* **75**, 555 (2006).

[134] M. Zaccanti, B. Deissler, C. DErrico, M. Fattori, M. Jona-Lasinio, S. Müller, G. Roati, M. Inguscio and G. Modugno, 'Observation of an efimov spectrum in an atomic system,' *Nature Physics* **5**, 586 (2009).

[135] M. Zwierlein, C. Stan, C. Schunck, S. Raupach, A. Kerman and W. Ketterle, 'Condensation of pairs of fermionic atoms near a feshbach resonance,' *Physical Review Letters* **92**, 120403 (2004).

[136] M. W. Zwierlein, C. A. Stan, C. H. Schunck, S. M. Raupach, S. Gupta, Z. Hadzibabic and W. Ketterle, 'Observation of bose-einstein condensation of molecules,' *Physical review letters* **91**, 250401 (2003).